AUS DEM LEHRSTUHL FÜR BIOCHEMIE III
DER FAKULTÄT FÜR BIOLOGIE UND VORKLINISCHE MEDIZIN
DER UNIVERSITÄT REGENSBURG

Investigation of the effects of putative RNA Polymerase I-specific Inhibitors in the eukaryotic model organism *Saccharomyces cerevisiae*

Inaugural – Dissertation
zur Erlangung des Doktorgrades
der Zahnmedizin

der
Fakultät für Medizin
der Universität Regensburg

vorgelegt von
René Schlegel

2025

AUS DEM LEHRSTUHL FÜR BIOCHEMIE III
DER FAKULTÄT FÜR BIOLOGIE UND VORKLINISCHE MEDIZIN
DER UNIVERSITÄT REGENSBURG

Investigation of the effects of putative RNA Polymerase I-specific Inhibitors in the eukaryotic model organism *Saccharomyces cerevisiae*

Inaugural – Dissertation
zur Erlangung des Doktorgrades
der Zahnmedizin

der
Fakultät für Medizin
der Universität Regensburg

vorgelegt von
René Schlegel

2025

Dekan:	Prof. Dr. Dirk Hellwig
1. Berichterstatter:	Prof. Dr. Joachim Griesenbeck
2. Berichterstatter:	Prof. Dr. Ralf Wagner
3. Berichterstatter:	Prof. Dr. Wolfgang Seufert
Tag der mündlichen Prüfung:	21.10.2025

Selbstständigkeitserklärung

„Ich erkläre hiermit, dass ich die vorliegende Arbeit ohne unzulässige Hilfe Dritter und ohne Benutzung anderer als der angegebenen Hilfsmittel angefertigt habe. Die aus anderen Quellen direkt oder indirekt übernommenen Daten und Konzepte sind unter Angabe der Quelle gekennzeichnet. Insbesondere habe ich nicht die entgeltliche Hilfe von Vermittlungs- bzw. Beratungsdiensten (Promotionsberater oder andere Personen) in Anspruch genommen. Niemand hat von mir unmittelbar oder mittelbar geldwerte Leistungen für Arbeit erhalten, die im Zusammenhang mit dem Inhalt der vorgelegten Dissertation stehen. Die Arbeit wurde bisher weder im In- noch im Ausland in gleicher oder ähnlicher Form einer anderen Prüfungsbehörde vorgelegt“

Regensburg, 23. März 2025 _____

René Schlegel

Table of Contents

1. Summary

A dividing cell's demand for ribosomes hinges on the synthesis of ribosomal RNA (rRNA), a process mainly carried out by DNA-dependent RNA Polymerase I (Pol I). In many cancers, elevated Pol I activity accelerates rRNA production, fueling rapid cell division and tumor progression. Consequently, Pol I has emerged as an attractive target for therapeutic intervention, prompting extensive efforts to discover and characterize small-molecule inhibitors.

In this study, we investigate two putative Pol I inhibitors, CX-5461 and BMH-21, both of which display distinctive effects on cell growth and division. To dissect their mechanisms of action, we employed the eukaryotic model organism *Saccharomyces cerevisiae*, which shares fundamental aspects of Pol I transcription with higher eukaryotes. The yeast system enables precise genetic manipulation of cellular pathways and therefore provides a robust platform to assess inhibitor specificity. The focus of the present study is to investigate the role of Hmo1, a chromatin-associated protein - a putative functional homolog of mammalian UBF1 - in mediating the response of yeast cells upon exposure to the inhibitors. We explored how CX-5461 and BMH-21 disrupt rRNA synthesis and inhibit cellular growth, depending on endogenous Hmo1 levels *in vivo*.

Our findings reveal that CX-5461's effects on yeast cell growth are not primarily caused by Pol I inhibition, whereas BMH-21 more directly targets Pol I by triggering subunit degradation. As a crucial factor, Hmo1 stabilizes Pol I and mitigates drug toxicity. Ultimately, this work confirms BMH-21 as a promising compound whose main effects on cellular growth can be explained by Pol I inhibition while emphasizing the need for eukaryotic model systems to understand the molecular basis for the observed phenomena and minimize off-target effects.

2. Zusammenfassung

Der Bedarf einer sich teilenden Zelle an Ribosomen beruht auf der Synthese von ribosomaler RNA (rRNA), einem Prozess, der hauptsächlich von der DNA-abhängigen RNA-Polymerase I (Pol I) durchgeführt wird. In vielen Krebserkrankungen führt eine erhöhte Pol I-Aktivität zu einer beschleunigten rRNA-Produktion, was das schnelle Zellwachstum und die Tumorprogression fördert. Folglich hat sich Pol I als attraktives therapeutisches Ziel etabliert, was umfangreiche Bemühungen zur Identifizierung und Charakterisierung von kleinen Molekülinhibitoren nach sich gezogen hat.

In dieser Studie untersuchen wir zwei potenzielle Pol I-Inhibitoren, CX-5461 und BMH-21, die beide markante Effekte auf Zellwachstum und Zellteilung zeigen. Zur Analyse ihrer Wirkmechanismen nutzten wir den eukaryotischen Modellorganismus *Saccharomyces cerevisiae*, der fundamentale Aspekte der Pol I-Transkription mit höheren Eukaryoten teilt. Das Hefesystem ermöglicht eine präzise genetische Manipulation zellulärer Signalwege und bietet somit eine robuste Plattform zur Bewertung der Spezifität der Inhibitoren. Im Fokus unserer Studie steht die Frage wie Hmo1, ein chromatinassoziiertes Protein, das weithin als funktionelles Homolog von UBF1 in Säugetieren angesehen wird, die Sensitivität von Hefezellen bei Behandlung mit den Inhibitoren beeinflusst. Hierzu haben wir untersucht wie CX-5461- und BMH-21-Behandlung die rRNA-Synthese und das Wachstum von Hefestämmen mit unterschiedlichen Hmo1 Expressionsniveaus beeinflussen.

Unsere Ergebnisse zeigen, dass die Effekte von CX-5461 auf das Zellwachstum in Hefen nicht primär auf einer Pol-I-Hemmung beruhen, wohingegen BMH-21 Pol I direkter angreift, indem es die Degradation ihrer Untereinheiten auslöst. Als wichtiger Faktor stabilisiert Hmo1 die Pol-I-Komplexe und reduziert somit die Toxizität der Wirkstoffe. Letztlich bestätigt diese Arbeit BMH-21 als vielversprechende Substanz, deren Auswirkungen auf das Zellwachstum hauptsächlich durch die Hemmung der Pol I erklärbar sind. Zugleich unterstreicht sie jedoch die Bedeutung eukaryotischer Modellsysteme, um die molekularen Grundlagen der beobachteten Phänomene besser zu verstehen und Nebeneffekte zu minimieren.

3. Introduction

3.1 Ribosome biogenesis and cell growth

Eukaryotic ribosomes are essential cellular organelles responsible for protein biosynthesis, comprising four distinct species of ribosomal RNA (rRNA) and ribosomal proteins (reviewed in Warner, 1999; Woolford Jr & Warner, 1991). In the model eukaryote *Saccharomyces cerevisiae* (hereafter called yeast), three of these rRNA species - 18S, 5.8S, and 25S - are synthesized by DNA-dependent RNA Polymerase I (Pol I), while the remaining 5S rRNA is produced by Pol III (reviewed in Nomura et al., 2013). The large scale of rRNA production is underscored by the observation that rRNA transcription by Pol I contributes about 60% of the total transcriptional activity in a dividing yeast cell, despite rRNA genes constituting only approximately 10% of the genome (reviewed in Warner, 1999; Woolford Jr & Warner, 1991). This high output is crucial for cell growth and proliferation, as each yeast cell must assemble around 200,000 ribosomes to complete one division cycle (reviewed in Warner, 1999; Woolford Jr & Warner, 1991). To achieve such elevated biosynthetic demands, the cell maintains multiple rDNA repeats, allowing numerous Pol I molecules to transcribe simultaneously along these gene clusters (Petes, 1979). In an exponentially growing yeast cell, around 50 Pol I molecules are simultaneously transcribing one 35S rRNA gene (French et al., 2003).

3.2 RNA polymerase I transcription in eukaryotes

3.2.1 The rDNA gene locus in *yeast*

In most eukaryotes, rDNA repeats are clustered within Nucleolar Organizer Regions (NORs), originally identified as sites responsible for nucleolus formation (McClintock, 1934). In yeast, the NOR occupies a specific locus on chromosome XII, comprising roughly 100-150 tandem repeats, each about 9.1 kb in length (Petes, 1979) (Fig. 1 a), top). Every repeat contains the 35S-rDNA (encompassing the information for the 18S, 5.8S, and 25S rRNA sequences, along with the Pol I promoter) and an Intergenic Spacer (IGS), which is subdivided into IGS1 and IGS2 by the 5S-rDNA gene (Philippsen, 1978; reviewed in Geiduschek & Kassavetis, 2001) (Fig. 1 a), middle). The 35S-rRNA precursor is transcribed by Pol I and subsequently processed into mature 18S, 5.8S, and 25S rRNAs, whereas the 5S-rDNA, located between IGS1 and IGS2, is transcribed by Pol III (Philippsen, 1978). Regulatory elements in the rDNA repeat include the 35S

rDNA promoter composed of an Upstream Element (UE), which binds the Upstream Activation Factor (UAF), and a Core Promoter (CP), which binds the Core Factor (CF) (Keys et al., 1994, 1996; Lalo et al., 1996) (Fig. 1 a), bottom). At the 3' end of the 35S rDNA, the Termination Site (T) and an Enhancer (E) help modulate transcription termination and may also stimulate promoter activity (Elion & Warner, 1984). Additionally, the Replication Fork Barrier (RFB) in IGS1 prevents replication-transcription collisions by halting the replication fork initiating at an Autonomous Replicating Sequence (ARS) within IGS2 and moving opposite to the direction of Pol I transcription (Brewer & Fangman, 1988; Kobayashi et al., 1992). Additionally, the rDNA repeat contains a Pol II-dependent promoter termed E-pro. E-pro (sometimes referred to as a "cryptic" or "non-coding" promoter) can drive low-level transcription that may influence the local chromatin landscape and help modulate rDNA copy number (Ganley et al., 2005; Kobayashi & Ganley, 2005).

Through the arrangement of repeated units, specialized cis-elements, and dedicated transcription factors, yeast enables the high-throughput synthesis of rRNAs and the accurate replication of the rDNA locus - both essential for robust ribosome biogenesis and, consequently, cell division.

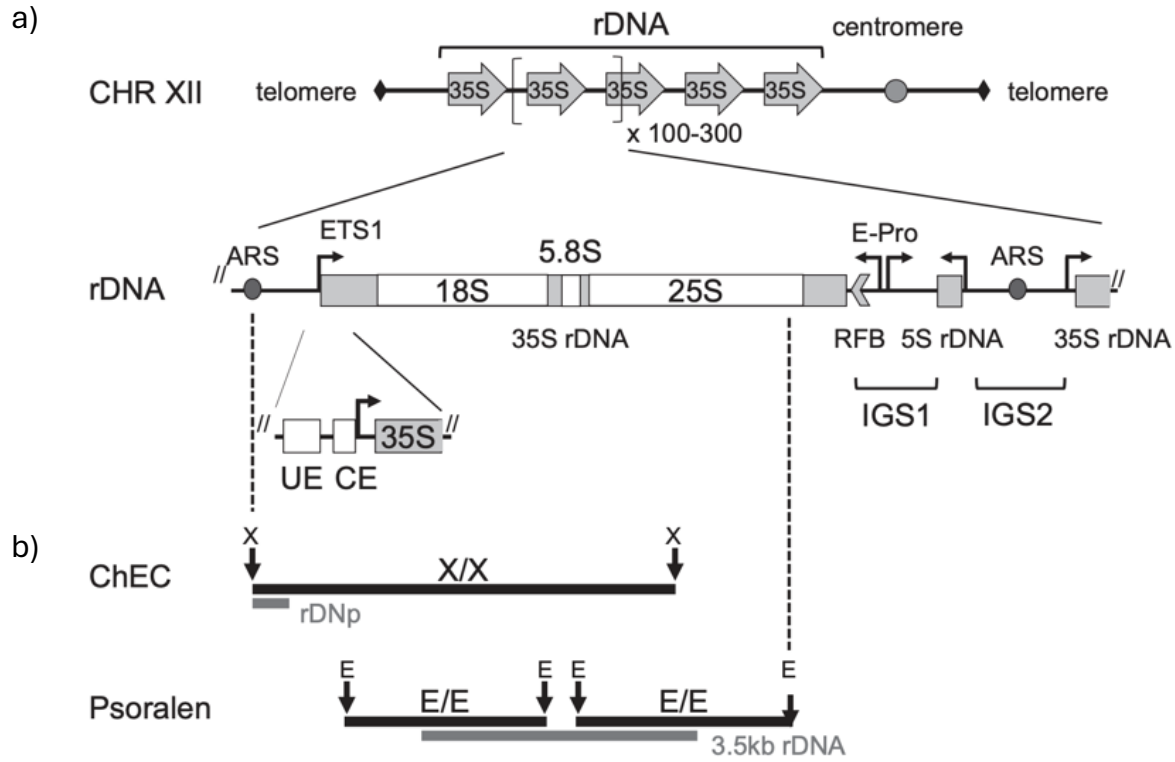

Figure 1: Schematic representation of the yeast rDNA locus
a) Depiction of the yeast rDNA locus on chromosome XII, which contains 100–300 transcription units in tandem array (top). In the middle Panel, a single rDNA transcription unit is illustrated along with its key genetic elements. Here, the 5S rDNA - transcribed by RNA polymerase III - is separated by intergenic spacers (IGS1 and IGS2) from two copies of the 35S rRNA gene. Within IGS1, a replication fork barrier (RFB) and a bidirectional expansion promoter (E-Pro) that is dependent on RNA polymerase II are found, while IGS2 houses an autonomous replication sequence (ARS). The 35S rDNA is transcribed by RNA polymerase I, producing a large precursor molecule that is subsequently processed into the mature 18S, 5.8S, and 25S rRNAs; the 5' external transcribed spacer (ETS1) is also indicated. At the bottom, the 35S rDNA promoter is shown, comprising an upstream element (UE) and a core element (CE), with arrows marking the direction of transcription.
b) Illustration of the specific rDNA fragments examined in the ChEC and psoralen photo-crosslinking experiments. These fragments are marked with restriction sites labeled X (for XcmI) and E (for EcoRI). Below the fragments, the radioactively labeled probes used in Southern blot analysis are shown as grey bars, indicating their hybridization sites (further explained in 5.3.6) (Figure taken from Babl et al. 2024)

3.2.2 Pol I transcription in yeast

3.2.2.1 The RNA polymerase I transcription cycle in yeast

The 35S rDNA promoter designates the DNA region immediately upstream of the transcription start site (TSS) - nucleotides -146 to +8 - where the Pol I pre-initiation complex (PIC) assembles (Keys et al., 1994, 1996; Lalo et al., 1996; Musters, 1989). Within this promoter, two main cis-elements have been defined: the UE, spanning roughly nucleotides -146 to -51, and the CP, spanning -28 to +8 (Keys et al., 1996; Musters, 1989). The UE is recognized by UAF, a complex composed of Rrn5, Rrn9, Rrn10, Uaf30, and histones H3 and H4 (Keener et al., 1997; Keys et al., 1996; Siddiqi, Dodd, Vu, & Nomura, 2001). Uaf30, in particular, aids UAF's stable binding to the UE (Goetze et al., 2010; Siddiqi, Dodd, Vu, & Nomura, 2001), while the presence of H3 and H4 may explain UAF's strong DNA affinity (Baudin et al., 2022; Keener et al., 1997) (Fig. 2, top left).

Once the UE is occupied by UAF, CF - comprising Rrn6, Rrn7, and Rrn11 - associates with the CP in a process that also depends on the TATA-binding protein (TBP, or Spt15 in yeast) (Cormack & Struhl, 1992; Steffan et al., 1996). TBP interacts with UAF subunits to recruit CF, enabling CF to bind the core promoter and stabilize early PIC formation (Keys et al., 1994, 1996; Lalo et al., 1996) (Fig. 2, middle left). Another critical protein is Rrn3, which first binds Pol I and then recruits the complex to the promoter (Milkereit & Tschochner, 1998; Yamamoto et al., 1996) (Fig. 2, step 1) (Fig. 2, middle). Notably, in minimal reconstituted systems only CF and Pol I-Rrn3 suffice to initiate promoter-specific transcription (Steffan et al., 1996), although a full factor set is essential for robust PIC assembly under physiological conditions (Goetze et al., 2010; Hontz et al., 2008; Siddiqi, Dodd, Vu, Eliason, et al., 2001).

After promoter engagement, Rrn3 dissociates from Pol I, allowing the polymerase to transition from initiation to elongation (Beckouet et al., 2008; Yamamoto et al., 1996) (Fig. 2, bottom middle). During this elongation phase, DNA topoisomerases I and II (Top I and Top II) are crucial for resolving negative and positive DNA supercoils that accumulate behind or in front of Pol I, respectively (Brill et al., 1987; French et al., 2011; Schultz et al., 1992). In the absence of these enzymes, torsional stress stalls polymerase movement and compromises rRNA synthesis. Moreover, the HMG-box protein Hmo1 has been observed to enhance Pol I transcription probably at the elongation phase, likely by stabilizing the open, nucleosome-depleted chromatin state within actively transcribed rDNA repeats (Gadal et al., 2002; Merz et al., 2008) (Fig. 2, bottom middle).

Ultimately, Pol I transcription terminates at the 3' termination site T1, located 93 base pairs downstream of the 25S rRNA 3' end (Lang & Reeder, 1993, 1995) (Fig. 2, bottom right). The Pol I termination factor Nsi1 is critical for efficient termination at T1, promoting proper Pol I dissociation and transcript release. Nevertheless, *in vivo* studies indicate that roughly 10% of Pol I transcripts bypass T1 and terminate at a secondary "fail-safe" site positioned about 250 base pairs further downstream (Reeder et al., 1999). This additional termination mechanism may safeguard cells against polymerases failing to disengage at the primary termination site, thereby preserving correct rRNA processing and ensuring the integrity of the rDNA locus (Reeder et al., 1999; Reiter et al., 2012).

As an additional level of regulation, the 35S rDNA can exist in either a closed, nucleosome-associated chromatin state or an open, actively transcribed nucleosome-depleted chromatin state stabilized by the HMG-box protein Hmo1 (Merz et al., 2008; Wittner et al., 2011). Typically, only about half of the around 150 rDNA repeats are active at any time, reflecting the cell's ability to modulate rRNA synthesis in response to growth demands (Dammann et al., 1993; Fahy et al., 2005; French et al., 2003). The dynamic regulation of transcription initiation at promoter cis-elements and changes in chromatin states ensures that Pol I transcription can be adjusted to support cellular ribosome biogenesis.

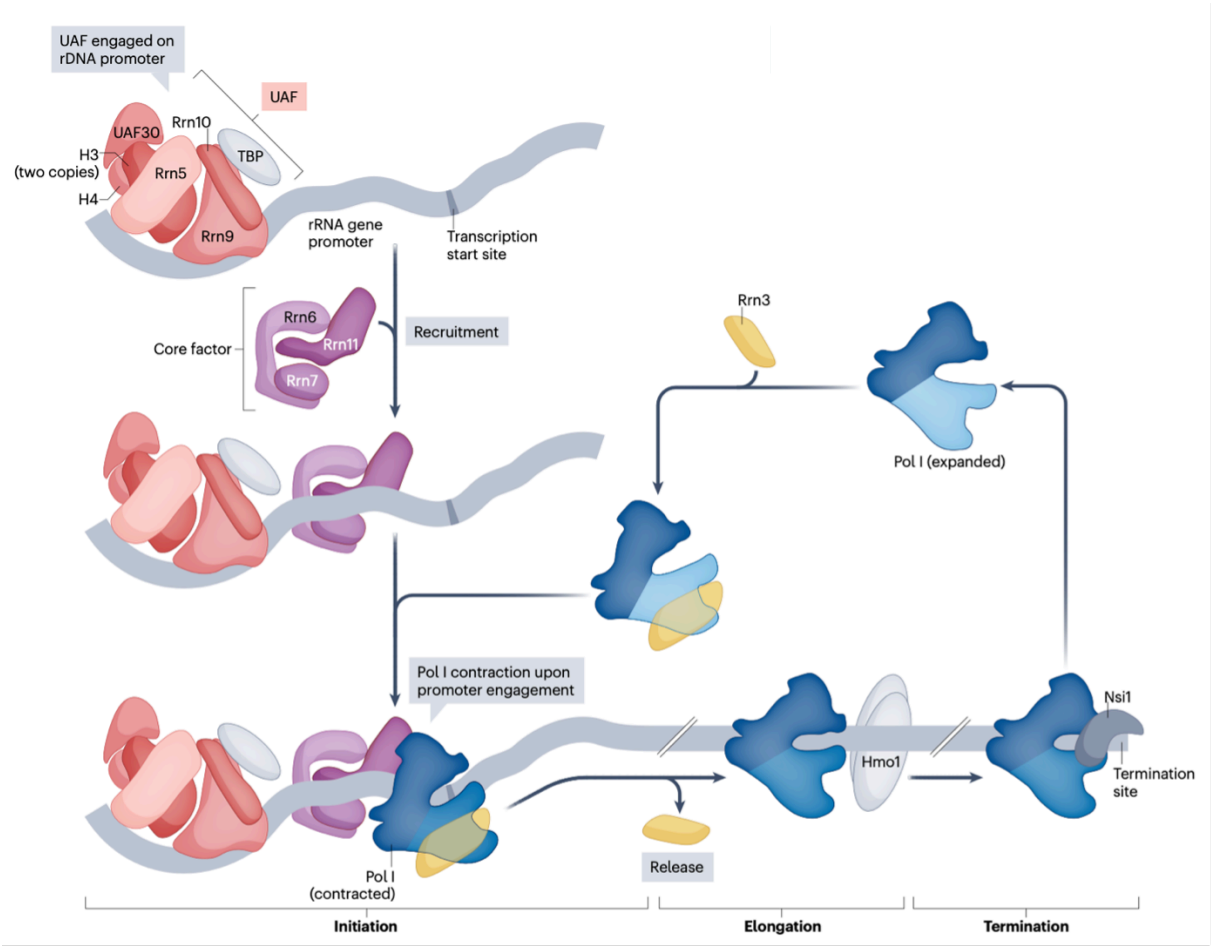

Figure 2: Schematic representation of the Pol I transcription cycle
In yeast, the upstream activating factor (UAF) attaches to an element upstream of the promoter, which facilitates the subsequent recruitment of TATA-binding protein (TBP) and the core factor complex (top left). When the transcription initiation factor Rrn3 binds to Pol I (middle right), it enables recruitment of the complex to the ribosomal RNA (rRNA) gene promoter. A particular DNA conformation assists the Pol I-Rrn3 complex to associate with the core factor (bottom left). As transcription proceeds and the polymerase escapes the promoter, Rrn3 is released, allowing Pol I to continue elongation. Additionally, Hmo1 - likely as dimer -are involved in binding along active rRNA genes to support transcript elongation (bottom middle), while transcription termination is achieved when the protein Nsi1 binds to a specific termination sequence, effectively acting as a roadblock for Pol I (bottom right). (Figure taken from Hori et al., 2023)

3.2.3 35S rDNA gene chromatin states in yeast

Chromatin is a large nucleoprotein complex which is important to package eukaryotic DNA in the limited space of the nucleus. The main repeating subunit of chromatin is called the nucleosome and consists of around 147 bp of DNA wrapped around a disc-shaped core of an octameric complex of histone proteins formed by a histone H3 and H4 tetramer and two associated H2A/H2B dimers (Luger et al., 1997; White et al., 2001; reviewed in Kornberg & Lorch, 1999). Chromatin may exert profound control over gene expression by regulating DNA accessibility through nucleosome positioning, and higher-order folding (Finch & Klug, 1976;

Kornberg, 1974; reviewed in Kornberg & Lorch, 1999). At the Pol I-transcribed 35S rDNA locus chromatin may switch between an open, nucleosome-depleted state that supports high-level rRNA synthesis (Dammann et al., 1993; French et al., 2003; Merz et al., 2008; Wittner et al., 2011) and a condensed, transcriptionally silent state packaged into nucleosomes. Examples of such dynamic shifts include the transient closing of rRNA genes during S-phase in yeast and their subsequent re-opening in other cell cycle stages, or transitions to a closed state in response to UV-induced DNA damage followed by re-opening upon DNA repair (Hamperl et al., 2013).

3.2.4 Hmo1 and its role in Pol I transcription

The HMG-box protein Hmo1, estimated at roughly 19,000 to 25,000 molecules per cell (reviewed in Cherry et al., 2012; Ghaemmaghami et al., 2003), stands out as a multifunctional DNA-binding factor. Genome-wide analyses indicate that Hmo1 interacts with nearly 290 genes or gene products, underscoring its potential to influence numerous cellular pathways (Berger et al., 2007; Hall et al., 2006; K. Kasahara et al., 2007). Thus, Hmo1 has been detected particularly at genes linked to ribosome biogenesis through techniques such as chromatin immunoprecipitation (ChIP) and microarray analyses. Within the rRNA gene locus, Hmo1 specifically associates with open, actively transcribed rRNA genes, where it stabilizes nucleosome-free DNA (Merz et al., 2008; Wittner et al., 2011). Intriguingly, Hmo1 can preserve this open chromatin state even in the absence of active Pol I transcription, suggesting a structural or architectural role (Wittner et al., 2011).

Hmo1 has been implicated in the regulation of DNA topology, particularly through its ability to induce negative supercoiling at gene boundaries. Hmo1 binding preserves localized negative supercoils, influencing chromatin conformation and modulating the accessibility and structural integrity of DNA regions (Achar et al., 2020).

Beyond its function in Pol I-driven transcription of the 35S rDNA, Hmo1 also supports transcription by Pol II. For example, Hmo1 localizes to promoters of ribosomal protein (RP) genes, helping to sustain a nucleosome-free region that facilitates the assembly of transcription factors and the Pol II preinitiation complex (Hall et al., 2006; M. Kasahara et al., 2011). Furthermore, Hmo1 has been shown to bind to its own promoter, indicative of a negative feedback mechanism controlling its expression (Xiao et al., 2011). In addition to its transcription-related

responsibilities, Hmo1 participates in DNA damage responses and the repair of double-strand breaks, highlighting its broader significance in genomic maintenance (reviewed in Panday & Grove, 2016). Moreover, shifts in Hmo1 occupancy at rRNA genes occur when rDNA chromatin undergoes dynamic changes, such as those associated with the cell cycle or replication stress (Bermejo et al., 2009). Collectively, these observations emphasize Hmo1's critical roles in both Pol I and Pol II transcription, as well as its importance in safeguarding genome integrity.

A closely related HMG-box protein in mammals is Upstream Binding Factor 1 (UBF1). Like Hmo1, UBF1 is integral to Pol I transcription, binding rDNA and maintaining an open chromatin configuration at rRNA gene promoters (Herdman et al., 2017; Jantzen et al., 1990; Moss et al., 2019; reviewed in Sanij & Hannan, 2009). This architectural role helps recruit and stabilize the Pol I transcription machinery, paralleling Hmo1's function in yeast (Mais et al., 2005; Stefanovsky et al., 2001). Beyond transcription, UBF1 contributes to rDNA organization and may influence the overall nucleolar architecture (van de Nobelen et al., 2010; reviewed in Hernandez-Verdun, 2006). Thus, Hmo1 in yeast and UBF1 in mammals may be considered as functionally analogous HMG-box proteins that facilitate high-level rRNA production and safeguard the genomic integrity of rDNA repeats (reviewed in Sanij & Hannan, 2009).

3.3 Similarities and differences between mammalian and yeast Pol I transcription

As in yeast, the human rDNA gene locus is a highly complex and dynamic genomic region that plays a central role in ribosome biogenesis and cellular homeostasis (reviewed in Hori et al., 2023; Potapova & Gerton, 2019). Situated in NORs on the short arms of the five acrocentric chromosomes (Henderson et al., 1972; reviewed in McStay, 2016), these loci contain hundreds of tandemly repeated units - each encompassing a 45S rRNA gene transcribed by Pol I and flanked by extensive intergenic spacer sequences (reviewed in Moss et al., 2007; Potapova & Gerton, 2019). Notably, rDNA organization in other higher eukaryotes follows a similar pattern of tandem repeats with specialized regulatory regions (Moss et al., 2019; reviewed in Potapova & Gerton, 2019), underscoring the conserved strategies for rRNA gene regulation across species. The IGS regions host various cis-regulatory elements - including enhancers, promoters, and upstream control elements - that help the recruitment of essential transcription factors, such as UBF1 and the Selective Factor 1 (SL1), which are components of

the Pol I pre-initiation complex (reviewed in Daiß et al., 2023; Moss et al., 2007). In humans, the Pol I pre-initiation complex is assembled by UBF1 and SL1, which comprises TBP and four TBP-associated factors (TAFs), and binds the core promoter leading to the recruitment of the initiation competent Rrn3-Pol I complex (Bell et al., 1988; Moorefield et al., 2000). UBF1 functions as a dimer that induces the formation of an enhanceosome - a loop structure that brings the activating sequence into close proximity with the core promoter element - and thereby stabilizes SL1 binding (Bell et al., 1990; Friedrich et al., 2005; Stefanovsky et al., 1996) (Fig. 3, bottom). In addition, UBF1 not only associates with promoter elements but also binds along the transcribed region to regulate Pol I elongation, with its activity modulated by posttranslational modifications (Hamdane et al., 2014; reviewed in Sanij & Hannan, 2009).

The yeast components Pol I, Rrn3, CF, and Hmo1 are functionally and structural analogous to transcription factors found in mammalian cells (Fig. 3, top). This is reflected by the structure of the Rrn3-Pol I complex (Engel et al., 2016; Misiaszek et al., 2021; Pilsl et al., 2016), and the fact that human Rrn3 can rescue lethality in a yeast strain lacking the *RRN3* gene (Moorefield et al., 2000; reviewed in Girbig et al., 2022). Furthermore, there is bioinformatic evidence that CF shares structural similarities with SL1, which is supported by functional complementation *in vivo* (Knutson & Hahn, 2011; Naidu et al., 2011). Additionally, sequence alignments show that UBF1 HMG boxes 1 and 2 are similar to Hmo1, and overexpression of these UBF1 domains can rescue synthetic lethality of a yeast strain carrying deletions in the genes coding for the Pol I subunit Rpa49 and Hmo1 (Albert et al., 2013). These parallels reflect deeper functional and structural homologies among the core Pol I machinery (Fig. 3, top).

In addition to transcriptional regulation, the human rDNA locus is subject to intricate epigenetic control: DNA methylation patterns and selective histone modifications generate a mix of active and silent rDNA repeats (Bird, 1986; Sanij et al., 2008; Zentner et al., 2011), enabling cells to modulate ribosome production in response to developmental cues, stress, or metabolic needs. As observed in yeast, only a fraction of the rDNA repeats is actively transcribed at any given time (Conconi et al., 1989), thereby allowing regulation of rRNA synthesis at the level of gene activation (Sanij et al., 2008; reviewed in Hori et al., 2023).

Despite the structural and regulatory complexity evident in the human rDNA locus, many fundamental processes that govern rRNA synthesis, chromatin dynamics, and ribosome assembly are evolutionarily conserved (reviewed in Nomura et al., 2013). Accordingly, yeast remains an indispensable model organism: investigations in yeast continue to illuminate core aspects of

rDNA transcription and epigenetic regulation, and these insights may translate directly to understanding the human rDNA system.

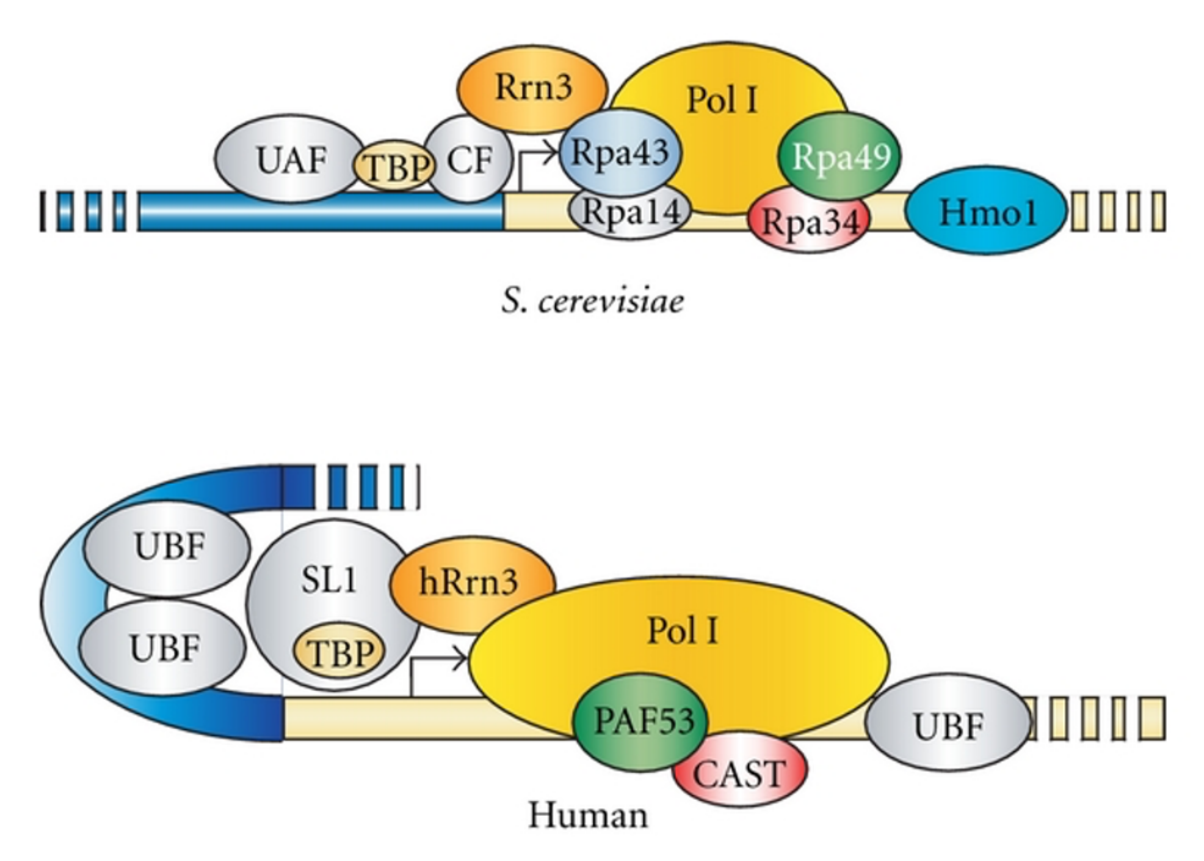

Figure 3: Structural comparison between yeast and human PIC
Comparison of the Pol I pre-initiation complexes (PICs) assembled on the rDNA promoter in yeast (top) and in hu-mans (bottom). In yeast, upstream factors (UAF, TBP, CF) recruit Rrn3, which in turn bridges the upstream elements to Pol I (yellow), while Hmo1 (blue) associates with the DNA. In humans, UBF may play a role analogous to UAF, in wrapping the rDNA promoter region and collaborating with SL1 (containing TBP) and hRrn3 to recruit Pol I, along with additional factors like PAF53 and CAST, which are homologous to the yeast Pol I subunits Rpa49 and Rpa34, respectively. Despite functional parallels, the subunit compositions and promoter-binding factors differ between the yeast and human Pol I PIC architectures. See text for detailed information about the single components. (Figure taken from Albert et al., 2012)

3.4 Pol I transcription as a target in cancer therapy

Altered ribosome biogenesis is a common hallmark of cancer cells, where heightened rRNA transcription by Pol I accommodates the increased demand for protein synthesis necessary for rapid tumor growth. This dysregulated Pol I activity drives excessive ribosome assembly and often manifests as nucleolar enlargement, a feature correlated with aggressive cellular behavior and resistance to apoptosis (Bywater, 2012; reviewed in Drygin et al., 2010; Pelletier et al., 2018; van Riggelen et al., 2010). Accordingly, targeting the mechanisms underlying this

altered ribosome biogenesis - such as reducing Pol I-mediated rRNA synthesis - has emerged as a promising approach for novel cancer therapies designed to exploit the heightened dependence of tumor cells on ribosome production (Bywater, 2012; reviewed in Ferreira et al., 2020). For instance, the platinum-based antineoplastic Cisplatin induces DNA damage that sequesters UBF1, thereby indirectly hampering ribosome production (Burger et al., 2010; Jordan & Carmo-Fonseca, 1998). Likewise, antimetabolites like 5-Fluorouracil can be misincorporated into rRNA, impairing its processing and obstructing ribosome assembly (reviewed in Longley et al., 2003). Plant alkaloids and antibiotics - e.g., Mitomycin C - also hinder Pol I transcription, though their precise modes of action remain unclear (Burger et al., 2010; Snodgrass et al., 2010).

A principal complication with these established therapeutic agents is their broad impact on multiple cellular pathways beyond Pol I-mediated rRNA synthesis, frequently culminating in cytotoxic effects across both tumor and normal tissues (Drygin et al., 2010). Nevertheless, growing mechanistic insights into Pol I transcription support the discovery of more selective inhibitors targeting specific steps of the Pol I cycle, potentially minimizing off-target toxicity and improving the therapeutic index (reviewed in Pelletier et al., 2018). These developments underscore the promise of focused Pol I inhibition as a foundation for novel, tumor-specific interventions, while continuous efforts seek to refine the safety and efficacy of these approaches in clinical oncology (reviewed in Ferreira et al., 2020).

3.4.1 The small molecule inhibitor CX-5461

CX-5461 is a small heterocyclic compound primarily known for selectively inhibiting Pol I-driven transcription (Drygin et al., 2011). In mammalian systems, CX-5461 impedes Pol I function by reducing the binding of SL1 to rDNA promoters or by preventing promoter release, ultimately leading to DNA damage accumulation (Mars et al., 2020). This nucleolar stress response can induce autophagy and apoptosis - partly by liberating p53 from its negative regulator, Mdm2 (Lane, 1992; reviewed in Deisenroth & Zhang, 2010) - and also causes G2 cell cycle arrest via ATM/ATR signaling (reviewed in Jackson & Bartek, 2009). In support to a Pol I specific function, the ratio of active to inactive rDNA repeats appears to modulate cytotoxic responses (Son et al., 2020). These observations make CX-5461 attractive for use in combination therapies, including ATR kinase inhibitors (Negi & Brown, 2015) or topoisomerase I inhibitors (Yan et al., 2021). Beyond preclinical efficacy in mouse models of small cell lung cancer,

ovarian cancer, and neuroblastoma (Cornelison et al., 2017; Kim et al., 2016; Taylor, 2019), CX-5461 is undergoing clinical trials for advanced cancers with *BRCA1/2* aberrations or homologous recombination deficiencies (Canadian Cancer Trials Group, 2022).

Although several studies (Mars et al., 2020; Tan & Awuah, 2019; reviewed in Drygin et al., 2011) are in support of a Pol I-specific mechanism for CX-5461 - e.g. by inhibiting SL1-recruitment to the rDNA promoter - there is increasing evidence that its cytotoxicity involves additional targets. Thus, other studies demonstrate that CX-5461 can stabilize G-quadruplex structures, thereby exacerbating replication stress (Xu et al., 2017), and act as a topoisomerase II poison (Bruno et al., 2020). A study of our working group could confirm that CX-5461's effects on growth of yeast cells are not mainly due to specific Pol I inhibition (Nagler, 2022), underscoring a multifaceted mode of action for this compound.

3.4.2 The small molecule inhibitor BMH-21

BMH-21 is a small molecule belonging to the pyridoquinazolinecarboxamides class originally identified in a screen for p53 pathway activation in a human cancer cell line devised to identify hits with potent antitumor activity and was subsequently described as a Pol I specific inhibitor (Peltonen et al., 2010, 2014). It achieves this inhibition by intercalating into GC-rich DNA, making ribosomal DNA (rDNA) a prime target due to its high GC content, or because of the increased DNA-accessibility of the open rDNA chromatin state. Such intercalation stalls transcribing Pol I and triggers degradation of its largest subunit, thereby compromising transcription initiation, promoter escape, and elongation in human and yeast cells (Jacobs, Huffines, Laiho, et al., 2021; Wei et al., 2018). Thus, there is strong evidence that BMH-21's Pol I-targeting mechanism may be conserved in diverse species.

Beyond its effects on Pol I transcription, BMH-21 also interacts with G4 quadruplex structures for example at the c-MYC promoter, correlating with down-regulation of c-MYC in cancer cells. It was shown, however, that BMH-21 does not stabilize these G-quadruplexes in certain assays (Musso et al., 2018). Preclinical studies further demonstrate its antitumor activity in prostate cancer cell lines, enzalutamide-resistant xenografts, and an aggressive mouse tumor model (Low et al., 2019), as well as in *SKOV3* ovarian cancer cells, where it triggers nucleolar stress-induced apoptosis (Fu et al., 2017). Despite these promising findings, BMH-21 has yet to advance into clinical trials involving patients.

3.5 Objectives

The primary research objectives of this thesis focus on elucidating the mode of action of CX-5461 and BMH-21 on Pol I in yeast. Building on a previous study by Christoph Nagler - which yielded key findings regarding the role of Hmo1 in BMH-21 treated cells - this work shall extend our understanding of how these inhibitors affect cellular processes.

Firstly, growth experiments will be carried out using genetically modified yeast strains. These include strains which do not depend on Pol I transcription to synthesize rRNA to assess the impact of the inhibitors when Pol I is no longer essential for cell survival, as well as strains with altered Hmo1 levels to investigate how variations in this critical factor influence the response to CX-5461 and BMH-21 treatment.

Secondly, protein analysis will be employed to examine the effects of these drugs on the degradation of Rpa190, the largest subunit of Pol I, in the context of varying Hmo1 levels. This approach is designed to provide mechanistical insights into how Hmo1 levels may influence Pol I stability in the presence of the small molecule inhibitors.

Finally, the molecular effects of the treatments will be investigated using Chromatin Endogenous Cleavage (ChEC) and ChEC-psoralen crosslinking experiments in strains expressing a Pol I enzyme in which micrococcus nuclease is C-terminally fused to the largest subunit Rpa190. These techniques offer the possibility to examine the effects of CX-5461 and BMH-21 on Pol I association with the rDNA gene as well as on rDNA gene chromatin structure.

In summary, these comprehensive experiments aim to unravel the intricate details of how CX-5461 and BMH-21 exert their effects on Pol I in yeast, shedding light on potential therapeutic implications and deepening our understanding of the molecular processes involved.

4. Materials

4.1 Chemicals, buffers and media

Table 1: Chemicals and solutions used in this work. Solutions are in water if not indicated otherwise

Chemical/Solution	Manufacturer	Item number
ROTIPHORESE®NF-Acrylamide/Bis-solution 30 (29:1)	Carl Roth GmbH & Co. KG	A124.2
Ammonia vapor (from ammonia hydroxide solution)	Carl Roth GmbH & Co. KG	CP17.1
10% ammonium persulfate	Carl Roth GmbH & Co. KG	9592.2
BMH-21	Hölzel Biotech	HY-12484-50mg
100 mM CaCl2	Sigma-Aldrich	1.02378
CX-5461 (-dihydrochloride)	Hölzel Biotech	HY-13323A-10mg
DMSO	Carl Roth GmbH & Co. KG	A994.2
10 mM dNTP mix	New England Biolabs	NO447S
0.1 M DTT	Sigma-Aldrich	D9779-10G
100% Ethanol	Carl Roth GmbH & Co. KG	9065.1
37% Formaldehyde	Sigma-Aldrich	F1635-500ml
G 418 (Geneticin)	Gibco (Life Technologies)	10131019
Glassbeads (Ø 0.75–1 µm)	BiospecProducts	11079105
Glycine	Serva	23391.03
100% Isopropanol	Carl Roth GmbH & Co. KG	9781.2
1% and 5% milk-powder solution (w/v) in PBS-T	Sufocin GmbH	N/A
NaH_2PO_4	Carl Roth GmbH & Co. KG	T879.2
NH_4Ac	Carl Roth GmbH & Co. KG	7869.1
PCI (phenol/chloroform/isoamyl alcohol)	Carl Roth GmbH & Co. KG	A156.2
1 kb Plus DNA-Leiter	New England Biolabs	N3200S
TCA (trichloroacetic acid)	Merck	T6399-500G
TMP (trimethylpsoralen) (0.2 mg/ml) in ethanol	Thermo Scientific	29986
SDS (sodium dodecyl sulfate)	Serva	2076503
SS salmon sperm DNA (10 mg/ml)	Invitrogen	15632-011
SYBR-Green	Invitrogen	S-7564
SYBR-Safe	Invitrogen	S33102
TEMED (tetra methyl ethylene diamide)	Carl Roth GmbH & Co. KG	2367.1
Tween 20	Carl Roth GmbH & Co. KG	9127.2
UltraPure Agarose	Life technologies	16500500

Table 2: Buffers and solutions used in this work

Buffer	Composition
100x Protease-Inhibitor (PIs)	33 mg/ml Benzamidine 17 mg/ml PMSF 137 µg/ml Pepstatin A 28.4 µg/ml Leupeptin 200 µl/ml Chymostatin
10x DNA loading dye	0.25% bromophenol blue 0.25% xylene cyanol 40% glycerol
10x SDS gel running buffer	250 mM Tris 2 M Glycine 1% SDS (w/v)
1x PBS	137 mM NaCl 2.7 mM KCl 10 mM Na2HPO4 2 mM KH2PO4
1x SDS gel running buffer	1/10 dilution 10× SDS gel running buffer
1x TBE	90mM Tris 90mM boric acid 1mM EDTA
20x SSC	3 M NaCl 0.3 M tri-sodium citrate dihydrate Adjust pH 7 with HCl
4x Lower Tris	1.5 M Tris-HCl pH 8.8 0.1% SDS (w/v)
4x SDS sample buffer	250 mM Tris pH 6.8 40% Glycerol 8.4% SDS (w/v) 0.04% β-Mercaptoethanol (v/v) Bromophenol blue (spatula tip)
4x Upper Tris	500 mM Tris-HCl pH 8.8 0.1% SDS (w/v)
6x DNA loading dye	15% Ficoll®-400 60 mM EDTA 19.8 mM Tris-HCl 0.48% SDS 0.12% Dye1 0.006% Dye2
AE	50mM NaAc pH5.3 10mM EDTA
Buffer A + PIs	15 mM Tris-HCl pH 7.4 80 mM KCl 4 mM EDTA 0.5 mM Spermidine 0.2 mM Spermine 1× Protease-Inhibitor (PIs)
Buffer Ag + PIs	15 mM Tris-HCl pH 7.4 80 mM KCl 0.1 mM EGTA 0.5 mM Spermidine 0.2 mM Spermine 1× Protease-Inhibitor (PIs)
Denaturing solution	1.5 M NaCl 0.5 M NaOH

HU buffer	5% SDS (w/v) 200 mM Tris pH 6.8 1 mM EDTA 1.5% β-Mercaptoethanol (v/v) 8 M urea Bromophenol blue (spatula tip)
Hybridization buffer	0.5 M Na-Pi pH 7.2 7% SDS (w/v)
IRN	50 mM Tris-HCl pH8 20 mM EDTA 0.5 M NaCl
0.5 M Na-Pi pH7.2	22.6% 1 M NaH2PO4 · $2H_2O$ (v/v) 77.4% 1 M Na2HPO4 · H_2O (v/v) Adjust pH with acidic buffer
3 M NaAc pH 5.3	41.024% NaAc · $3H_2O$ (w/v) Adjust pH with glacial acetic acid
Ponceau solution	0.5% Ponceau-S (w/v) 1% glacial acetic acid
Pretreatment solution	7.5% β-Mercaptoethanol 1.85 M NaOH
qPCR MM mix	10× PCR-buffer (Qiagen) 25 mM MgCl2 25 mM dNTP's Bidest. H_2O
Rinse buffer	3× SSC 0.1% SDS (w/v)
Stripping buffer	0.1× SSPE 0.5% SDS (w/v)
TE	10 mM Tris-HCl pH8 1 mM EDTA pH8
TE_{RNase}	10 mM Tris-HCl pH8 1 mM EDTA pH8 0.05 mg/ml RNase
Wash buffer I	0.3× SSC 0.1% SDS (w/v)
Wash buffer II	0.1× SSC 0.1% SDS (w/v)
Wash buffer III	0.1× SSC 1.5% SDS (w/v)
Western transfer buffer	20% Methanol 40 mM Glycine 50 mM Tris 0.037% SDS

Table 3: List of media used in this work

Medium	Composition
SCD	0.675% Yeast nitrogen base without amino acids (w/v) 0.063% CSM -His -Leu -Ura 2% of 50× Histidine stock-solution (v/v) 2% of 50× Leucine stock-solution (v/v) 2% of 50× Uracil stock-solution (v/v)
SCD-Ura	0.675% Yeast nitrogen base without amino acids (w/v) 0.063% CSM -His -Leu -Ura 2% of 50× Histidine stock-solution (v/v) 2% of 50× Leucin stock-solution (v/v)

YPAD	1% Bacto Yeast Extract (w/v) 2% Bacto Peptone (w/v) 2% Glucose (w/v) 0.004% Adenine-thiosulfate (w/v)
YPAD-Geneticin	1% Bacto Yeast Extract (w/v) 2% Bacto Peptone (w/v) 2% Glucose (w/v) 0.004% Adenine-hemisulfate (w/v) 250 µg/ml Geneticin

For agar plates, 2% (w/v) agar was added to the medium prior to autoclaving.

4.2 Yeast strains used during this work

Table 4: Yeast strains used in this work

Database	Name	Parent	Used in section	Genotype
Y207	BY4742		6.1.1	MATa; his31; leu20; lys20; ura30
Y348	NOY505		6.1.1, 6.1.2, 6.1.3	ade2-1 ura3-1 his3-11 trp1-1 ; leu2-3,112 can1-100
Y352	NOY1064		6.1.1, 6.1.2	MATa; ade2-1; ura3-1; trp1-1; leu2-3,112; his3-11; can1-100; fob1::HIS3; RDN: ~190 copies
Y353	NOY1071		6.1.1, 6.1.2	MATa; ade2-1; ura3-1; trp1-1; leu2-3,112; his3-11; can1-100; fob1::HIS3; RDN: ~25 copies
Y624	YKM08		6.1.2, 6.2.2	MATa; ade2-1; ura3-1; trp1-1; leu2-3,112; his3-11; can1-100; RPA190_MNase_3xHA_KAN_MX6; ;
Y640	YKM24	YKM1	6.2.1	MATa; ade2-1; ura3-1; trp1-1; leu2-3,112; his3-11; can1-100; rdn::HIS3; RPA190_MNase_3xHA_KAN_MX6; pKM6 [2µ, RDN(RS_LEXA_35S_RS), URA3]
Y1117	yR44	348	6.1.2	MATa; ade2-1; ura3-1; trp1-1; leu2-3,112; his3-11; can1-100; hmo1::TRP_KL;
Y1332	yR69	YKM08 (624)	6.2.2	MATa; ade2-1; ura3-1; trp1-1; leu2-3,112; his3-11; can1-100; hmo1::URA3_KL; RPA190_MNase_3xHA_KAN_MX6;
Y1587	ySH7	NOY505	6.2.1	MATa; ade2-1; ura3-1; trp1-1; leu2-3,112; his3-11; can1-100; RPA190_3xHA_KanMX6
Y1743	YR115		6.1.1, 6.1.2	MATa; ade2-1; ura3-1; trp1-1; leu2-3,112; his3-11; can1-100; rdn::URA3; pNOY373 [2µ, RDN, LEU2]
Y2441	NOY891_pNOY373	NOY891	6.1.1, 6.1.2	MATa; ade2-1; ura3-1; trp1-1; leu2-3,112; his3-11; can1-100; rdn-::HIS3; pNOY373 [2µ, RDN, LEU2]
Y4256	yCS58		6.1.1, 6.1.2	MATa, ade2-1; ura3-1; trp1-1; leu2-3,112; his3-11; can1-100; rdn::HIS3; K2708 [2µ, TEF1-35S rDNA, 5S rDNA,LEU2]
Y4412	4256_2808	4256	6.1.1, 6.1.2	MATa, ade2-1; ura3-1; trp1-1; leu2-3,112; his3-11; can1-100; rdn::HIS3; rpa135::TRP1 K.l; K2708 [2µ, TEF1-35S rDNA, 5S rDNA,LEU2]
Y4449	4183_RPA190-MN_1	4183	6.1.2, 6.2.3, 6.3.1, 9.	MATa his3Δ1 leu2Δ0 met15Δ0 ura3Δ0 RAD52-GFP-HIS3; RPA190-MN::pTEF-URA3

Y4499	yCS158	yCS58	6.2.2	MATa, ade2-1; ura3-1; trp1-1; leu2-3,112; his3-11;can1-100; rdn::HIS3; RPA190-Mnase:KANMX6; K2708 [TEF1-35S rDNA, 5S rDNA,LEU2]
Y4500	yCS159	yCS58	6.2.1	MATa, ade2-1; ura3-1; trp1-1; leu2-3,112; his3-11; can1-100; rdn::HIS3; RPA190-Mnase:KANMX6; K2708 [TEF1-35S rDNA, 5S rDNA,LEU2]
Y4695	4183-2968_1	4183	9.	MATa his3Δ1 leu2Δ0 met15Δ0 ura3Δ0 RAD52-GFP-HIS3; RPA43-MN-3xHA:URA3kl
Y4762	348_2971_1	348	6.1.2	MATa; ade2-1; trp1-1; leu2-3,112; his3-11; can1-100; ura3-1::pTEF2-HMO1_URA3Kl

4.3 Yeast strains generated during this work

Table 5: Yeast strains generated during this work

Database	Name	Parent	Plasmid used for construction	Used in section	Genotype
Y4979	4708_2850_1	4708	K2850	9.	MATa his3Δ1 leu2Δ0 met15Δ0 ura3Δ0 RAD52-GFP-HIS3; hmo1Δ::URA3Kl; RPA43-MN-3xHA::KANMX6
Y4980	4708_2850_2	4708	K2850		MATa his3Δ1 leu2Δ0 met15Δ0 ura3Δ0 RAD52-GFP-HIS4; hmo1Δ::URA3Kl; RPA43-MN-3xHA::KANMX6
Y4981	4714_2850_1	4714	K2850	9.	MATa his3Δ1 leu2Δ0 met15Δ0 ura3Δ0 RAD52-GFP-HIS3; ura3Δ0::pTEF2-HMO1_URA3Kl; RPA43-MN-3xHA::KANMX6
Y4982	4714_2850_2	4714	K2850		MATa his3Δ1 leu2Δ0 met15Δ0 ura3Δ0 RAD52-GFP-HIS3; ura3Δ0::pTEF2-HMO1_URA3Kl; RPA43-MN-3xHA::KANMX6
Y4983	4762_2850_1	4762	K2850		MATa; ade2-1; ura3-1; trp1-1; leu2-3,112; his3-11; can1-100; ura3Δ0::pTEF2-HMO1_URA3Kl; RPA43-MN-3xHA::KANMX6
Y4984	4762_2850_2	4762	K2850		MATa; ade2-1; ura3-1; trp1-1; leu2-3,112; his3-11; can1-100; ura3Δ0::pTEF2-HMO1_URA3Kl; RPA43-MN-3xHA::KANMX6
Y4985	4708_2851_1	4708	K2851	6.1.2, 6.3.1	MATa his3Δ1 leu2Δ0 met15Δ0 ura3Δ0 RAD52-GFP-HIS3; hmo1Δ::URA3Kl; RPA190-MN-3xHA::KANMX6
Y4986	4708_2851_2	4708	K2851	6.2.3	MATa his3Δ1 leu2Δ0 met15Δ0 ura3Δ0 RAD52-GFP-HIS4; hmo1Δ::URA3Kl; RPA190-MN-3xHA::KANMX6
Y4987	4714_2851_1	4714	K2851	6.1.2, 6.3.1	MATa his3Δ1 leu2Δ0 met15Δ0 ura3Δ0 RAD52-GFP-HIS3; ura3Δ0::pTEF2-HMO1_URA3Kl; RPA190-MN-3xHA::KANMX6
Y4988	4714_2851_2	4714	K2851	6.2.3	MATa his3Δ1 leu2Δ0 met15Δ0 ura3Δ0 RAD52-GFP-HIS3; ura3Δ0::pTEF2-HMO1_URA3Kl; RPA190-MN-3xHA::KANMX6

Y4989	4762_2851_1	4762	K2851		MATa; ade2-1; ura3-1; trp1-1; leu2-3,112; his3-11; can1-100; ura3Δ0::pTEF2-HMO1_URA3Kl; RPA190-MN-3xHA::KANMX6
Y4990	4762_2851_2	4762	K2851		MATa; ade2-1; ura3-1; trp1-1; leu2-3,112; his3-11; can1-100; ura3Δ0::pTEF2-HMO1_URA3Kl; RPA190-MN-3xHA::KANMX6
Y4991	348_2969_1	348	K2969		MATa; ade2-1; ura3-1; trp1-1; leu2-3,112; his3-11; can1-100; hmo1::URA3_KL
Y4992	348_2969_2	348	K2969		MATa; ade2-1; ura3-1; trp1-1; leu2-3,112; his3-11; can1-100; hmo1::URA3_KL
Y5054	2441_2969_1	2441	K2969		MATa ade2-1 ura3-1 his3-11 trp1-1 leu2-3,112 can1-100 rdnΔΔ::HIS3; hmo1::URA3_KL; #190 pNOY373 (35S rDNA, 5S rDNA, LEU2, 2µ, amp)
Y5055	2441_2969_2	2441	K2969	6.1.2	MATa ade2-1 ura3-1 his3-11 trp1-1 leu2-3,112 can1-100 rdnΔΔ::HIS3; hmo1::URA3_KL; #190 pNOY373 (35S rDNA, 5S rDNA, LEU2, 2µ, amp)
Y5056	4256_2969_1	4256	K2969		MATa ade2-1 ura3-1 trp1-1 leu2-3,112 his3-11 can1-100 rdnΔΔ::HIS3; hmo1::URA3_KL; K2708 [TEF1-35S rDNA, 5S rDNA, 2µ, LEU2]
Y5057	4256_2969_2	4256	K2969	6.1.2	MATa ade2-1 ura3-1 trp1-1 leu2-3,112 his3-11 can1-100 rdnΔΔ::HIS3; hmo1::URA3_KL; K2708 [TEF1-35S rDNA, 5S rDNA, 2µ, LEU2]

4.4 Southern probes

Table 6: List of Southern probes used in this work

Probe	Name	Usage	Gene locus
#5	XcmI_prom	For indirect endlabeling at XcmI site in direction of the rDNA promoter	rDNA
#34	RDN_NcoI_3.5kb	For detection of 18S rDNA and 25 rDNA fragments obtained after EcoRI restriction digestion	rDNA

4.5 Enzymes

Table 7: List of enzymes and related buffers used in this work

Enzyme	Manufacturer
5X Green GoTaq® Reaction Buffer	Promega
CutSmart Buffer	New England Biolabs (NEB)
Go-Taq Polymerase	Promega
Proteinase K (20 mg/ml)	Sigma-Aldrich
Restriction Enzymes: EcoRI, SacII, XcmI, XhoI	New England Biolabs (NEB)
RNAse A (20 mg/ml)	Invitrogen
Zymolyase T100	Seikagaku Corporation

4.6 Kits

Table 8: List of kits used in this work

Kit	Manufacturer
BCABest Labeling Kit	Takara Bio
BM Chemiluminescence Western Blotting Kit	Roche
SuperSignal™ West Femto kit	Thermo Fischer

4.6 Antibodies

Table 9: List of antibodies used in this work

Database	Epitope	Manufacturer	Species	Dilution for western Blot
#68	S8	Roche	Rabbit	1:3.000
#75	HA (3F10)	Roche	Rat	1:1.000
#78	Rabbit IgG (H+L)-Peroxidase	Dianova	Goat	1:5.000
#79	Mouse IgG (H+L)-Peroxidase	Dianova	Goat	1:10.000
#81	Rat IgG-Peroxidase	DIanova	Goat	1:2.500

4.7 Primers

Table 10: List of primers used in this work

Database	Sequence	Gene	Purpose
O1543	TCGTTCCCAAGCTGAAAGTT	RPA43	Genotyping
O1947	GCGGCCATCAAAATGTATGGATGCA	MED20	Genotyping
O4277	TGCTGCTGTGTTGAAAACGT	RPA190	Genotyping
O4697	CGCTAGCCCACGTCCATATT	MN	Genotyping
O4930	ATCCAAGAGCACAAGGGAGC	ARG82	Genotyping

4.8 Plasmids

Table 11: List of plasmids used in this work

Database	Name	Description
K2850	pBS_RPA43-MN_long	vector for homologous recombination at the RPA43 gene locus carrying around 100-400bp of homologous sequence to the 3'CDS and 3'UTR of RPA43 at the 5' & 3' end of a KpnI/SacII-fragment, respectively -> replaces the endogenous RPA43 locus by a RPA43-MN-3xHA_KANMX6 expression cassette
K2851	pBS_RPA190-MN_long	Vector for homologous recombination at the RPA190 gene locus carrying around 100-400bp of homologous sequence to the 3'CDS and 3'UTR of RPA190 at the 5' & 3' end of a KpnI/SacII-fragment, respectively -> replaces the endogenous RPA190 locus by a RPA190-MN-3xHA_KANMX6 expression cassette
K2969	pBS_hmo1::ura3kl	Plasmid for deletion of the HMO1 CDS. Contains >200bp of 5' and 3' IGS of HMO1 flanking a pTEF:URA3kl cassette

4.9 Devices, equipment and software

Table 12: Devices and Equipment used in this work

Equipment	Manufacturer
Autoclaves LTA32/25, HST32/25, LVSA50/70	Zirbus Apparate- und Maschinenbau GmbH
Balances	Sartorius/Kern
Biospectrophotometer basic	Eppendorf
C1000 Touch	Bio-Rad
Digital pH-meter FiveEasyTM	Mettler Toledo
DNA cross-linking system Fluo-Link tFL20.M	Vilber Lourmat
Electrophoresis System Model 45-2010-i	Peqlab
Erlenmeyer flasks	Schott/VWR
Gel Max UV transilluminator	Intas
Gel-doc. system	Intas
Hand-Fuss-Monitor	Berthold
Hybridization oven	Grant Boeckel
Hybridization oven	Peqlab
Hybridization tube	Bachofer, Rettberg
Ice Machine	Ziegra
Incubator	Memmert
LAS-3000 Chemiluminescence Imager	Fujifilm
Magnetic stirrer	Heidolph
Millipore water system (ELGA)	Purelab
PierceG2 Fast Blotter	BioRad
Pipettes	Gilson
Polymax 2040	Heidolph
Rotor-Shake Genie	Scientific Industries, Inc.

Safe-Imager	Invitrogen
Shake incubators Multitron/Minitron	Infors
Sub-Cell GT	BioRad
Thermomixer compact	Eppendorf
Typhoon FLA-9500 Imager	Fujifilm
VIBRAX VXR basic	IKA

Table 13: Centrifuges used in this work

Equipment	Rotor	Manufacturer	Rotor identificaiton number
Biofuge Fresco refrigerated tab-letop centrifuge	Standard (24x1.5/2.0 ml)	Heraeus	#1
Biofuge Pico tabletop centrifuge	Standard (24x1.5/2.0 ml)	Heraeus	#2
CR4i centrifuge [M4 High Throughput Swing-Out]	M4 (4x 750 ml)	Jouan	#3
Eppendorf 5430R refrigerated tabletop centrifuge	FA-45-48-11 (48 × 1.5/2.0 ml)	Eppendorf	#4

Table 14: Software used for editing and analysis

Software	Developer
Adobe Acrobat DC	Adobe
ChatGPT	OpenAI
GelDoc	Intas
Image Reader FLA-3000	Fujifilm
Image Reader LAS-3000	Fujifilm
ImageJ	FIJI
Microsoft Excel	Microsoft
Microsoft PowerPoint	Microsoft
Microsoft Word	Microsoft
MultiGauge v.3.0	Fujifilm
Rotor-Gene 6000 Series Software 1.7	Corbett Research
SnapGene Viewer	SnapGene

5. Methods

5.1 Working with *Saccharomyces cerevisiae*

All chemicals, media, flasks, and other materials used for cultivation of yeast cells were handled under sterile conditions. For monitoring cell amounts, we used OD600. This parameter measures the optical density at 600 nm, providing an indirect estimate of yeast cell density. As the culture grows, increased cell numbers lead to greater light scattering and higher OD600 values. An OD600 of 1 generally corresponds to roughly 1-3x10^7 cells per ml.

5.1.1 Preparation of competent yeast cells

Yeast cells were prepared for competence following a systematic protocol. Initially, a preculture was set up by inoculating 5 ml of YPAD medium with yeast cells and incubating overnight at 30°C with shaking at 180 rpm. This preculture was then used to inoculate a 50 ml main culture of YPAD medium, adjusting the starting OD600 to 0.1. The main culture was grown until an OD600 of approximately 0.6-0.8 was reached, after which the cells were harvested by centrifugation at 4,000 rpm (rotor #3) for 10 minutes at room temperature. The cell pellet was washed with 10 ml of sterile water, followed by a second centrifugation at 4,000 rpm (rotor #3) for 5 minutes at room temperature, and then washed again using 2.5 ml of SORB buffer. After sedimentation, the cells were resuspended in 750 µl of SORB and transferred to a 1.5 ml reaction tube. A subsequent centrifugation at 13,000 rpm for 1 minute at room temperature (rotor #1) concentrated the cells further, and the supernatant was discarded. The cells were then resuspended in 540 µl of SORB, and 60 µl of Salmon-Sperm DNA was added to facilitate transformation. Finally, the competent yeast cells were stored at -80°C until further use.

5.1.2 Transformation of competent yeast cells via homologue recombination

For the transformation, 2.5 µg of digested plasmid DNA was added to 50 µl of competent yeast cell suspension. Subsequently, six volumes of polyethylene glycol (PEG) were incorporated into the mixture, which was then thoroughly mixed and incubated for 30 minutes at room temperature. Following this, sterile DMSO - amounting to 1/9 of the total volume - was added,

and the cells were subjected to a heat shock at 42°C for 15 minutes. The cells were then pelleted by centrifugation at 2,000 rpm (rotor #1) for 2 minutes at room temperature and resuspended in 200 µl of selective media and subsequently plated to selective media for auxotrophic markers or 3 ml of YPAD for resistance markers. This suspension was incubated for 3 hours at 30°C with shaking at 800 rpm to allow the expression of the resistant markers. After another round of centrifugation, the cells were resuspended in 100 µl of selective media and plated on selective media. Finally, to confirm the stability of the transformants, the resulting colonies were replicated onto fresh selective media. Further, genomic DNA of the transformants was analyzed as described in 5.1.3 and 5.1.4.

5.1.3 Preparation of genomic yeast DNA

An overnight yeast culture (1 ml) was first sedimented by centrifugation at 12.7 k rpm for 1 min at room temperature (rotor #1), followed by a wash with 500 µl H_2O and a subsequent re-centrifugation to discard the supernatant. The resulting pellet was then resuspended in 500 µl of a solution containing 1 M Sorbitol/0.1 M EDTA and 2 µl Zymolyase T100 and incubated for 30 min at 37°C with shaking in a thermoshaker to generate spheroplasts. After centrifugation at 5k rpm for 2 min at room temperature (rotor #1) to collect the spheroplasts, the supernatant was discarded. The pellet was subsequently resuspended in 417 µl IR buffer supplemented with 83 µl of 10% SDS and incubated under vigorous shaking for 15 min at 65°C to achieve cell lysis. Following lysis, 200 µl of 5 M KOAc was added, and the precipitate was sedimented by centrifugation at 12.7 k rpm for 20 min at 4°C (rotor #4). The supernatant was then transferred into a new 1.5 ml tube containing 500 µl isopropanol to precipitate the genomic DNA. After a 5 min incubation at room temperature, the sample was centrifuged at 12.7 k rpm for 5 min (rotor #4). The DNA pellet was washed with 150 µl of 70% ethanol and centrifuged again at 12.7 k rpm for 2 min at room temperature (rotor #4), after which the supernatant was discarded, and the pellet was allowed to air-dry. Finally, the dried pellet was resuspended in 50 µl of TE buffer containing RNase (0.05 mg/ml) and incubated with shaking for 30 min at 37°C to ensure complete dissolution. The extracted genomic DNA was subsequently analyzed by PCR and agarose gel electrophoresis.

5.1.4 Polymerase Chain Reaction (PCR)

All reaction components were assembled on ice, with thorough mixing and a brief centrifugation performed prior to use. A mastermix was prepared on ice according to the specifications outlined in Table 15 and then transferred into PCR reaction tubes.

Table 15: Composition of GO TAQ PCR reaction mix

Reagent	Volume
5x PCR buffer	6 µl
40 mM dNTPs	0.6 µl
GO TAQ Polymerase	0.15 µl
10 mM forward-primer	0.6 µl
10 mM reverse-primer	0.6 µl
Template	1 µl
H_2O	22.25 µl
Total volume	30 µl

The amplification program was subsequently executed following the protocol described in Table 16.

Table 16: PCR cycling program used for GO TAQ PCR reactions

PCR reaction step	Time	Temperature
1	180s	95°C
2	10s	95°C
3	20s	54°C
4	Primer dependent	72°C
5	Go to 2	x34
6	420s	72°C

The PCR product was analyzed by AGE or used for further experiments.

5.1.3 Cultivation of cells for BMH-21 or CX-5461 treatment

Overnight cultures were prepared by inoculating yeast cells from backup plates into YPAD medium and incubating them at 30°C with gentle shaking until they reached stationary phase. After measuring the cell concentration, a main culture was inoculated at an initial OD600 of 0.2 and cultivated at 30°C until the OD600 reached approximately 0.5.

If cells were treated with BMH-21, it was either added directly to the culture at the required concentration for each experiment or introduced into fresh YPAD medium prior to transferring

the desired volume of cell culture, ensuring the correct cell density. For subsequent protein or DNA analyses, 10 ml samples were collected at various time points and centrifuged at 4°C (rotor #3) for 10 minutes. The resulting pellet was resuspended in 500 µl of sterile H_2O, transferred to a 1.5 ml tube, and centrifuged again for 1 minute at maximum speed (rotor #1). Finally, the cell pellet was snap-frozen in liquid nitrogen and stored at -80°C until protein or DNA extraction.

If cells were treated with CX-5461, the overnight cultures were first pelleted, washed with sterile H_2O, and then resuspended in selective medium to achieve the desired cell density. CX-5461 was then subsequently added at the appropriate concentration in each experiment.

5.1.4 Growth analysis in a TECAN plate reader

For growth analysis in liquid media, cells were first grown to stationary phase overnight. OD600 of each culture was measured. Cells were diluted to an OD600 of 0.05 in water and a 20 µl aliquot of this suspension was transferred into a well of a 96-well plate containing 200 µl of YPAD or complete selective medium supplemented with the desired concentration of BMH-21 or CX-5461, respectively. The 96-well plates were then transferred into a TECAN infinite500 reader, which measured cell density (at an optical density of 612 nm) over a two- to four-day period. The collected data were documented and analyzed using Microsoft Excel, allowing for a detailed assessment of growth dynamics under the given treatment conditions.

Table 17: TECAN measuring parameters

Parameter	Value
Target Temperature	30 °C (Valid Range: 29.5 - 30.5 °C)
Kinetic Cycles	600
Shaking (Orbital) Duration	60 s
Shaking (Orbital) Amplitude	5 mm
Wait (Time)	00:00:30
Interval Time	00:15:00
Mode	Absorbance
Multiple Reads per Well (Circle (filles))	4x4
Multiple Reads per Well (Border)	450 µm
Wavelength	612 nm
Bandwidth	10 nm
Number of Flashed	10
Settle Time	10 ms

5.2 Protein analysis

5.2.1 Denaturing protein extraction

For the protein extraction, 3 OD600 units of yeast cells were harvested (rotor #3) and resuspended in 1 ml of cold, deionized water. 150 µl of pretreatment solution was added, followed by a 15-minute incubation on ice to prepare the proteins for subsequent precipitation. Next, 150 µl of 55% TCA was introduced and after thorough mixing, and the samples were returned to ice for an additional 10 minutes. The protein pellet was isolated by centrifugation at 12.7 k rpm for 20 min at 4°C (rotor #1), after which the supernatant was discarded, and the pellet resuspended in 100 µl of HU buffer. If the solution exhibited a yellow hue - indicating increased acidity - ammonia vapor was used to neutralize the sample. Finally, the proteins were solubilized by heating at 65°C for 10 minutes, followed by a brief high-speed centrifugation at room temperature (rotor #1) to remove any residual debris. The resulting extracts were either stored at -20°C or immediately subjected to SDS-PAGE and Western blot analysis.

5.2.2 SDS-Page

Proteins extracted and denatured in HU buffer were separated by molecular weight using a 10% SDS-polyacrylamide gel. First, the gel solution was prepared and poured into a suitable mold (Table 18), either specialized plastic forms or two glass plates separated by plastic spacers. The separating gel was cast and topped with isopropanol to create a smooth interface and ensure uniform polymerization. Once the isopropanol was removed, the stacking gel containing the sample wells was layered on top and allowed to polymerize fully (Table 18). The gel assembly was then placed in the electrophoresis apparatus, filled with 1x SDS running buffer, and 20 µl of each protein sample in HU buffer was loaded alongside a colored protein standard to serve as a molecular weight marker. An initial voltage of 80-120 V was applied until the samples reached the interface between the stacking and separating gels, at which point the voltage was increased to 130-170 V to optimize resolution. Electrophoresis concluded once the bromophenol blue tracking dye approached the gel's lower edge. Finally, the apparatus was disassembled, and the gel was placed into a blotting setup so the separated proteins could be transferred onto a nitrocellulose membrane for further analysis.

Table 18: Composition of polyacrylamide gels

Component	Separating gel (10%)	Stacking gel (10%)
AA (Acrylamide/Bisacrylamide)	6.16 ml	1.01 ml
H_2O	7.45 ml	4.05 ml
Lower Tris	4.54 ml	-
Upper Tris	-	1.01 ml
SDS	183.1 µl	81 µl
APS	178.2 µl	178.2 µl
TEMED	6.2 µl	4.1 µl

5.2.3 Western blotting

After the SDS-PAGE separation, proteins were immediately transferred onto a nitrocellulose membrane through a semi-dry blotting process. The membrane was first equilibrated by dipping it briefly in water, followed by transfer buffer, which equilibrates the membrane and ensure consistent protein binding. It was then placed on top of three layers of transfer buffer-soaked Whatman paper laid on the anode plate, while the SDS gel was carefully positioned against the membrane. Three additional layers of soaked Whatman paper were placed over the gel, and the cathode plate was attached, forming a “blotting sandwich” (Fig. 4). The transfer was carried out at 25 V with a 1 A limit for 60 minutes, allowing proteins to migrate out of the gel and bind to the nitrocellulose surface. Afterward, the membrane was stained with ponceau red to verify that the proteins had successfully transferred.

Subsequently, the membrane was placed in a PBS-T containing 5% (w/v) milk powder, blocking the membrane to prevent nonspecific antibody binding and minimizing background signals. This incubation took place for either one hour at room temperature or overnight at 4°C.

Figure 4: Schematic picture of western blot semi-dry blotting sandwich
This schematic shows the layered setup used to transfer proteins from the polyacrylamide gel onto a nitrocellulose (NC) membrane. From bottom to top: three layers of Whatman filter paper, the NC membrane, the gel, and another three layers of Whatman filter paper. Under an electric field, proteins migrate from the gel onto the membrane for subsequent detection.

The membrane was then exposed to a primary antibody specific for the target protein, diluted in a 1% (w/v) milk powder-PBS-T solution. Following thorough washing with PBS-T, a secondary antibody conjugated to an enzyme that enables chemiluminescent detection was applied for 45 minutes, followed by three additional washes to remove any unbound reagent. Finally, the membrane was briefly rinsed once more before a chemiluminescent substrate was added, causing the bound secondary antibody to emit light detectable by an imaging system. Detection was typically carried out using the BM chemiluminescence kit from Roche in conjunction with the Bio-Rad ChemiDoc system. In instances where the signal was faint or undetectable, the more sensitive SuperSignal™ West Femto kit from Thermo Scientific was used instead.

5.3 DNA analysis

5.3.1 Formaldehyde fixation of yeast cells

Yeast strains expressing an MNase fusion protein were cultured to the exponential phase, and 50 ml of cell culture at an OD600 of approximately 0.5 was transferred into a 50 ml Falcon tube. For formaldehyde fixation, 1.35 ml of 37% formaldehyde was added, and the culture was incubated for 15 min at 30°C under continuous shaking. The fixation reaction was then

quenched by adding 2.5 ml of 2.5 M glycine, followed by an additional 5 min of shaking at 30°C. After quenching, cells were harvested by centrifugation at 4000 rpm for 8 min at 4°C (rotor #3). The cell pellet was resuspended in 500 µl of H_2O, transferred to a 1.5 ml tube, and centrifuged at full speed at room temperature (rotor #1). Finally, the pellet was flash-frozen in liquid nitrogen and stored at -80°C until further processing.

5.3.2 Preparation of crude nuclei

All procedures were carried out on ice or at 4°C in a cold room. Starting with cell pellets obtained from the cultivation and fixation process (as described in 5.3.1), the pellet was resuspended in 500 µl of cold buffer A containing Proteinase Inhibitors (PIs) at a 1:100 dilution. This suspension was centrifuged at 4°C for 2 minutes at full speed (rotor #1), after which the supernatant was discarded. This washing step was repeated two additional times to ensure thorough removal of contaminants. The resulting pellet was then resuspended in 350 µl of cold buffer A + PIs, and an appropriate amount of glass beads (0.75-1.0 µm) was added until only a small layer of cell suspension remained above the beads. The cells were mechanically lysed by vigorous shaking for 15 minutes at 4°C using the VIBRAX VXR basic. To remove the glass beads, the bottom and lid of the 1.5 ml microtubes was pierced with a heated needle, and the tubes were placed into 15 ml Falcon tubes and centrifuged for 2 minutes at 2000 rpm (rotor #3), resulting in the crude nuclei collecting in the Falcon tubes. These crude nuclei were then quantitatively transferred into new 1.5 ml tubes and washed once with 500 µl of cold buffer A + PIs, followed by an additional wash with 500 µl of cold buffer Ag + PIs, using the same centrifugation procedure as before. The final crude nuclei preparation was kept on ice until used for the subsequent ChEC reaction.

5.3.3 ChEC reaction

The crude nuclei prepared in section 5.3.2 were used to initiate the ChEC reaction by first splitting the suspension into three aliquots: 380 µl for the main ChEC reaction, 100 µl for the 0 min ChEC sample, and 50 µl for the 0 min ChEC-Psoralen sample. The 380 µl and 100 µl aliquots were pre-warmed at 30°C in an Eppendorf Thermomixer compact, while the 50 µl aliquot was kept on ice after the addition of 50 µl IRN buffer. In preparation for sampling, 100 µl of IRN buffer was aliquoted into 1.5 ml tubes for the 10, 30, and 60 min timepoints, and a

separate tube was prepared with 50 µl IRN buffer for the 60 min ChEC-Psoralen sample. To activate MNase activity, 7.5 µl of 100 mM $CaCl_2$ was added to the 380 µl ChEC reaction aliquot, and the reaction was incubated at 30°C with vigorous shaking at 1000 rpm. Samples of 100 µl were taken at 10, 30, and 60 min and immediately transferred into the corresponding IRN buffer tubes to stop the reaction; additionally, after 60 min, 50 µl was added to the tube for the ChEC-Psoralen sample. The 0 min and 60 min ChEC-Psoralen samples were subsequently centrifuged for 1 min at full speed at room temperature, flash-frozen in liquid nitrogen, and stored at -80°C until further crosslinking with TMP, as described in section 5.3.9. Finally, following a 60 min incubation at 30°C, 100 µl of IRN buffer was added to the 0 min ChEC samples, and the reactions were processed directly for DNA extraction via phenol/chloroform/isoamyl alcohol (PCI) extraction.

5.3.4 ChEC-Psoralen

ChEC-Psoralen crude nuclei pellets stored at -80°C (as described in section 5.3.3) were retrieved, placed on ice, and directly resuspended in 200 µl IRN buffer. The suspension was then transferred to a pre-cooled 24-well plate maintained on ice, where 10 µl of TMP - pre-stirred at room temperature for at least 30°C - was added to the solution. After mixing, the plate was incubated for 5 min on ice in the dark, followed by UVA irradiation at 8 mW/cm² using 15 W Blacklight blue lamps (315-400 nm) (Sankyo-Denki) for 5 min. This process of adding 10 µl TMP and UV irradiation was repeated three additional times, with the UV exposure time extended by 1 min at each step (resulting in irradiation periods of 6, 7, and finally 8 min). Following these treatments, the samples were transferred into new 1.5 ml tubes and subjected to the DNA workup protocol outlined in section 5.3.5.

5.3.5 DNA workup

For the DNA extraction, 10 µl of 10% SDS and 10 µl of Proteinase K solution were added to the samples, which were then incubated for 1 h at 56°C for protein digestion followed by an overnight incubation at 65°C in a Hybridization oven to revert formaldehyde cross links. After incubation, 150 µl of PCI (phenol/chloroform/isopropanol) was added, and the samples were mixed thoroughly for 20 seconds before being centrifuged for 10 minutes at room temperature at full speed (rotor #2). After centrifugation 150ul of the upper aqueous phase was care-

fully transferred to a new 1.5 ml tube, and DNA precipitation was initiated by the addition of 350 µl of cold 100% ethanol. The samples were centrifuged for at least 20 minutes at 4°C (rotor #4). Following precipitation, the supernatant was discarded, and the DNA pellet was washed with 300 µl of cold 70% ethanol, followed by centrifugation for 5 minutes or longer at 4°C at full speed (rotor #4). After discarding the supernatant, the pellet was air-dried either at room temperature or at 37°C in an Eppendorf Thermomixer Compact, and finally, the purified DNA was dissolved in 50 µl TE buffer containing RNase (5 mg/ml) for subsequent analyses.

5.3.6 Restriction digestion and agarose gel electrophoresis

Extracted DNA from both ChEC and ChEC-Psoralen experiments was subjected to restriction digestion using a reaction mixture prepared according to Table 19 that was subsequently added to a 1.5 ml tube containing the nucleic acid.

Table 19: Composition of reaction mix for restriction digestion of ChEC- or ChEC-Psoralen DNA

Component	ChEC	ChEC-Psoralen
DNA	15 µl	15 µl
10x *CutSmart*	2.5 µl	2 µl
Restriction enzyme	0.5 µl [XcmI-HF]	0.5 µl [EcoRI-HF]
H_2O	7 µl	2,5 µl
Total volume	25 µl	20 µl

The restriction digestion was performed at 37°C for 2.5 h, after which the samples were either stored at -20°C or prepared immediately for agarose gel electrophoresis (AGE). For ChEC samples, 4 µl of 6x purple DNA loading dye was added, and the entire digestion reaction was loaded onto a 1% agarose gel containing 0.01% SYBR-Safe. Electrophoresis was carried out for approximately 3 h at an electric field strength of 5 V/cm until the purple band migrated to a position 2 cm above the lower end of the gel. In contrast, for ChEC-Psoralen samples, 4 µl of 10× DNA loading dye was used to prevent fading of the colored bands during overnight separation on a 1% agarose gel without SYBR-Safe. The gel was initially run overnight at 1 V/cm, and subsequently the electric field strength was increased until the blue band reached 2 cm from the lower end of the gel. At this point the TMP crosslinked DNA was de-crosslinked by exposing it to UV irradiation three times for 3 min each using a Gel Max UV transilluminator. The gel was then stained for 20 min with 500 ml of 0.01% SYBR-Safe in TBE. Finally, the gel

separations were documented using the Typhoon FLA-9500 imaging system, and the resulting images were analyzed with MultiGauge v.3.0 software and edited with Microsoft Excel. From this point forward both ChEC- and ChEC-Psoralen gels were treated equally.

5.3.7 Southern blotting

Immediately following documentation with the Typhoon FLA-9500 imaging system, the 1% agarose gel was incubated twice for 15 minutes each with a denaturing solution under gentle shaking. Subsequently, the gel was further incubated twice for 15 minutes or longer with 1 M ammonium acetate under similar gentle shaking conditions. The Southern blot was then assembled in the following order: a plastic support, a Whatman paper soaked in 1 M ammonium acetate (acting as a bridge in contact with the same buffer), the agarose gel positioned upside-down, a Nylon membrane, two additional Whatman papers soaked in 1 M ammonium acetate, a stack of absorbent paper, a plastic plate, and finally a metal rack to serve as a weight. The transfer of the separated DNA from the agarose gel to the Nylon membrane was performed in an anti-gravitational manner, carried out either overnight or over several days. After disassembling the blotting sandwich, the Nylon membrane was allowed to dry for a few minutes, and the transferred DNA was covalently crosslinked to the membrane via UV irradiation at 0.3 J/cm². The resulting blot was stored at room temperature until further processing.

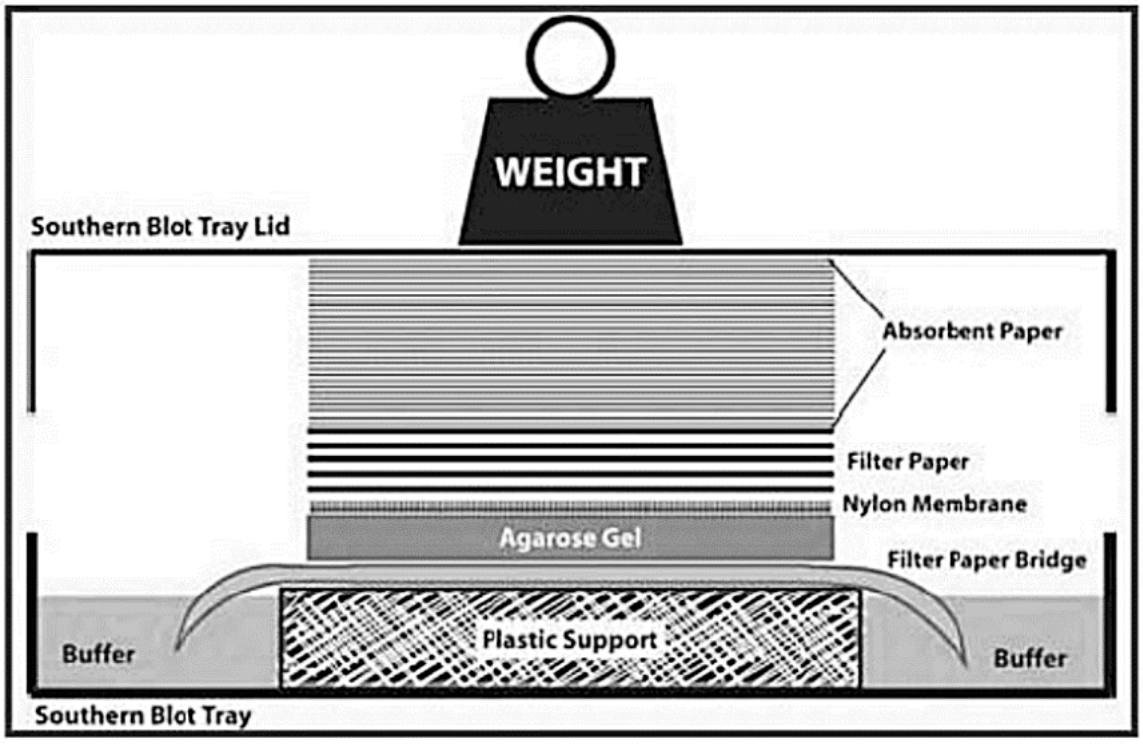

Figure 5: Assembly of the Southern blot
This schematic illustrates how DNA is transferred from an agarose gel onto a membrane by capillary action. From bottom to top: a buffer reservoir, a Whatman filter paper bridge, the agarose gel, the nylon membrane, additional Whatman filter paper, an absorbent stack of filter paper, and a weight on top. As buffer travels upward, it carries DNA out of the gel onto the membrane for subsequent analysis.

5.3.8 Labeling of radioactive probes for Southern blot analysis

A Southern probe was prepared using the BcaBEST DNA labeling kit by initially mixing 1 µl of Southern probe DNA (30-50 ng) with 2 µl random primers and 11 µl sterile purified H_2O, followed by heating for 3 minutes at 95°C in an Eppendorf Thermomixer Compact and cooling on ice for 5 minutes. Subsequently, 2.5 µl of 10x buffer and 2.5 µl of a dNTP mixture lacking dCTP were added to the mixture, after which the working area was shifted to the isotope laboratory. There, 5 µl of radioactive labeled dCTP and 1 µl of BcaBEST DNA Polymerase incorporated, and the reaction was incubated for 10 minutes at 55°C. The polymerization reaction was then halted by adding 5 µl of 0.5 M EDTA and incubating for 3 minutes at 95°C, followed by cooling on ice. For the clean-up, a size exclusion spin chromatography column was prepared, mixed, and centrifuged at 2800 rpm for 1 minute at room temperature (rotor #1). After discarding the initial flowthrough, the radioactive reaction mix was applied to the column and centrifuged again under the same conditions, and the resulting flowthrough was transferred into a 1.5 ml screw cap tube. Labeling and clean-up efficiency were confirmed using a Geiger-Müller counter. Finally, 120 µl of single-stranded salmon sperm DNA was added to the labeled probe to achieve a concentration of 100 µg/ml in the hybridization solution, and the mixture was boiled for 5 minutes at 95°C, cooled on ice, and transferred to a hybridization tube containing the blots and 12 ml of hybridization buffer.

5.3.8 Hybridization, washing and exposition

All hybridization and washing steps were conducted at 65°C under rotation in a hybridization tube. Initially, Southern blots were pre-hybridized by incubating them with 35 ml of hybridization buffer in hybridization tubes, rotated in a Hybridization oven for 1-3 h. During this pre-hybridization period, a radioactive labeled Southern probe was prepared as described in section 5.3.7. Once ready, the pre-hybridization buffer was discarded and replaced with 12 ml of fresh hybridization buffer before the radioactive probe was added; the blots were then incubated overnight at 65°C under rotation. On the following day, the hybridization solution was

discarded, and the blots were rinsed with 35 ml of rinse buffer at room temperature, followed by sequential washing with Wash buffers I, II, and III, with each washing step performed twice for 15 min or longer at 65°C using pre-warmed solutions. After washing, the blots were air-dried briefly, and their radioactivity was measured using a Geiger-Müller counter. The dried blots were then placed in a BAS cassette (model 2040, Fujifilm) with BAS-III imaging plates and exposed for a period ranging from a few hours to several days, depending on hybridization efficiency and the gene locus of interest. Subsequent imaging was carried out using the FLA-9500 imager, and the images were analyzed with MultiGauge v.3.0 and Microsoft Excel. After documentation, the BAS-III imaging plates were erased using the Eraser from Raytest, and the blots were stripped of residual radioactivity by incubating them with 100 ml of boiled stripping buffer for at least 20 min at 80°C in a hybridization oven. This stripping procedure was repeated 3-4 times, with additional cycles performed, if necessary, until the residual radioactivity approximated background levels. Following stripping, the blots were either re-hybridized with a new Southern probe or stored in foil at room temperature until further use.

6. Results

6.1 Analyzing cell growth in the presence of CX-5461 or BMH-21 in different yeast genotypes

In the following results section, we examine the effects of CX-5461 and BMH-21, on several yeast genotypes. Thus, we examined strains carrying a low rRNA gene copy number in which the individual genes are transcribed at a higher rate than in yeast strains carrying wild-type gene copy numbers (hereafter referred to as $RDN_{25copies}$, and *RDN* strains, respectively). Additionally, we analyzed strains in which the native rDNA locus was deleted (hereafter referred to as *rdnΔ* strains), and 35S rRNA was instead produced from a multicopy plasmid via either Pol I or II (hereafter referred to as "pPol I" and "pPol II" strains, respectively). Using these strains, it was possible to rigorously test the Pol I specificity of the two different compounds. Subsequently, we investigated strains that either lack the *HMO1* gene or overexpress *HMO1*. By comparing these distinct genetic backgrounds, we aim to investigate the possibility that the rRNA gene chromatin component Hmo1 plays a role in supporting Pol I transcription under chemical stress induced by CX-5461 and BMH-21.

6.1.1 Yeast cell growth in the presence of CX-5461

The use of selective media allows to study yeast cell growth in the presence of CX-5461

Earlier studies suggested that CX-5461 might also function as a Pol I-specific inhibitor in yeast (Jackobel et al., 2019). In the latter study it was found that CX-5461 tends to precipitate in YPAD which prevented the analysis of yeast cell growth in liquid media in the presence of the compound. Therefore, cells had to be pre-treated with CX-5461 in water before being transferred to solid YPAD media to investigate the effects on growth. This type of treatment was also used in a study of the working group in which it was concluded that CX-5461 might not exert Pol I specificity (Nagler, 2022). In the present work, we found that CX-5461 could be added to selective complete media (ScD), where it exerted an inhibitory effect on yeast growth in liquid media. To this end, yeast strains were cultured overnight in YPAD media to stationary phase. Cells from this overnight culture were then diluted in water and a defined cell number

was used to inoculate a 96-well culture plate containing either YPAD or selective growth media in the presence or absence of CX-5461. Additionally, the compound CX-5461-dihydrochloride was tested in this experiment. Growth in the 96-well plate was automatically detected using a TECAN plate reader system. In Figure 6 an example of a growth experiment with a haploid yeast strain Y207 [*RDN*] carrying an in-tact wild-type chromosomal ribosomal gene locus (*RDN*) is shown. Similar results were obtained with other yeast strains. Whereas no significant impact of the CX-5461 compounds on yeast cell growth could be detected in YPAD media (Fig. 6, Panel II, yellow and orange graphs), growth was retarded in the presence of CX-5461 and even more in the presence of the same concentration of CX-5461-dihydrochloride (Fig. 6, Panel I, yellow and orange graphs).

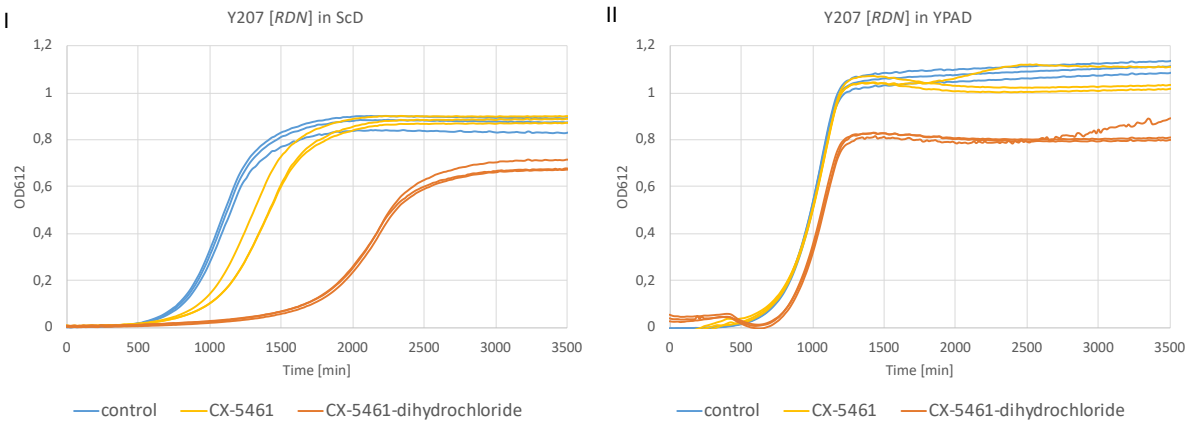

Figure 6: The use of selective liquid media allows to analyze yeast cell growth in the presence of CX-5461
The strain Y207 [*RDN*] carrying a wild-type rDNA locus was grown in **(I)** liquid selective media (ScD) and **(II)** YPAD at 30 °C in the absence (control) or presence of 250 µM CX-5461, or 250 µM CX-5461-dihydrochloride. Yeast cells from a stationary culture were inoculated in the respective liquid media in a 96-well plate and analyzed in a TECAN reader (as described in 5.1.2). The optical densities of the cultures at 612 nm (OD612) were measured every 15 minutes and plotted against the time of growth. The growth graphs for the different conditions are color-coded as indicated in the legends of the diagrams. Cells were grown in three independent cultures for each condition.

CX-5461 doesn't show Pol I-specific effects in yeast

To analyze if CX-5461 has features of a Pol I-specific inhibitor in yeast three different genotypes were examined: one laboratory wild-type strain, Y348 [*RDN*]; and two strains in which the quantity of rDNA transcription unit repetitions has been increased (Y352 [*fob1Δ*; $RDN_{190\ copies}$]) or lowered (Y353 [*fob1Δ*; $RDN_{25\ copies}$]) (Cioci et al., 2003). To ensure stability of the rDNA copy number in both strains, the *FOB1* gene has been deleted (Kobayashi et al., 1998).

As observed for *RDN* strain Y207 (Fig. 6), strain Y348 was affected in growth in the presence of CX-5461 (Fig. 7, Panel I, orange graphs). In strain Y353 carrying only 25 copies of the

transcription units, all copies of the 35S rRNA gene are densely packed with Pol I molecules to ensure robust rRNA production (Albert et al., 2011). This increase in transcriptional activity within individual rRNA genes should likely lead to a higher sensitivity of Y353 to a Pol I-specific inhibitor, when compared to the 190 rRNA gene copies containing but otherwise isogenic Y352. Contrary to these assumptions, however, in the presence of CX-5461 growth of Y352 [*fob1Δ*; $RDN_{190\ copies}$] was more strongly affected than growth of Y353 [*fob1Δ*; $RDN_{25\ copies}$] (Fig. 7, compare orange graphs in Panels II and III). These results suggest that CX-5461's mode of action in yeast may not strictly target Pol I transcription.

Furthermore, growth of strain Y352 [*fob1Δ*; $RDN_{190\ copies}$] appeared to be more strongly inhibited by CX-5461 than growth of strain Y348, although both strains contained a similar rDNA copy number. This could indicate that the lack of the *FOB1* gene product might increase the sensitivity towards CX-5461.

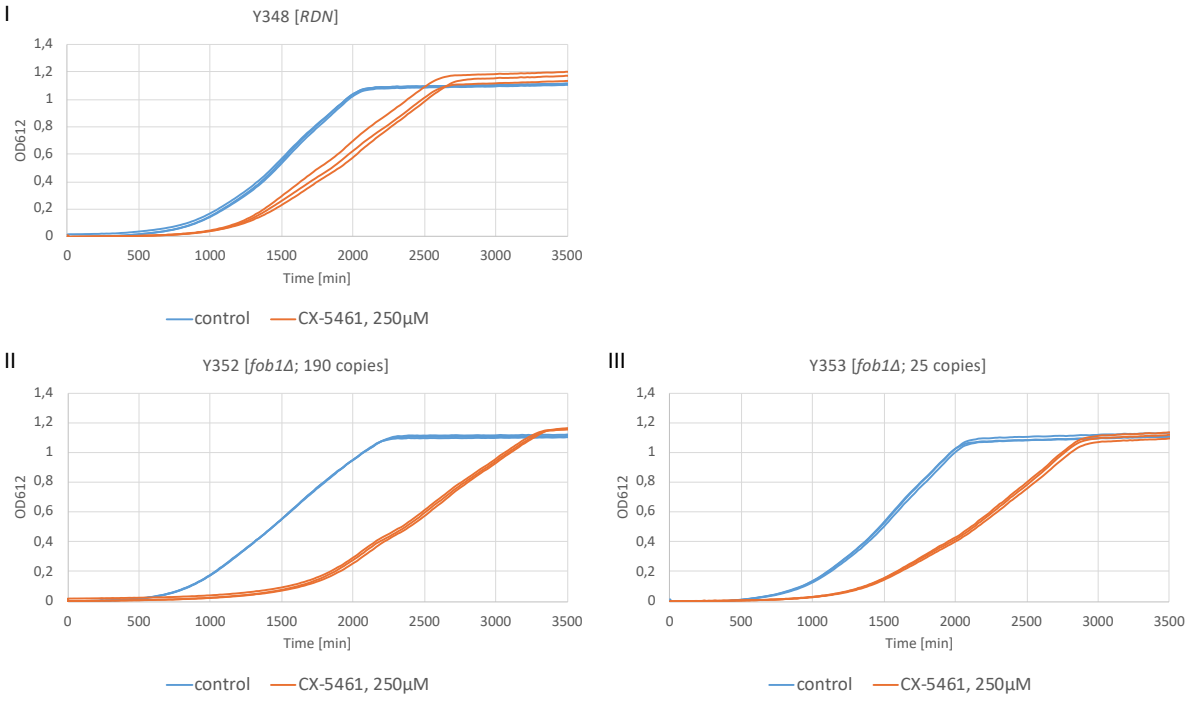

Figure 7: Different quantities of *RDN* copies suggest that CX-5461 doesn't act as a Pol I specific inhibitor in yeast
The three yeast strains indicated - **(I)** Y348 [*RDN*], **(II)** Y352 [*fob1Δ*; $RDN_{190\ copies}$] and **(III)** Y353 [*fob1Δ*; $RDN_{25\ copies}$] - were cultivated at 30 °C in the absence (control) or presence of 250 µM CX-5461. Cells from stationary-phase cultures were inoculated into the respective media in a 96-well plate and monitored using a TECAN plate reader. The optical density at 612 nm (OD612) was measured every 15 minutes, and the resulting growth graphs were plotted against time. Each condition is color-coded as shown in the legend, and three independent cultures were analyzed per condition. Two **(II, III)** or three **(I)** technical replicates have been created of this experiment.

In another experiment, *rdnΔ*, pPol I strains Y1743 and Y2441 were compared to *rdnΔ,* pPol II strains Y4256 and Y4412, the latter of which has an additional deletion of the gene coding for the second largest Pol I subunit (*rpa135Δ*), therefore completely lacking Pol I transcriptional activity. In principle, a purely Pol I-specific inhibitor would allow the *rdnΔ,* pPol II strains Y4256 and Y4412 to remain largely unaffected, while *rdnΔ*, pPol I strains Y1743 and Y2441 - in both of which the essential 35S rRNA is synthesized by Pol I - would be expected to exhibit a more pronounced response. Contrary to this prediction, the Pol II-dependent strains Y4256 and Y4412 proved highly sensitive to CX-5461, displaying no growth at all (Fig. 8, orange graphs in Panels I & II), whereas strains Y1743 and Y2441 weren't affected much (Fig. 8, orange graphs in Panels I & II). Interestingly strain Y2441 reacted more strongly than strain Y1743. These strains only differ in the marker gene which replaces the endogenous chromosomal rDNA locus (see 4.2, Tab. 4). The cause for this observation remains elusive.

The significant impact of CX-5461 on Y4256 and Y4412 growth, despite a lack of 35S rRNA transcription by Pol I in these strains, aligns with published evidence that CX-5461 may affect growth by targeting pathways beyond Pol I transcription (reviewed in Ferreira et al., 2020). Together, these findings support that CX-5461 does not act primarily by inhibiting Pol I.

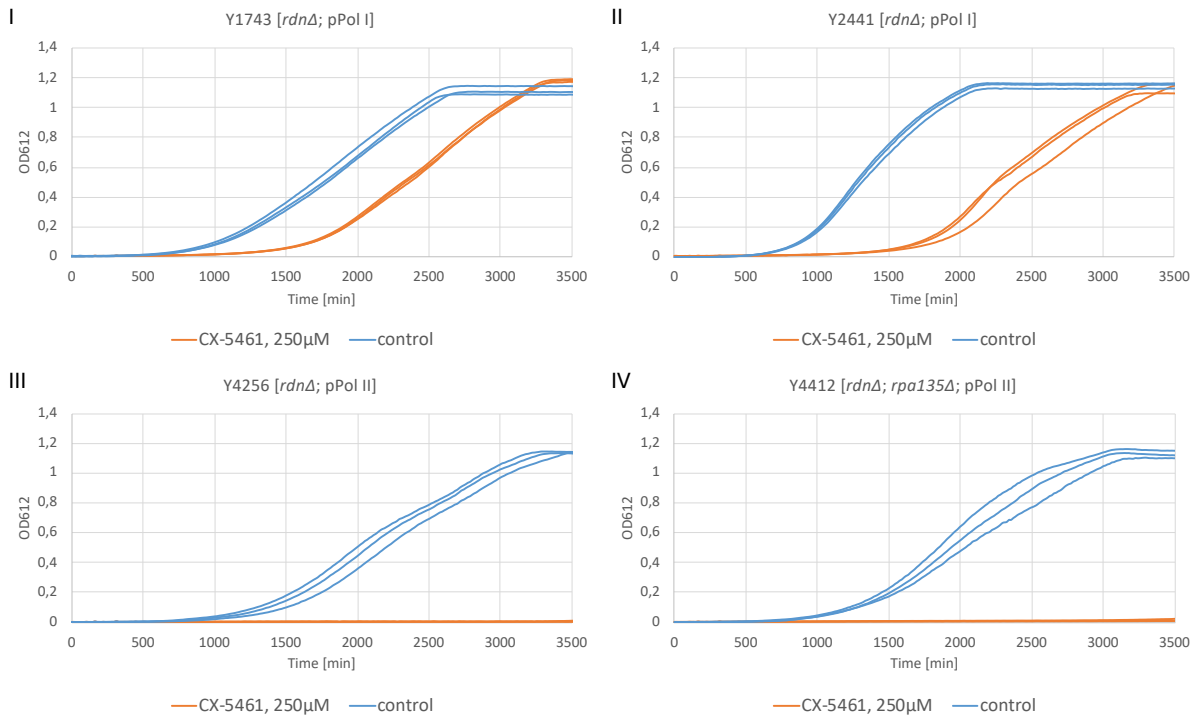

Figure 8: CX-5461 doesn't seem to exert a Pol I-specific effect in yeast
The four yeast strains indicated - **(I)** and **(II)** Y1743 and Y2441 [*rdnΔ*, pPol I], **(III)** Y4256 [*rdnΔ*, pPol II], and **(IV)** Y4412 [*rdnΔ*, *rpa135Δ*, pPol II] - were grown at 30 °C in the absence (control) or presence of 250 µM CX-5461. Yeast cells from stationary cultures were inoculated into the respective media in a 96-well plate and analyzed in a TECAN plate reader. The optical density at 612 nm (OD612) was measured every 15 minutes and plotted against the time of growth. The growth graphs for the different conditions are color-coded as indicated in the legend. Cells were grown in three independent cultures for each condition. Two technical replicates have been created of this experiment. Two **(I, IV)** or three **(II, III)** technical replicates have been created of this experiment.

6.1.2 Yeast cell growth under the influence of BMH-21

Frequent freeze-thaw cycles compromise the efficacy of BMH-21

BMH-21 solution was initially prepared according to the manufacturer's protocol by dissolving the compound in DMSO at a final concentration of 10 mM. To ensure complete dissolution of the stock solution, BMH-21 in DMSO was heated to 43°C under rotation in a hybridization oven. The stock solution was then divided into 1 mL aliquots and stored at -20°C. When needed for an experiment, a single aliquot was thawed, reheated to 43°C, and shaken at 1000 rpm in a thermoshaker to restore full solubility. Any leftover volume was refrozen at -20°C for future use.

During our experiments we suspected that repeatedly thawing, heating, and refreezing the same aliquots compromised the effectiveness of BMH-21. Tests conducted with the *RDN* strain Y348 showed that repeatedly cycled aliquots revealed a marked decline in the efficiency by which BMH-21 inhibited yeast cell growth (Fig. 9, compare orange graphs in Panels I and II). Recognizing this issue, we discarded the data associated with these problematic aliquots and repeated all important experiments with freshly prepared BMH-21 solutions. To prevent future complications, we switched from the 1 mL aliquot size to 100 µL aliquots, allowing each aliquot to undergo only one freeze-thaw cycle. This procedure helped to preserve BMH-21's potency and ensured more reliable and reproducible results in subsequent experiments.

It should be noted that growth of yeast strains was only compared within one individual experiment in which all the strains were grown under the same culture conditions in the same 96-well plate.

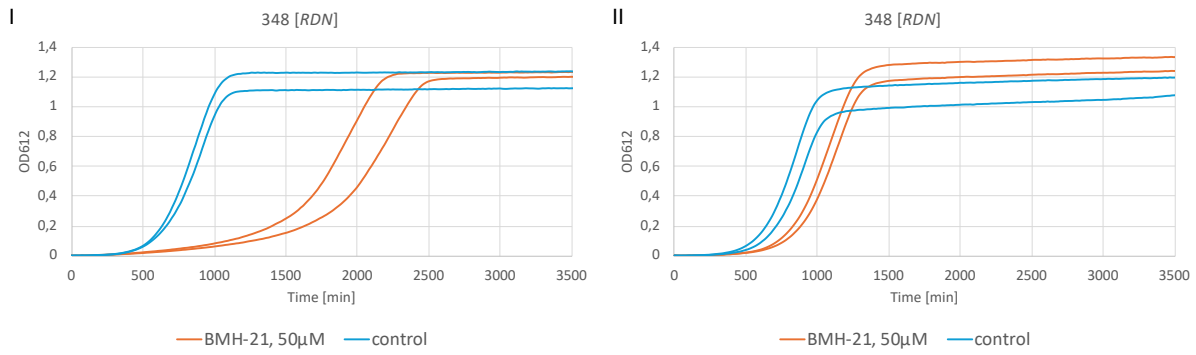

Figure 9: Frequent freeze-thaw cycles compromise the efficacy of BMH-21
The yeast strain Y348 was grown at 30 °C in two independent TECAN experiments using the same protocol. **(I)** A fresh aliquot of BMH-21 was used at concentration of 50 µM, with DMSO as the control. **(II)** An aliquot of BMH-21 that had been exposed to multiple freeze-thaw cycles was tested at 2 µM, 10 µM, and 50 µM, again with DMSO as the control. Yeast cells from stationary cultures were inoculated into a 96-well plate and monitored in a TECAN reader. The optical density at 612 nm (OD612) was measured over time and plotted, with each condition color-coded as indicated in the legend. Cells were grown in two independent cultures for each condition.

BMH-21 affects yeast cell growth in YPAD but not in selective growth media

In contrast to CX-5461, the compound BMH-21 had been used in YPAD in the past to investigate yeast cell growth in liquid media (Jacobs et al., 2021). To test whether BMH-21 exerts different effects on yeast cell growth in dependence of the culture media, we examined the *RDN* strain Y624 grown in either YPAD or ScD in the absence of presence of BMH-21. Strain Y624 is a derivative of Y348 and expresses the largest subunit of Pol I, Rpa190, as a fusion-protein with a C-terminal micrococcal nuclease (MN) tagged with a threefold hemagglutinin epitope (3xHA). This genetic modification has no significant effect on growth but allowed to investigate Rpa190 protein levels via detection of the HA-epitope (see Section 6.2) and DNA association due to the MN tag in Chromatin Endogenous Cleavage (ChEC) analyses (see Section 6.3). Notably, a strong inhibitory effect of BMH-21 on growth of Y624 was observed in YPAD (Fig. 10, orange graphs in Panel II), while no detectable effect was observed in ScD (Fig. 10, all graphs in Panel I). Thus, the growth medium also plays a critical role in how the presence of BMH-21 affects yeast cell growth. The underlying mechanism, however, remains elusive and needs further investigation.

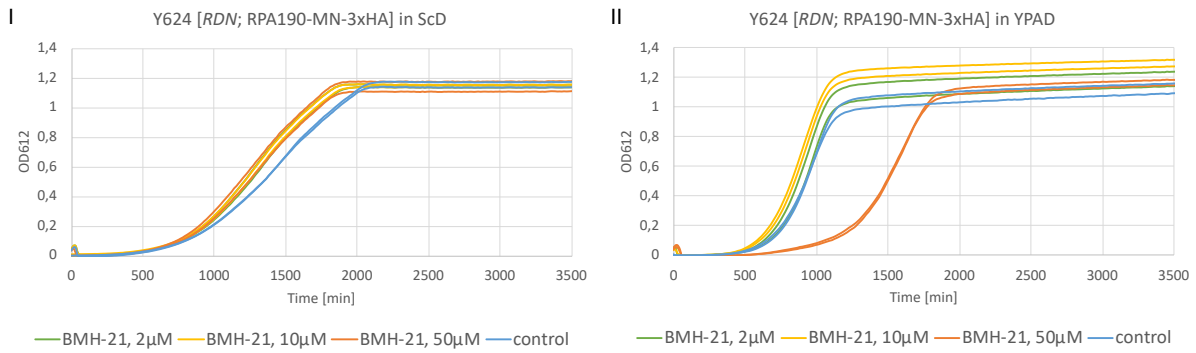

Figure 10: BMH-21 doesn't exert an effect in selective growth media
The strains Y624 [*RDN*; RPA190-MN-3×HA] and Y1332 [*RDN*; *hmo1Δ*; RPA190-MN-3×HA] were grown at 30 °C in **a)** ScD and **b)** YPAD media in the absence (control) or presence of 2 µM, 10 µM, or 50 µM BMH-21. Yeast cells from stationary cultures were inoculated into the respective liquid media in a 96-well plate and analyzed in a TECAN reader. The optical densities of the cultures at 612 nm (OD612) were measured every 15 minutes and plotted against the time of growth. The growth graphs for each condition are color-coded as indicated in the legends. Cells were grown in two independent cultures for each condition. Two technical replicates have been created of this experiment.

The degree of growth inhibition by BMH-21 correlates with Pol I transcriptional activity

First, we analyzed three yeast strains - Y348 [*RDN*], Y352 [*fob1Δ*; $RDN_{190\ copies}$], and Y353 [*fob1Δ*; $RDN_{25copies}$] - that were previously tested with CX-5461 (see Section 6.1.1). Here, we examined their responses to BMH-21, allowing us to compare its effects with those observed using CX-5461 (Fig. 7).

In good agreement with the assumption that BMH-21 is a Pol I specific inhibitor our results showed that Y353 in which only 25 rRNA genes are highly transcribed by densely packed Pol I molecules experienced the strongest inhibition of growth in the presence of BMH-21 (Fig. 11, orange graphs in Panel III). Growth of Y352 carrying 190 rRNA Gene copies was not as strongly affected but still substantially delayed, very similar to the growth delay observed for RDN strain Y348 (Fig. 10, orange graphs in Panels I and II). Thus, contrary to the results obtained with CX-5461 increased rRNA gene transcription correlated with increased sensitivity to the compound. Additionally, the lack of *FOB1* appeared to have no significant effect on BMH-21 sensitivity.

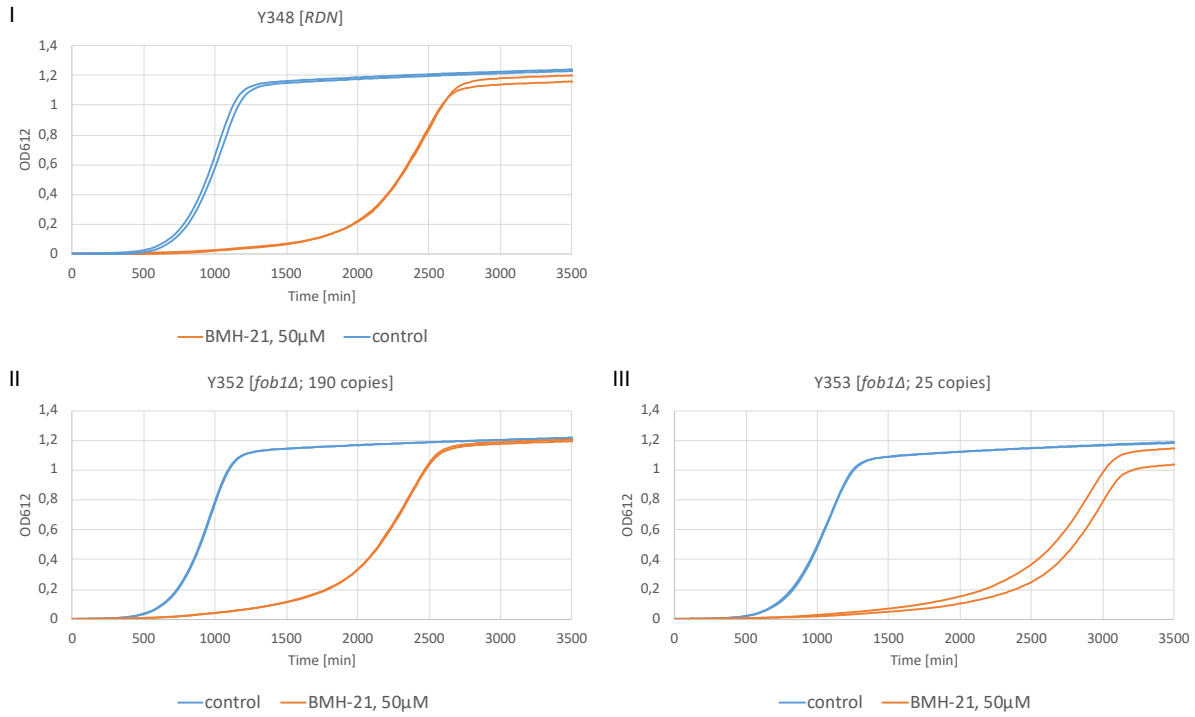

Figure 11: The degree of growth inhibition by BMH-21 correlates with Pol I transcriptional activity
The three yeast strains indicated - **(I)** Y348 [*RDN*], **(II)** Y352 [*fob1Δ*; $RDN_{190\ copies}$] and **(III)** Y353 [*fob1Δ*; $RDN_{25\ copies}$] - were cultivated at 30 °C in the absence (control) or presence of 50 µM BMH-21, respectively. Cells from stationary-phase cultures were inoculated into the respective media in a 96-well plate and monitored using a TECAN plate reader. The optical density at 612 nm (OD612) was measured every 15 minutes, and the resulting growth graphs were plotted against time. Each condition is color-coded as shown in the legend, and two independent cultures were analyzed per condition. Two **(II, III)** or three **(I)** technical replicates have been created of this experiment.

As for CX-5461 (see Section 6.1.1) we then examined *rdnΔ*, pPol I strains Y1743 and Y2441, and *rdnΔ*, pPol II strains Y4256 and Y4412, in which the 35S rRNA is synthesized by Pol I or Pol II, respectively.

In these experiments the *rdnΔ*, pPol I strains Y1743 and Y2441 showed a profound sensitivity to BMH-21 (Fig. 12, orange graphs in Panels I and II) while growth of *rdnΔ*, pPol II strains, Y4256 and Y4412, was significantly less affected (Fig. 12, orange graphs in Panels III and IV).

Taken together these data strengthen the hypothesis that synthesis of 35S rRNA by Pol I sensitizes yeast cells for growth inhibition by BMH-21.

As observed with CX-5461 (see Section 6.1.1), the almost isogenic *rdnΔ*, pPol I strains, Y1743 and Y2441, did not behave identically upon exposure to BMH-21. In contrast to the effects observed in the presence of CX-5461, growth of strain Y1743 was more strongly affected than growth of strain Y2441 in the presence of BMH-21 (Fig. 12, orange graphs in Panels I and II).

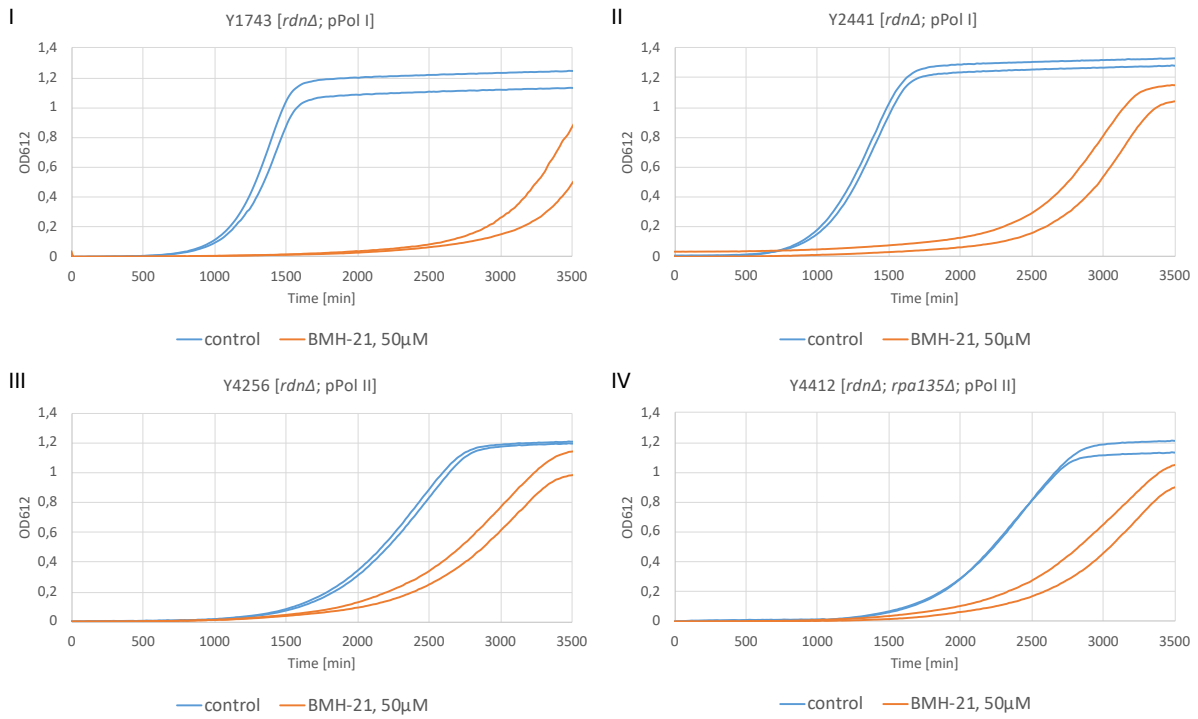

Figure 12: BMH-21 exhibits a Pol I-specific mode of action in the *rdnΔ* genetic system
The four yeast strains indicated - **(I)** and **(II)** Y1743 and Y2441 [*rdnΔ*, pPol I], **(III)** Y4256 [*rdnΔ*, pPol II], and **(IV)** Y4412 [*rdnΔ*, *rpa135Δ*, pPol II] - were grown in YPAD at 30 °C in the absence (control) or presence of 50 µM BMH-21. Yeast cells from stationary cultures were inoculated into 96-well plates and analyzed in a TECAN reader. The optical densities of the cultures at 612 nm (OD612) were measured every 15 minutes and plotted against the time of growth. The growth graphs for the different conditions are color-coded as indicated in the legend of the diagrams. Cells were grown in two independent cultures for each condition. Two **(I, IV)** or three **(II, III)** technical replicates have been created of this experiment.

Hmo1 expression levels play a crucial role in how severely BMH-21 affects yeast cell growth

In a previous study, it has been observed that association of the chromatin component Hmo1 with 35S rRNA genes was increased in the presence of BMH-21. Therefore, we analyzed if endogenous Hmo1 levels might influence the BMH-21 sensitivity of yeast cells.

In yeast strains Y1117, Y4762 derived from the *RDN* strain Y348 - which is a derivative of the yeast model strain W303 (Ralser et al., 2012) - we observed that deletion of *HMO1* severely inhibited yeast cell growth (Fig. 13, orange graphs in Panels I and III), whereas overexpressing *HMO1* using a strong *pTEF2* promoter from a chromosomally integrated expression cassette reduced the BMH-21 sensitivity of the corresponding yeast strain (Fig. 13, orange graphs in Panels I and IV). The same tendencies were observed in strains Y4449, Y4985, Y4987 - which are derivatives of another laboratory model strain S288C (Brachmann et al., 1998). These strains were modified to express Rpa190-MN-3xHA and a fusion-protein of Rad52 with a C-

terminal green fluorescent protein (Rad52-GFP) and carried either a wild-type copy of the *HMO1* gene (*HMO1*), a full deletion (*hmo1Δ*), or an additional chromosomally integrated *pTEF2-HMO1* overexpression cassette, respectively (Fig. 13. orange graphs in Panels II, IV, and VI). Another set of otherwise isogenic strains Y4695, Y4979, and Y4981 expressing the Pol I subunit, Rpa43, as an MN-3xHA-fusion protein instead of Rpa190-MN-3xHA behaved virtually identical to strains Y4449, Y4985, and Y4987 (Suppl. Fig. 1, Panels II, IV, and VI). Interestingly, W303 derivatives were generally more sensitive to BMH-21 treatment than the corresponding S288C derivatives (Fig. 13., compare orange graphs in Panels I and II, II, and IV, V and VI).

In summary, this indicates that the presence of the chromatin component Hmo1 may suppress BMH-21 sensitivity of yeast strains.

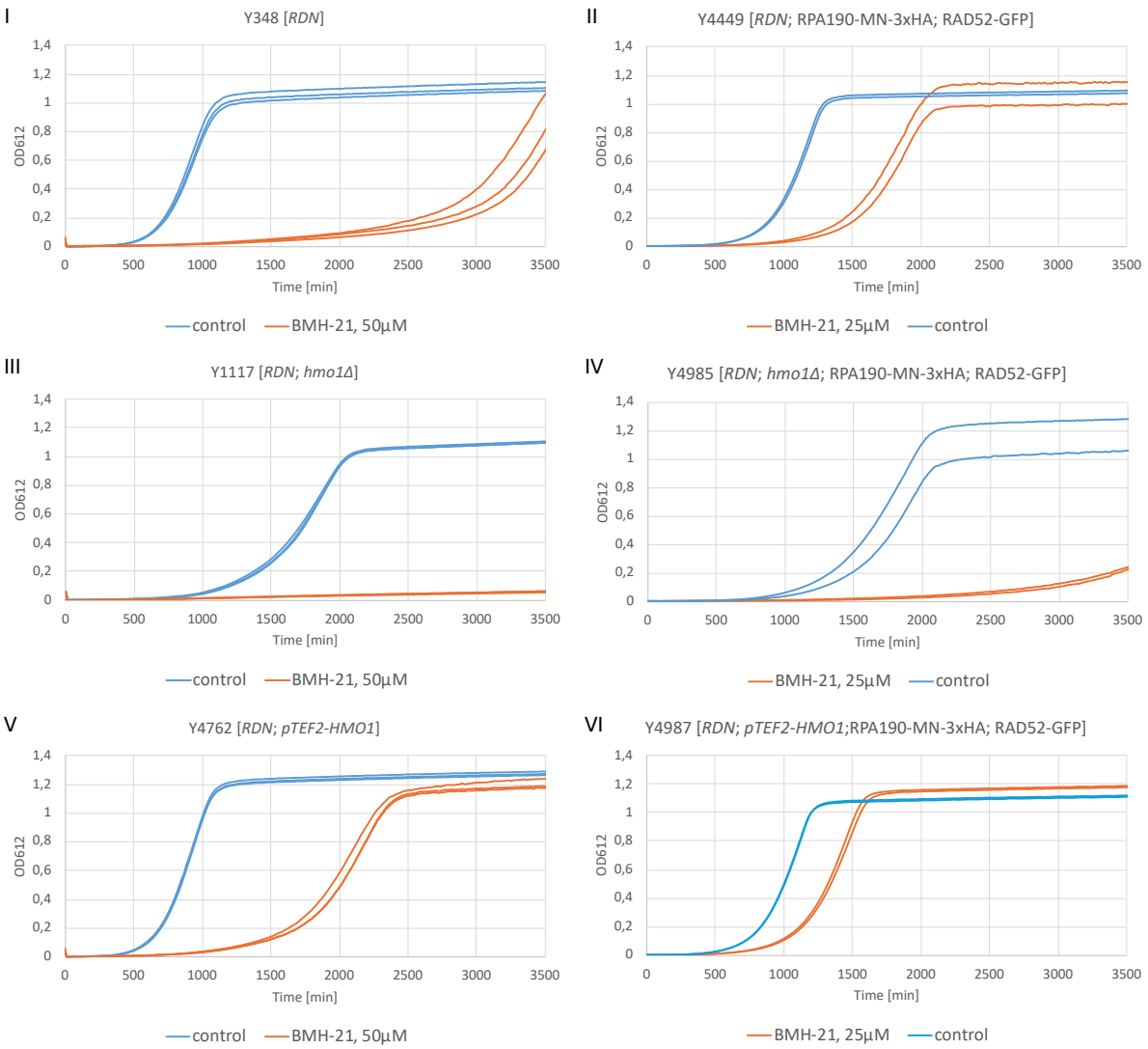

Figure 13: Overexpression of Hmo1 protects yeast cells from inhibitory BMH-21 effects
Growth graphs (OD612) were recorded over time for six yeast strains cultured in a TECAN plate reader at 30 °C, with cells exposed to either 25 µM (**I, III, V**) or 50 µM BMH-21 (**II, IV, VI**), or an equivalent volume of DMSO (control). The six genotypes examined were: **(I)** Y348 [*RDN*]; **(II)** Y4449 [RDN; RPA190-MN-3×HA; RAD52-GFP],; **(III)** Y1117 [*RDN*; *hmo1Δ*]; **(IV)** Y4985 [*RDN*; *hmo1Δ*; RPA190-MN-3×HA; RAD52-GFP],; **(V)** Y4762 [*RDN*; *pTEF2-HMO1*]; and **(VI)** Y4987 [*RDN*; *pTEF2-HMO1*; RPA190-MN-3×HA; RAD52-GFP],. The optical density at 612 nm (OD612) was measured every 15 minutes and plotted against the time of growth. The growth graphs for the different conditions are color-coded as indicated in the legend. Cells were grown in three (**I**, **II, V**) or two (**II, IV, VI**) independent cultures for each condition, respectively. Two **(III, IV, VI)** or three **(I, II, V)** technical replicates have been created of this experiment.

Suppression of BMH-21 mediated growth inhibition by Hmo1 is dependent on Pol I transcription

Besides being a bona fide 35S rRNA gene chromatin component, Hmo1 associates with many promoter regions of Pol II transcribed genes (see 3.1.4). To further discriminate if the observed effects of endogenous Hmo1 levels on BMH-21 sensitivity of yeast cells relies on the role of Hmo1 in Pol I or Pol II transcription we generated new strains. Specifically, we constructed strains Y5055 [*rdnΔ*, *hmo1Δ*, pPol I] and Y5057 [*rdnΔ*, *hmo1Δ*, pPol II], both lacking *HMO1* but relying on RNA polymerase I or II, respectively, for 35S rRNA transcription from a multicopy plasmid. Growth analysis with these strains allowed us to determine whether the Hmo1-depenent BMH-21-sensitivity was Pol I- or Pol II-specific.

HMO1 deletion led to a growth delay in both pPol I and pPol II *rdnΔ* strains (Fig. 14, compare blue graphs in Panel I with Panel III, and in Panel II with Panel IV). The results confirmed that in strains that depend on Pol I for 35S rRNA synthesis, such as Y5055, deleting *HMO1* further increased susceptibility to BMH-21 (Fig. 14, compare orange graphs in Panels I and III). In contrast, in strain Y5057 that relies on Pol II for 35S rRNA production, deleting *HMO1* did not augment sensitivity to BMH-21 (Fig. 14, compare orange graphs in Panels II and IV).

Overall, these observations reinforce that the inhibitory effects of BMH-21 are closely tied to Pol I activity and highlight the critical role of Hmo1 in safeguarding cells from chemical stress targeting 35S rRNA synthesis by Pol I.

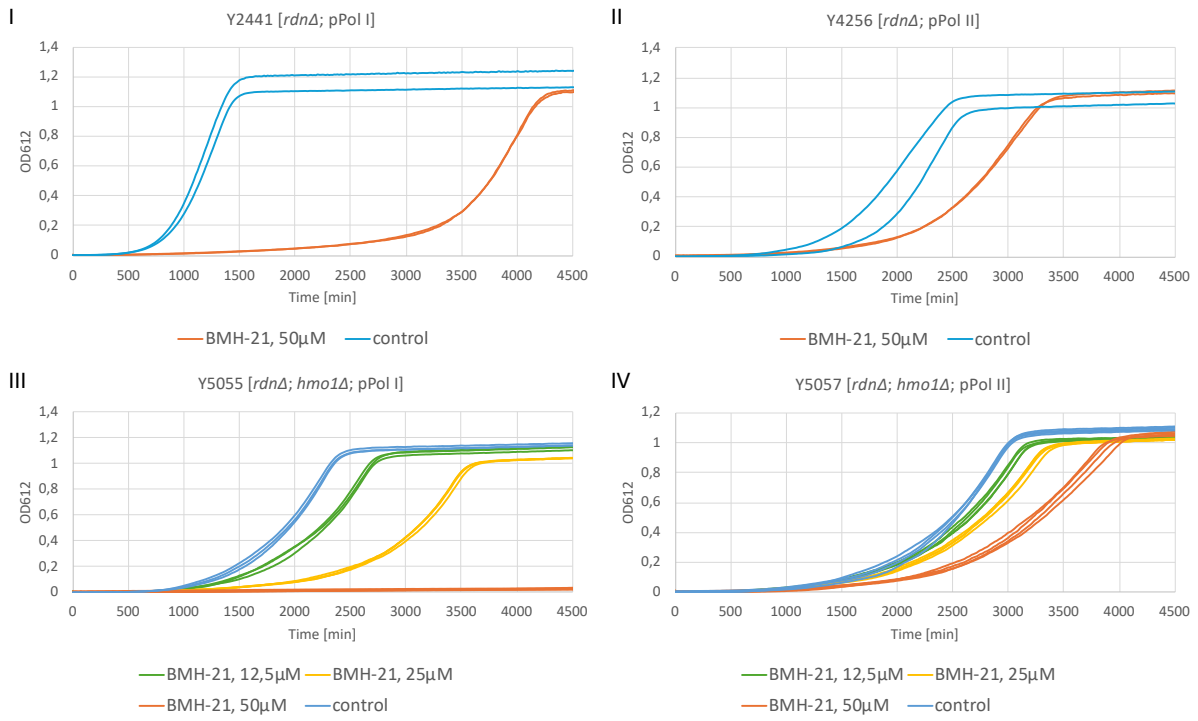

Figure 14: Suppression of BMH-21 mediated growth inhibition by Hmo1 is dependent on Pol I transcription The strains **(I)** Y2441 [*rdnΔ*, pPol I], **(II)** Y4256 [*rdnΔ*, pPol II], **(III)** Y5055 [*rdnΔ*, *hmo1Δ*, pPol I], and **(IV)** Y5057 [*rdnΔ*, *hmo1Δ*, pPol II] were grown at 30 °C in the absence (DMSO) or presence of 50 µM BMH-21. For strains Y5055 and Y5057, a dose-response experiment was performed using 12.5 µM, 25 µM, and 50 µM BMH-21. Yeast cells from stationary cultures were inoculated into 96-well plates and analyzed in a TECAN plate reader. The optical density at 612 nm (OD612) was measured every 15 minutes and plotted against the time of growth. The growth graphs for the different conditions are color-coded as indicated in the legend. Cells were grown in two (**I**, **II**) or three (**III, IV**) independent cultures for each condition, respectively. Two **(III, IV)** or three **(I, II)** technical replicates have been created of this experiment.

6.2 Investigating Rpa190 degradation in the presence of BMH-21

In the second part of this study, we investigated the previously reported degradation of the largest Pol I subunit, Rpa190, under the influence of BMH-21. We confirmed earlier findings and used our genetic system to correlate Rpa190 degradation with 35S rRNA transcription by Pol I. We further aimed at studying the impact of the endogenous Hmo1 level on Rpa190 degradation.

6.2.1 Analysis of Rpa190 degradation in the presence of BMH-21 in dependence on 35S rRNA gene transcription by Pol I

Protein analysis reveals that Rpa190 degradation in the presence of BMH-21 correlates with 35S rRNA transcription by Pol I

Previous work (Wei et al., 2018) established that BMH-21 leads to a degradation of Rpa190, the largest Pol I subunit - a finding further corroborated by our working group (Nagler, 2022). Whereas in human cell lines there was evidence that degradation of the largest Pol I subunit correlated with active Pol I transcription, similar experiments had so far not been conducted in yeast. Therefore, three distinct yeast strains were examined in the present study: Y1587 [*RDN*, RPA190-MN-3xHA], which carries a wild-type *RDN* locus, and two *rdnΔ* strains, Y640 [*rdnΔ*, RPA190-MN-3xHA, pPol I] and Y4500 [*rdnΔ*, RPA190-MN-3xHA, pPol II], where rDNA transcription is driven by a multicopy plasmid via Pol I or Pol II, respectively. All these strains were expressing an Rpa190-MN-3xHA fusion protein from the endogenous *RPA190* locus. This allowed to detect the fusion-proteins with a monoclonal antibody against the HA-epitope in subsequent analyses. To investigate how these different genetic backgrounds responded to BMH-21, exponential-phase cultures were transferred to YPAD medium containing either DMSO (control) or 50 µM BMH-21 and incubated at 30°C under continuous shaking. Samples of the culture were withdrawn at defined intervals for protein extraction and western blot analysis using antibodies directed against the HA-tag of Rpa190-MN-3xHA and the ribosomal protein of the small subunit S8 (rpS8) (Fig. 15 a)). The band intensities of both proteins allowed the calculation and comparison of Rpa190-MN-3xHA levels relative to rpS8 between the different samples (Fig. 15, b)).

In both Y1587 and Y640, the levels of Rpa190-MN-3xHA (normalized against rpS8) remained essentially constant for the first 30 minutes and dropped sharply after 90 minutes (Fig. 15, a), Lanes 2 to 7 and Lanes 9 to 12, see Fig. 15, b) for quantification). By contrast, Y4500 - which relies on Pol II for 35S rRNA transcription - remained largely unaffected until a slower decline in Rpa190-MN-3xHA levels began only after 180 minutes (Fig. 15, a), Lanes 16 to 21, see Fig. 15, b) for quantification). These findings indicate that - similar to the observations in human cell lines (Wei et al., 2018) - BMH-21 triggers Rpa190 degradation in dependence on 35S rRNA production by Pol I in yeast.

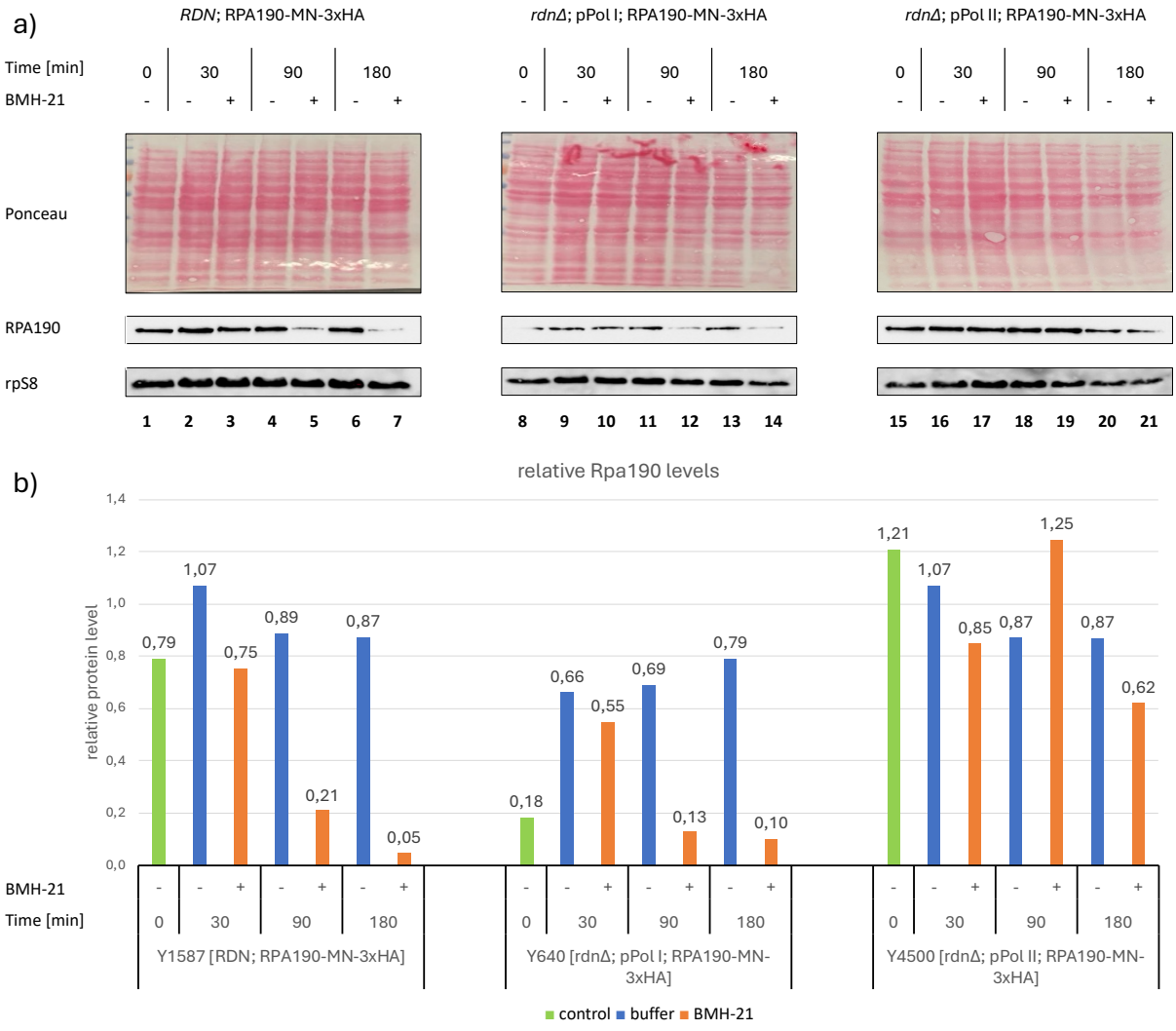

Figure 15: Rpa190 degradation in the presence of BMH-21 correlates with 35S rRNA synthesis by Pol I
Strains Y1587, Y640, and Y4500 all expressing an Rpa190-MN-3xHA, carrying a wildtype RDN locus or a complete deletion (*rdnΔ*), and transcribing 35S rRNA from a multicopy plasmid by Pol I (pPol I) or Pol II (pPol II) were grown overnight and inoculated into fresh YPAD. Cells were cultivated until they reached exponential phase. Then, equivalent volumes of DMSO (control) or BMH-21 (stock solution in DMSO to reach a final concentration of 50 µM) were added to each culture. Samples were withdrawn before (0) and 30, 90, and 180 minutes after addition of DMSO (-) and BMH-21 (+). Proteins were extracted, separated by SDS-PAGE, and transferred to membranes for western blot analysis.
a) Upper Panel: efficient transfer was verified by Ponceau red saining of the membrane. Rpa190-MN-3xHA was detected using rat-IgG #75 (monoclonal anti-HA antibody) and a horseradish peroxidase (HRP)-goat-IgG conjugate #81 (anti-rat-IgG) secondary antibody. The ribosomal protein S8 was detected using rabbit-IgG #68 (anti-rpS8) and a chemiluminescent HRP-goat-IgG conjugate #78 (anti-rabbit-IgG) secondary antibody. Chemiluminescent signals on the membranes were imaged using the Bio-Rad ChemiDoc system.
b) Depicts normalized Rpa190-MN-3xHA levels, calculated by dividing the Rpa190-MN-3xHA band intensities by the corresponding rpS8 band intensities (the normalized Rpa190-MN-3xHA level is indicated above each bar). Band intensities were measured with ImageJ, and the resulting ratios were calculated and plotted using Microsoft Excel. Bars were color-coded as explained in the legend on the bottom. Two technical replicates have been created of this experiment.

6.2.2 Analysis of Rpa190 degradation in the presence of BMH-21 in dependence on the endogenous Hmo1 level

The absence of Hmo1 increases degradation of Rpa190 in the presence of BMH-21

To further explore the impact of Hmo1 on BMH-21 susceptibility, we examined three different yeast strains: Y624 [*RDN*], harboring a wild-type RDN locus, Y1332 [*RDN*, *hmo1Δ*], which lacks the gene encoding Hmo1, and Y4499 [*rdnΔ*, pPol II], transcribing rDNA from a multi-copy plasmid via Pol II. As above (6.2.1), all these strains were expressing an Rpa190-MN-3xHA fusion protein from the endogenous RPA190 locus. The strains were then treated with BMH-21 and analyzed as described above (6.2.1).

Under BMH-21 treatment, strain Y624 (a biological replicate of Y1587) maintained Rpa190-MN-3xHA protein levels for the first 30 minutes but showed a sharp decline after 90 minutes, consistent with previous observations in strain Y1587 (Fig. 16, a), Lanes 2 to 7, see Fig. 16, b) for quantification). By contrast, in strain Y1332 Rpa190-MN-3xHA levels decreased already significantly after just 30 minutes of BMH-21 treatment, reflecting a crucial role of Hmo1 in maintaining Pol I stability in this condition (Fig. 16, a), Lanes 10, 12, 14, see Fig. 16, b) for quantification). Even in the control (DMSO) condition, Rpa190-MN-3xHA levels relative to rpS8 appeared to be lower than those in the wild-type strain at least in the samples withdrawn after 90 and 180 minutes (Fig. 16, a), Lanes 9, 11, 13, see Fig. 16, b) for quantification), suggesting that the lack of Hmo1 might decrease endogenous Rpa190 levels. Finally, Y4499 (a biological replicate of Y4500) displayed stable Rpa190-MN-3xHA protein levels across most of the time course (Fig. 16, a), Lanes 16 to 21, see Fig. 16, b) for quantification), showing only a gradual decline after 180 minutes.

Taken together, these observations suggest a function of Hmo1 in stabilizing the Pol I enzyme, particularly when the transcription machinery is challenged by an inhibitor such as BMH-21. Even in the absence of BMH-21, Hmo1 appears to be necessary for maintaining wild-type Rpa190 levels.

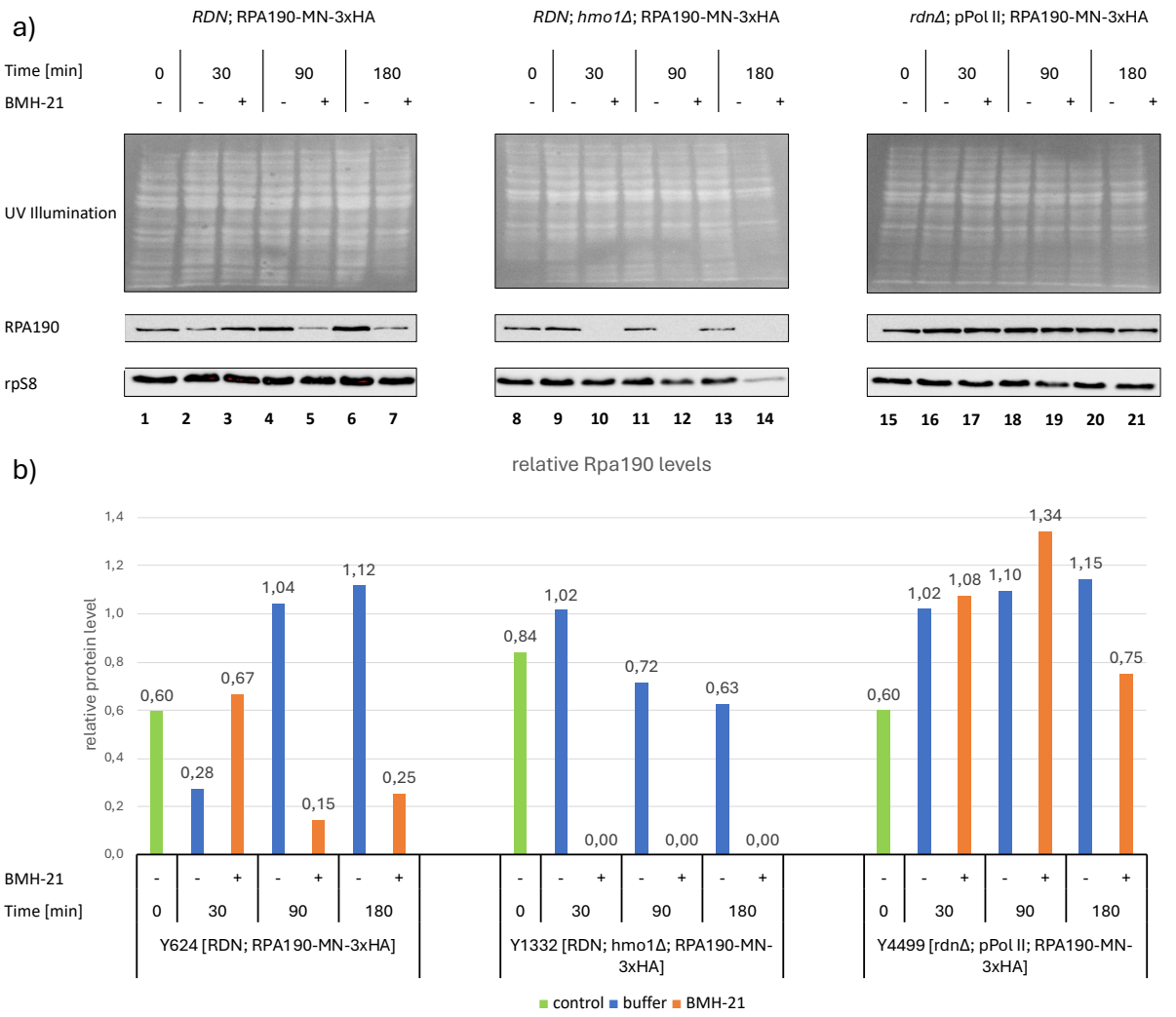

Figure 16: The absence of Hmo1 increases degradation of Rpa190 in the presence of BMH-21
Strains Y624 [*RDN*], Y1332 [*RDN*, *hmo1Δ*], and Y4499 [*rdnΔ*, pPol II] were treated and analyzed as in Figure 15. **a)** Upper Panel: Efficient protein transfer was verified by UV illumination of the membrane. Rpa190-MN-3xHA was detected using rat-IgG #75 (monoclonal anti-HA antibody) and a horseradish peroxidase (HRP)-goat-IgG conjugate #81 (anti-rat-IgG) secondary antibody. Ribosomal protein S8 was detected using rabbit-IgG #68 (anti-rpS8) and an HRP-goat-IgG conjugate #78 (anti-rabbit-IgG) secondary antibody. Chemiluminescent signals were visualized using the Bio-Rad ChemiDoc system. **b)** Lower Panel: Normalized Rpa190-MN-3xHA levels were calculated by dividing the Rpa190-MN-3xHA band intensity by the corresponding rpS8 band intensity (normalized values are indicated above each bar). Band intensities were quantified using ImageJ, and the resulting ratios were plotted using Microsoft Excel. Bars were color-coded as explained in the legend below. Two technical replicates have been created of this experiment.

6.2.3 Analysis of Rpa190 degradation in *HMO1* overexpression system

Overexpression of HMO1 protects Rpa190 from degradation in the presence of BMH-21

Since *HMO1* deletion resulted in an increase in Rpa190 degradation in the presence of BMH-21, we tested the possibility that overexpression of Hmo1 might help to stabilize the Pol I enzyme in this condition. We chose three yeast strains all carrying a wild-type *RDN* gene locus and expressing Rpa190-MN-3xHA and Rad52-GFP fusion-proteins for this experiment (Y4449

[*RDN*; RPA190-MN-3×HA; RAD52-GFP], Y4986 [*RDN*; *hmo1Δ*; RPA190-MN-3×HA; RAD52-GFP], and Y4988 [*RDN*; *pTEF2-HMO1*; RPA190-MN-3×HA; RAD52-GFP]). Y4449 carries a wild type *HMO1* locus, Y4986 lacks the *HMO1* locus, and Y4988 overexpresses *HMO1* via the pTEF2 promoter in addition to expressing endogenous Hmo1. Because *hmo1Δ* cells (Y4986) proved extremely sensitive to 50 µM BMH-21 in earlier tests the BMH-21 concentration was lowered to 25 µM to facilitate a more fine-grained analysis of how Rpa190-MN-3xHA levels change over time. The strains were then treated with BMH-21 and analyzed as described above (6.2.1).

In the presence of 25 µM BMH-21, Y4449 (*HMO1*) showed stable Rpa190-MN-3xHA levels, normalized to rpS8, for the first 30 minutes of incubation. After 90 minutes in the presence of BMH-21, the Rpa190-MN-3xHA protein levels had dropped noticeably, though less drastically than observed for Y1587 and Y624 in the presence of 50µM of BMH-21 (Compare Fig. 17 a), Lanes 2 to 7 with Lanes 2 to 7 in Figs 15 a) and 16 a), see Figs 15-17 b) for quantification), likely correlating with the dose-dependent impact of BMH-21 on cell growth (see Fig. 9 panel II as an example). In contrast, upon treatment of strain Y4986 - lacking Hmo1 - with 25 µM BMH-21 Rpa190-MN-3xHA levels decreased significantly after 30 minutes of incubation (Fig. 17 a), Lanes 9 to 14, see Fig. 17, b) for quantification). Meanwhile, Y4988, which overexpresses *HMO1*, largely preserved its Rpa190-MN-3xHA content throughout the observation period, revealing only a mild decrease in the sample withdrawn after 90 and 180 minutes of incubation (Fig. 17, Lanes 16 to 21, see Fig. 17, b) for quantification).

Taken together, these findings underscore the critical importance of Hmo1 in preserving Pol I integrity, highlighting that cells lacking Hmo1 are highly susceptible even to modest concentrations of BMH-21, whereas elevated Hmo1 levels, though not fully eliminating BMH-21's effects on Rpa190 degradation, significantly mitigate them.

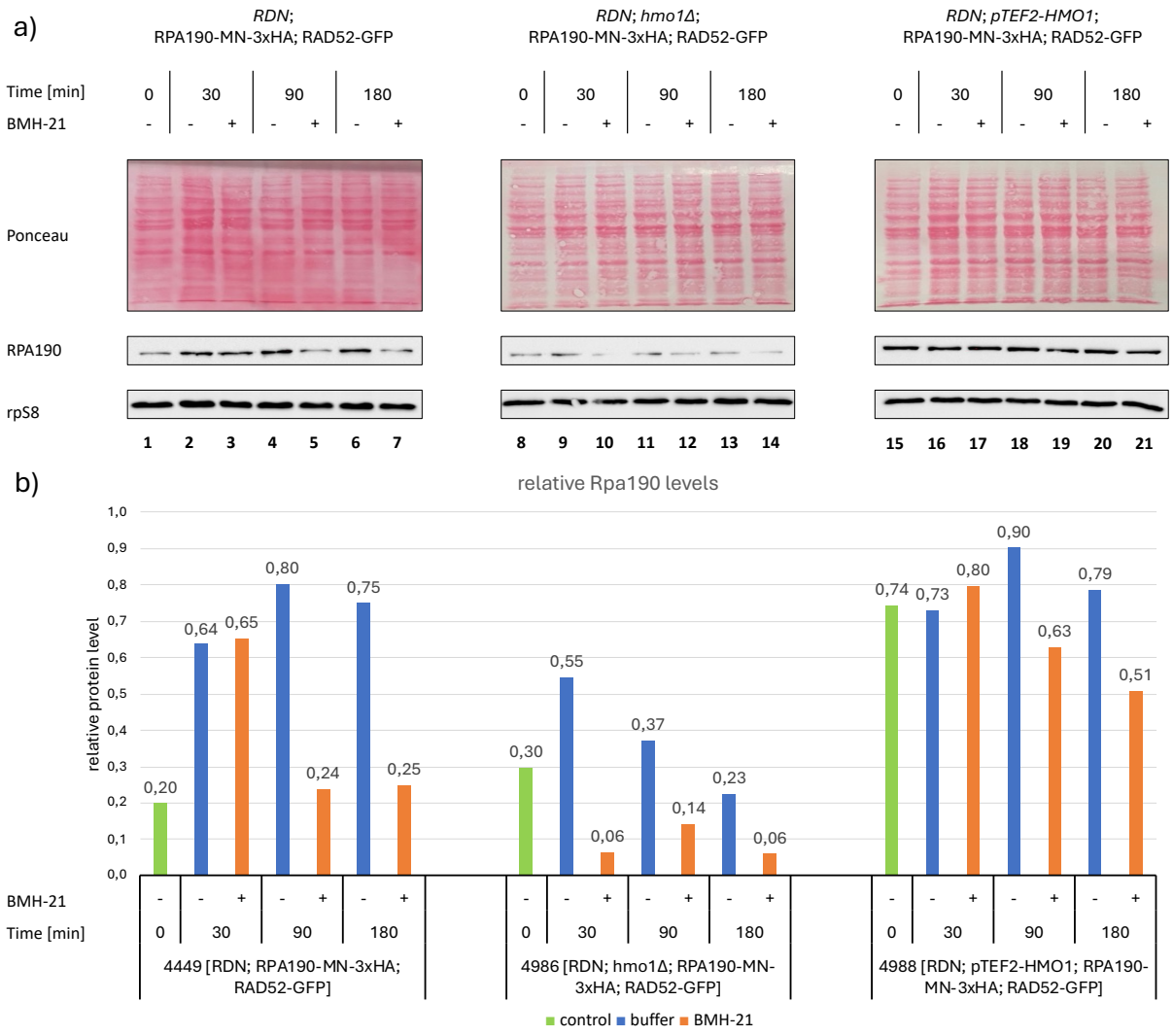

Figure 17: Overexpression of Hmo1 protects Rpa190 from degradation in the presence of BMH-21
Strains Y4449 [*RDN*, RPA190-MN-3xHA, RAD52-GFP], Y4986 [*RDN*, *hmo1Δ*, RPA190-MN-3xHA, RAD52-GFP], and Y4988 [*RDN*, *pTEF2-HMO1*, RPA190-MN-3xHA, RAD52-GFP] were treated and analyzed as in Figure 15, with a concentration of 25 µM at this instance.
a) Upper Panel: Efficient protein transfer was verified by Ponceau red staining of the membrane. Rpa190-MN-3xHA was detected using rat-IgG #75 (monoclonal anti-HA antibody) and a horseradish peroxidase (HRP)-goat-IgG conjugate #81 (anti-rat-IgG) secondary antibody. Ribosomal protein S8 was detected using rabbit-IgG #68 (anti-rpS8) and an HRP-goat-IgG conjugate #78 (anti-rabbit-IgG) secondary antibody. Chemiluminescent signals were visualized using the Bio-Rad ChemiDoc system.
b) Lower Panel: Normalized Rpa190-MN-3xHA levels were calculated by dividing the Rpa190-MN-3xHA band intensity by the corresponding rpS8 band intensity (normalized values are indicated above each bar). Band intensities were quantified using ImageJ, and the resulting ratios were plotted using Microsoft Excel. Bars were color-coded as explained in the legend below. Two technical replicates have been created of this experiment.

6.3 DNA Analysis

The data presented in this section are preliminary and have not been independently reproduced. While the observed trends are consistent with within an earlier study (Nagler, 2022) and other datasets from different experiments shown in this thesis, these findings should be regarded as initial observations. Due to time constraints, comprehensive reproduction and validation of these results were not possible within the scope of this thesis. Future research will be necessary to reproduce and confirm these results.

6.3.1 Analysis of Pol I occupancy upon BMH-21 treatment in strains with different endogenous Hmo1 levels

To gain insights in how different Hmo1 levels alter Pol I transcription in the absence and presence of BMH-21, we conducted a ChEC analysis using the strains also investigated in 6.1.2, and 6.2.3: Y4449 [*RDN*; RPA190-MN-3xHA; RAD52-GFP], Y4985 [*RDN*; *hmo1Δ*; RPA190-MN-3xHA; RAD52-GFP], and Y4987 [*RDN*; *pTEF2-HMO1*; RPA190-MN-3xHA; RAD52-GFP]. Exponential cultures of each strain were cultivated in YPAD medium supplemented with either 50 µM BMH-21 or DMSO, and cells were harvested for analysis at 0, 30, and 120 minutes post-treatment. The ChEC experiment was performed following the protocol detailed in section 5.3.3. Subsequently, DNA was transferred onto a nylon membrane via Southern blotting as described in section 5.3.5, and radioactive labeled probe #5 was used to visualize a XcmI- fragment including the 35S rRNA gene promoter as well as a large part of the Pol I transcribed 35S rRNA gene region. To better illustrate differences in cleavage events in the different strains and under different conditions, radioactive signal intensities in individual lanes of the blot membrane were read out and plotted against the migration of DNA fragments in the agarose gel. To investigate the possibility that BMH-21 treatment has an impact on 35S rRNA gene chromatin structure, aliquots of the 0 min and 60min ChEC samples were further subjected to psoralen crosslinking experiments. In these experiments psoralen intercalates efficiently in nucleosome-free DNA whereas psoralen intercalation is strongly impaired when the DNA is wrapped around histone octamers in nucleosomes. Since 35S rRNA genes coexist in a nucleosomal transcriptional inactive and a nucleosome depleted actively transcribed chromatin state, two distinct populations of 35S rDNA fragments are observed displaying a low and a

high degree of psoralen incorporation, respectively (Toussaint et al., 2005). The different degrees of psoralen incorporation correlate with a characteristic retardation of the migration of the respective 35S rDNA fragments in agarose gel electrophoresis. The fragments derived from the two different 35S rRNA gene chromatin states can subsequently be visualized by Southern blot analysis using a probe detecting different EcoRI fragments encompassing the 18S rDNA and the 25S rDNA, respectively. In combination with ChEC-psoralen crosslinking allows to obtain information if a certain fac-tor is a component of open or the closed 35S rRNA gene chromatin state (Griesenbeck et al., 2012).

Endogenous Hmo1 levels impact Pol I association with 35S rRNA genes in the presence of BMH-21

Whereas different endogenous Hmo1 levels had no significant impact on Rpa190-MN-3xHA mediated cleavage events before or 30 or 120 min after DMSO addition (Suppl. Fig. 2) characteristic changes were observed in the samples treated with BMH-21. In strains carrying a wild-type *HMO1* locus, treatment with BMH-21 resulted in a modest increase in longer fragments produced by Rpa190-MN cleavage within the transcribed 35S rRNA gene region (Fig. 18, a) compare lanes 1-4 with lanes 5-8, Fig. 19, Panel I, compare blue and orange graphs). While the overall cleavage was reduced in cells grown for 120min in the presence of DMSO and BMH-21 when compared to the overall cleavage 30min after addition of the compounds, the tendencies upon BMH-21 treatment were the same (Fig. 18, b), compare lanes 1-4 with lanes 5-8, Fig. 19, Panel II, compare blue and orange graphs). This change in cleavage pattern suggests that, under BMH-21 treatment, a greater number of rRNA genes may be transcribed; however, each gene is engaged by a lower density of Pol I, indicating a potential redistribution of transcriptional activity across the Pol I transcribed region. Interestingly, *hmo1Δ* strains exhibited a markedly different response, where just 30 minutes of BMH-21 treatment led to a pronounced decrease in Rpa190-MN-3xHA mediated cleavage events at the 5’ end of the 35S rRNA gene (Fig. 18, a), compare lanes 9-12 with lanes 13-16, Fig. 19, Panel III, compare blue and orange graphs). The simplest explanation for this phenomenon is that Pol I becomes limiting for transcription initiation (perhaps due to the degradation of Rpa190-MN-3xHA observed in 6.2.3). Thus, 35S rRNA genes might be only sparsely covered with Pol I molecules under those conditions. Moreover, after 120 minutes of exposure to BMH-21, Rpa190-MN-3xHA mediated cleavage was almost entirely abolished in the *hmo1Δ* background, correlating

with the compound's severe inhibitory effect on cellular growth when Hmo1 was absent (Fig. 18, a), compare lanes 9-12 with lanes 13-16, Fig. 19, Panel IV, compare blue and orange graphs). Conversely, in strains overexpressing *HMO1*, the cleavage of Rpa190-MN-3xHA is significantly enhanced at both the promoter and throughout the transcribed region upon treatment with BMH-21 (Fig. 18, a), compare lanes 9-12 with lanes 13-16, Fig. 19, Panels V and VI, compare blue and orange graphs). This effect was more pronounced after 120 minutes compared to 30 minutes, suggesting that elevated levels of Hmo1 may actively support Pol I recruitment to 35S rRNA genes in the presence of BMH-21 thereby mitigating the negative impact of the compound on cellular growth (compare to results shown in Fig. 13). Increased Pol I loading on 35S rRNA genes in the presence of BMH-21 upon *HMO1* overexpression might also be supported by stabilization of Rpa190-MN-3xHA protein levels in this condition (compare to results shown in Fig. 17).

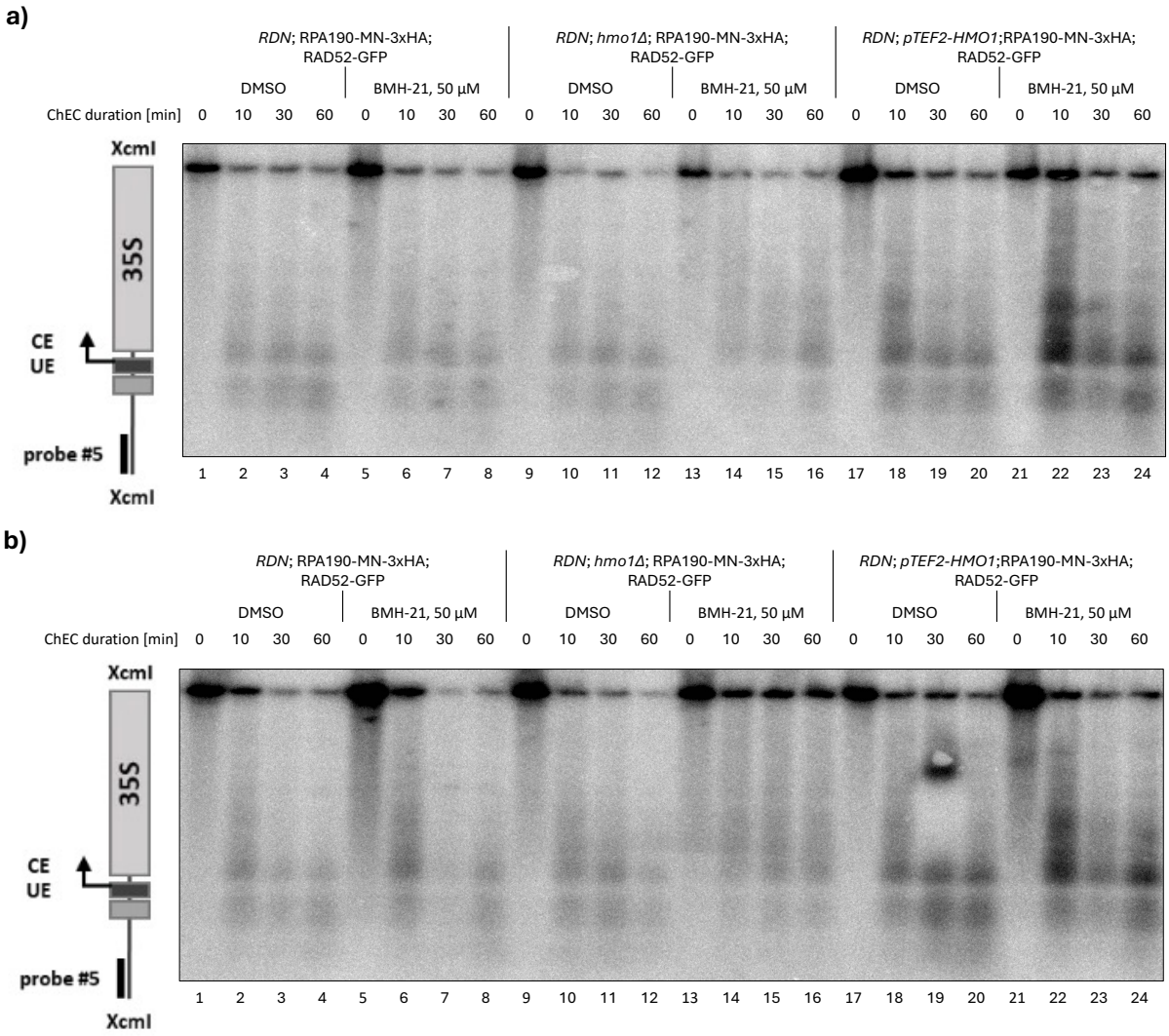

Figure 18: Rpa190-MN mediated cleavage events at rRNA genes are altered upon treatment with BMH-21 and depend on endogenous Hmo1 levels

Yeast strains Y4449 [*RDN*; RPA190-MN-3xHA; RAD52-GFP], Y4985 [*RDN*; *hmo1Δ*; RPA190-MN-3xHA; RAD52-GFP], and Y4987 [*RDN*; *pTEF2-HMO1*; RPA190-MN-3xHA; RAD52-GFP] were cultured in YPAD medium until reaching exponential phase. The cultures were then treated with either 50 µM BMH-21 or DMSO (control). For the ChEC analysis, samples were collected at 0 minutes (before compound addition), 30 minutes, and 120 minutes after treatment. The experiment was performed and analyzed as described in section 5.x.x, and the autoradiograms shown are derived from DNA samples that underwent extraction, XcmI digestion, agarose gel electrophoresis, Southern blotting, and subsequent radioactive labeling using Southern probe #5. Each blot displays ChEC time points at 0, 10, 30, and 60 minutes in cells treated with either DMSO or 50 µM BMH-21. The map presented on the left side of the autoradiograms illustrates the XcmI-digested fragment, indicating the positions of the Southern probe #5, the upstream element (UE), the core element (CE), the transcription start site (arrow), and a portion of the 35S rRNA gene. Each blot includes 24 sample lanes.

a) shows Rpa190-MN mediated cleavage events following 30 minutes of BMH-21 treatment. **b)** displays Rpa190-MN mediated cleavage events after 120 minutes of BMH-21 treatment.

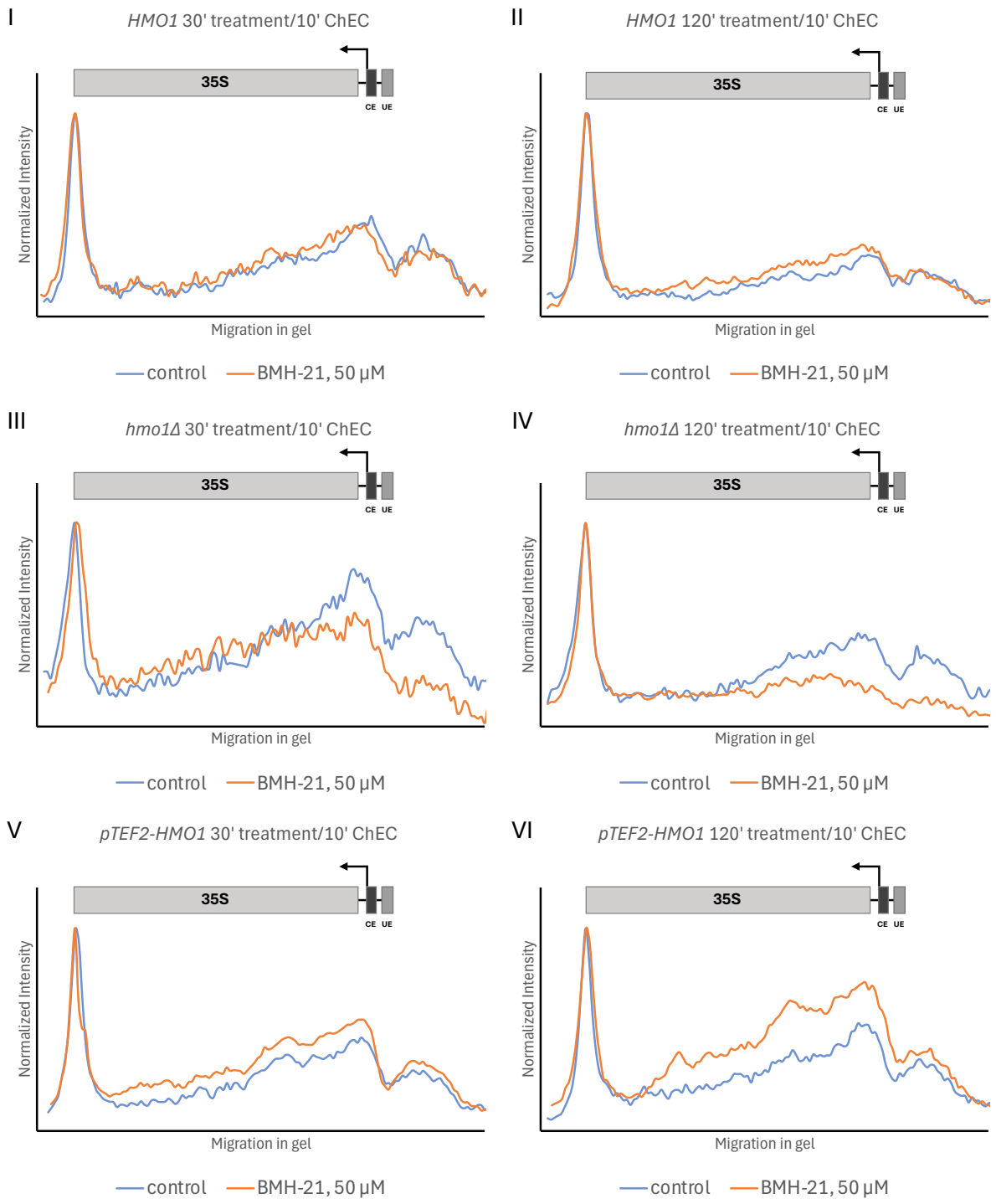

Figure 19: Profile analysis of Rpa190-MN mediated cleavage events at the endogenous rRNA gene after BMH-21 treatment

The Figure displays profiles of radioactive signal intensities plotted against the migration of DNA fragments on Southern membranes, as presented in Figure 18. The data were generated following the protocols detailed in section 5.3.4. Profiles were obtained from ChEC experiments at 10 minutes for both control (blue graphs) and BMH-21 treatments (orange graphs). The data were generated using MultiGauge software, which quantitatively captures the cleavage patterns. The profiles were generated using Microsoft Excel. Intensity values were normalized to the highest value, respectively. Schematics positioned above the profiles illustrate the XcmI-digested fragments and their corresponding features, in line with the descriptions provided in Figure 18.

6.3.2 Analysis of chromatin dynamics upon BMH-21 treatment in strains with different endogenous Hmo1 levels

BMH-21 treatment increases psoralen accessibility in rRNA genes and correlates with an increased number of rRNA genes in the open chromatin state

In all yeast strains analyzed, BMH-21 treatment markedly increased DNA accessibility to psoralen, especially after 30 minutes of incubation in the presence of the compound. This is evidenced by the observation that the 25S-rDNA fragments migrate with lower mobility in BMH-21-treated cells compared to those treated with DMSO. This was indicated by an upshift of the fragments in the autoradiograms (Fig. 20, Panels I and II, compare Lane 1 with 3, and 5 with 7), and a "left-shift" of the "BMH-21" profiles in Fig. 20 (Panels I, and II, orange graphs) when compared to the "DMSO" profiles (Panels I and II, blue graphs). The same tendencies were observed for the 18S-rDNA fragment also visualized in the Southern blot analysis (Suppl. Fig. 3). The decreased electrophoretic mobility strongly suggests that BMH-21 intercalates into the DNA, thereby facilitating subsequent psoralen intercalation. Although this tendencies might be also observed in samples 120 minutes of treatment (Fig. 20, Panels III, IV and V, compare Lane 9 with 11, 13 with 15, and 17 with 19 and see the corresponding graphs in each panel), an exception to this trend may occur in the *HMO1* overexpression strain, indicating that elevated Hmo1 levels can modulate the effects of BMH-21 on rDNA accessibility for psoralen under these conditions (Fig. 20, Panel V, compare Lane 17 with 19 and see the corresponding graphs in each panel).

Furthermore, treatment with BMH-21 consistently increased the fraction of open rRNA genes across all strains. This observation was supported by our ChEC experiments in the strain carrying a wild-type *HMO1* locus and the strain encompassing an additional chromosomally integrated cassette, which revealed both an increased degradation of the 35S rRNA gene fragment and presumably a lower density of Pol I molecules along the genes, indicated by an observed shift to higher fragment sizes. One plausible explanation is that BMH-21 interferes with the elongation phase of Pol I transcription. By blocking Pol I elongation, the drug prevents the initiation-competent Rrn3-Pol I complex from entering the gene, which may then relocate and assemble at an alternative promoter, converting that region into an open chromatin state. This effect is particularly pronounced in the *HMO1* overexpression strain, where chromatin appears to be especially susceptible to such alterations (Fig. 20, Panels II and V, compare Lane 5 with 7 and 17 with 19 and see the corresponding graphs in this panel). In *hmo1Δ* strains,

additional chromatin structural changes were observed. Not only was there an opening of the rRNA genes, but the distance between the two 25S-rDNA fragments derived from the open and the closed chromatin state became significantly reduced (Fig. 20, Panel IV, compare Lane 13 with 15 and see the corresponding graphs in this panel). Based on previous experience - indicating that a high-density of Pol I molecules increases accessibility of the transcribed region to psoralen (Ide et al., 2010; Wittner et al., 2011) - this narrowing suggests that very few Pol I enzymes are present in the transcribed region, further supporting the idea that the chromatin architecture in *hmo1Δ* strains in the presence of BMH-21 was markedly altered due to diminished Pol I occupancy and overall reduced transcriptional activity. Thus, despite the absence of Hmo1 and the strong decrease of Pol I transcription, rRNA genes remained in a partially open chromatin state in the presence of BMH-21.

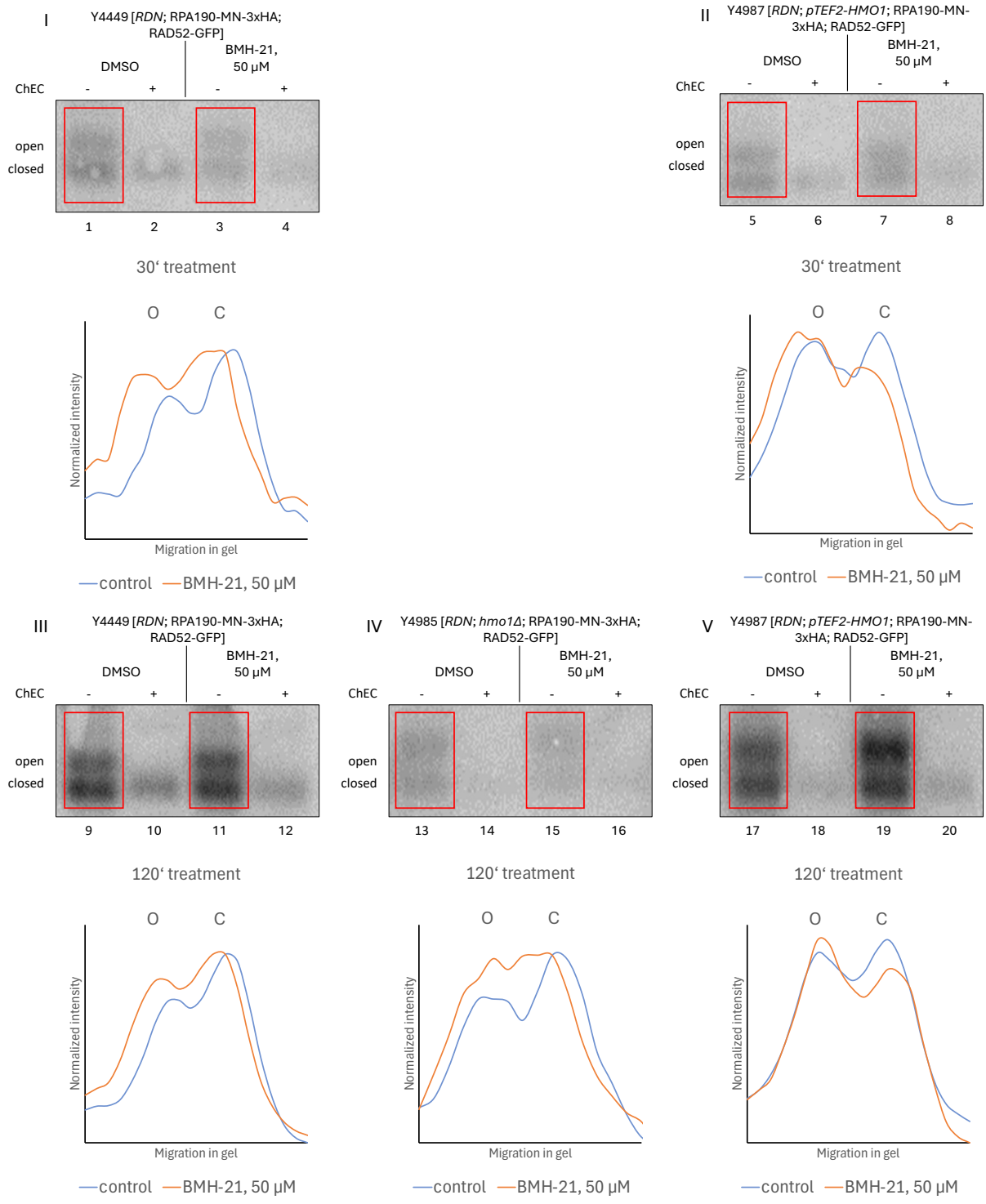

Figure 20: BMH-21 treatment increases psoralen accessibility in rRNA genes and correlates with an increased number of rRNA genes in the open chromatin state

Yeast strains Y4449 [*RDN*; RPA190-MN-3xHA; RAD52-GFP], Y4985 [*RDN*; *hmo1Δ*; RPA190-MN-3xHA; RAD52-GFP], and Y4987 [*RDN*; *pTEF2-HMO1*; RPA190-MN-3xHA; RAD52-GFP] were cultured in YPAD medium and treated with either DMSO (control) or 50 µM BMH-21. Samples were collected at 0, 30, and 120 minutes following treatment. ChEC analysis was performed as described in the legend of Figure 18, with samples taken at two time points: before (ChEC -) and after (ChEC +) the completion of the ChEC reaction. Further analysis of the psoralen cross-linked DNA was conducted as detailed in section 5.3.4, yielding a Southern membrane that was subsequently hybridized with Southern probe #34. This probe visualizes two EcoRI-digested fragments - one containing part of the 25S rDNA and the other part of the 18S rDNA - only the 25S rDNA is shown in this Figure. The autoradiograms

display the 0 ChEC samples from cells pretreated with DMSO and 50 µM BMH-21. The two bands correspond to the same 25S rDNA region and are annotated as representing either fragments derived from open state chromatin (O) or closed state chromatin (C). Profiles derived from the autoradiograms are provided, with the intensities of the bands (reflecting open and closed chromatin states) plotted against their migration in the agarose gel and normalized to the highest value of each graph, respectively, thus offering a quantitative representation of the chromatin state at the 25S rDNA region under the various treatment conditions.

Finally, upon induction of Rpa190-MN cleavage, the majority of 25S-rDNA fragments derived from open chromatin regions were degraded in both the DMSO control and in cells treated with BMH-21 for 120 minutes. This degradation indicates that Rpa190-MN remained bound to the 3' region of the rDNA gene even after prolonged BMH-21 treatment. Again, *hmo1Δ* strains behaved differently in this analysis since fragments derived from open 35S rRNA genes from cells cultured either in the presence of DMSO or BMH-21 were not as efficiently degraded as the corresponding fragments in *HMO1* wild-type and *HMO1* overexpression strains (Fig. 21, compare blue and yellow graphs in Panels II and V, I and IV, and III and VI).

Collectively, these findings reveal an important role for Hmo1 in the cellular response to the treatment with BMH-21. The data indicates that DNA-intercalating drugs, like BMH-21, may affect Pol I transcription likely by altering DNA-topology. In this scenario, Hmo1 might help to compensate topological changes, thereby assisting Pol I transcription in this condition.

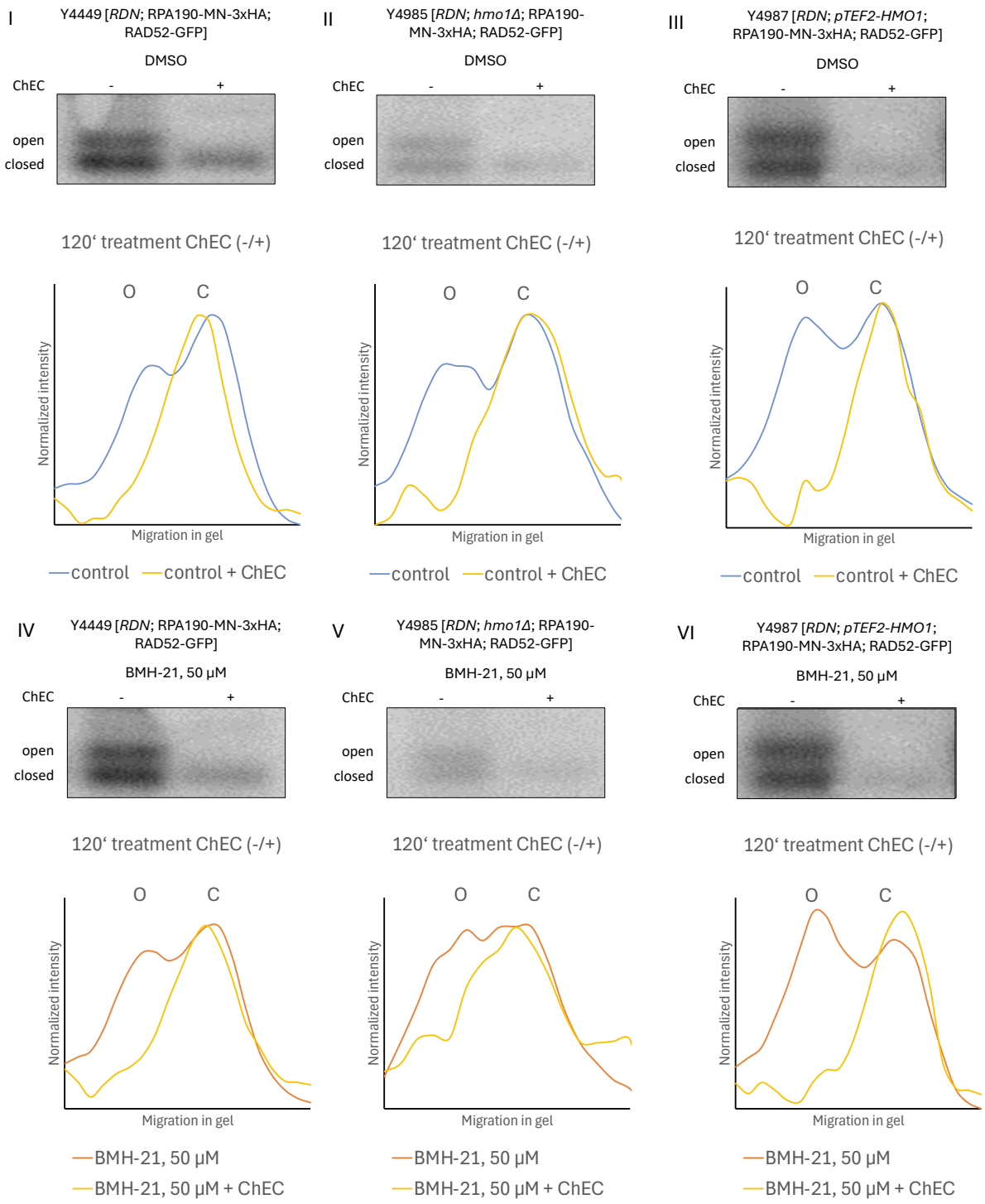

Figure 21: Rpa190-MN remains bound to the rDNA gene over the course of the experiment
Yeast strains Y4449 [*RDN*; RPA190-MN-3xHA; RAD52-GFP], Y4985 [*RDN*; *hmo1Δ*; RPA190-MN-3xHA; RAD52-GFP], and Y4987 [*RDN*; *pTEF2-HMO1*; RPA190-MN-3xHA; RAD52-GFP] were cultured in YPAD medium and treated as described in Figure 20. The autoradiograms display the 0 and 60-minute ChEC samples from cells pretreated with DMSO and 50 µM BMH-21. The two bands correspond to the same 25S rDNA region and are annotated as representing either fragments derived from open state chromatin (O) or closed state chromatin (C). Profiles derived from the autoradiograms are provided, with the intensities of the bands (reflecting open and closed chromatin states) plotted against their migration in the agarose gel and normalized to the highest value of each graph, respectively, thus offering a quantitative representation of the chromatin state at the 25S rDNA region under the various treatment conditions.

7. Discussion

The rDNA gene locus is among the most actively transcribed genomic regions in eukaryotic cells, reflecting its vital role in supporting cell growth and proliferation through robust ribosome biogenesis. The efficient production of ribosomes is tightly linked to chromatin organization, with the HMG-box protein Hmo1 playing a pivotal part in stabilizing an open chromatin conformation at the rDNA locus (Merz et al., 2008; Wittner et al., 2011). This arrangement ensures that rRNA genes remain accessible for transcription by Pol I - the enzyme responsible for synthesizing the majority of eukaryotic rRNA (reviewed in Nomura et al., 2013). Because Pol I-driven transcription underlies ribosome biogenesis, it has emerged as a prime target for anticancer strategies aimed at curtailing the unchecked proliferation of tumor cells (reviewed in Drygin et al., 2010; Ferreira et al., 2020; van Riggelen et al., 2010).

Among the small-molecule inhibitors that interfere with Pol I function, CX-5461 has been clinically investigated and holds promise for disrupting Pol I activity (Canadian Cancer Trials Group, 2022); however, yeast studies suggest that its cytotoxic effects may extend beyond Pol I inhibition, potentially implicating DNA damage pathways (Nagler, 2022; Xu et al., 2017). Another promising agent, BMH-21, interrupts Pol I transcription more directly through intercalation in the rDNA leading to the degradation of Pol I, thus positioning it as a compelling candidate for further development (Jacobs et al., 2021; Peltonen et al., 2010, 2014; Wei et al., 2018). Although both inhibitors reduce rRNA synthesis, they do so via distinct mechanisms, raising important questions regarding specificity, cellular impact, and overall therapeutic efficacy. Studies in yeast provide an ideal framework for dissecting these complexities, offering detailed insights into how such compounds engage Pol I and modulate chromatin architecture. Ultimately, this knowledge informs both the fundamental biology of ribosome biogenesis, and the ongoing refinement of clinical interventions designed to disrupt ribosome production in rapidly dividing cancer cells.

7.1 CX-5461 doesn't show Pol I-specific effects in yeast and leads to DNA fragmentation

The first aim of our study was to reproduce and confirm prior results from our laboratory (Nagler, 2022). Because CX-5461 precipitated in YPAD media (Jackobel et al., 2019) the latter work was conducted by pre-incubation of cells in the presence of the CX-5461 in buffer and subsequent plating on solid YPAD. Here, we found that the drug could be dissolved in minimal growth media. This allowed us to study yeast cell growth in the presence of CX-5461 in liquid media. Consistent with the earlier findings (Nagler, 2022), we observed a growth retardation at a concentration of 250 µM CX-5461. We additionally found, that CX-5461-dihydrochloride was an even more potent inhibitor of cell growth in liquid media (Fig. 6).

In accordance with Nagler, our data obtained upon treatment of *rdnΔ*, pPol II strains in which Pol I activity is no longer essential, treatment with CX-5461 more severely inhibited growth, although the opposite outcome was expected if the drug were a Pol I-specific inhibitor (Fig. 8). Furthermore, also in contrast to Pol I transcription being a primary CX-5461 target, growth of yeast strains carrying a lower rDNA copy number and highly transcribed individual rRNA genes with around 100 Pol I molecules per gene (French et al., 2003), was affected more than growth of an isogenic yeast strain carrying a wild-type number of rDNA repeats (Fig. 7). Taken together these results obtained in yeast diverge from the compound's selective Pol I-targeting profile reported in mammalian cells (Drygin et al., 2011; Mars et al., 2020) and instead align with the notion that CX-5461's cytotoxicity may involve additional mechanisms, such as DNA damage or replication stress (Bruno et al., 2020; Xu et al., 2017).

Indeed, while its ability to disrupt nucleolar function and rRNA synthesis is well-documented in higher eukaryotes - leading to apoptosis (through p53 pathway activation), G2 arrest, and heightened sensitivity to ATR or topoisomerase I inhibitors (Negi & Brown, 2015; Yan et al., 2021; reviewed in Deisenroth & Zhang, 2010; Jackson & Bartek, 2009) - our findings in yeast emphasize the multifaceted nature of CX-5461's action. Further dissecting these differences between yeast and mammalian systems will be essential for clarifying how best to exploit CX-5461's therapeutic potential, particularly as a component of combination regimens targeting ribosome biogenesis in rapidly dividing cancer cells.

7.2 BMH-21 triggers Rpa190 degradation and leads to increased susceptibility to psoralen crosslinking

In the next part of this study, we also aimed to reproduce and build upon previous observations from our laboratory regarding BMH-21 (Nagler, 2022). In line with experiments performed in the previous study, growth experiments indicated that 50 µM BMH-21 was the effective concentration in most experiments; however, in highly sensitive *hmo1Δ* cell lines, 25 µM BMH-21 were employed because treatment with 50 µM BMH-21 proved lethal. Moreover, we discovered that repeated freeze-thaw cycles markedly reduced the drug's effectiveness, suggesting that its stability is compromised under such conditions (Fig. 9).

The results of our growth analyses largely mirrored previous findings (Nagler, 2022), showing that BMH-21 treatment hinders yeast growth, apparently through Pol I-specific effects (Jacobs et al., 2021; Wei et al., 2018). Specifically, we observed that *rdnΔ*, pPol II strains - in contrast to yeast strains in which 35S rRNA was synthesized by Pol I - were only mildly affected in growth upon BMH-21 treatment, indicating a clear specificity for Pol I activity (Fig. 12). Additionally, yeast strains with a reduced rDNA copy number, characterized by increased Pol I activity and more open chromatin states, showed more pronounced growth impairment upon BMH-21 exposure compared to strains with wild-type copy number of rDNA repeats (Fig. 11). These observations collectively suggest that BMH-21 specifically inhibits Pol I-driven transcription rather than exerting cytotoxicity through other non-specific mechanisms.

In contrast to Nagler's observation of substantial Rpa190 degradation in *rdnΔ*, pPol II strains, our experiments revealed no significant degradation of this Pol I subunit in response to BMH-21, aligning more closely with the proposed mode of action (Fig. 15). Initially, we had also planned experiments analyzing if BMH-21 affected the stability of another Pol I subunit, Rpa43. Additionally, we started to investigate whether Pol II undergoes similar degradation upon treatment with BMH-21, to correlate the situation in yeast with recent findings in human cell-lines suggesting that chromatin damage by DNA intercalators can lead to RNA Polymerase II degradation (Espinoza et al., 2024). However, due to time constraints, these additional analyses could not be performed.

The impact of BMH-21 on Pol I-driven rRNA synthesis was proposed to involve its preferential intercalation into GC-rich DNA, making ribosomal DNA (rDNA) a prime target (Peltonen et al.,

2010, 2014). Besides its high GC content - e.g. ~45% in yeast rDNA compared to the genome-wide average of ~38% (Saccharomyces Cerevisiae S288c (ID 128) - BioProject - NCBI) - the open chromatin structure of rDNA may also contribute significantly to its susceptibility to BMH-21 binding. Consequently, BMH-21 could similarly affect other genomic regions characterized by high GC-content and accessible chromatin, which might explain the growth defects observed even in *rdnΔ*, pPol II strains.

7.3 Endogenous Hmo1 levels impact cellular growth, Pol I occupancy and alterations in rDNA chromatin structure upon BMH-21 treatment

The third major goal of this thesis was to examine how endogenous Hmo1 levels shape Pol I transcription and influence BMH-21 sensitivity. In our growth experiments, we initially observed that *hmo1Δ* cells were highly susceptible to BMH-21 treatment. This heightened sensitivity suggests that Hmo1 - likely through its direct physical association with the rRNA genes (Gadal et al., 2002; Merz et al., 2008; Wittner et al., 2011) - can effectively suppress or mitigate the inhibitory effects of BMH-21 on cell growth. By comparing the effects of BMH-21 in *rdnΔ*, pPol I and *rdnΔ*, pPol II strains carrying an *HMO1* deletion, we conclude that the elevated BMH-21 sensitivity observed in cells carrying a wildtype rDNA locus and lacking Hmo1 is primarily attributable to its function in Pol I transcription (Fig. 14).

At the protein level, our comprehensive analyses revealed a notable relationship between endogenous Hmo1 levels and Rpa190 stability upon BMH-21 treatment. While the loss of Hmo1 was found to enhance BMH-21 mediated degradation of Rpa190 (Fig. 16), the overexpression of *HMO1* partially prevented this degradation (Fig. 17). These findings correlated with the suppression of growth defects upon BMH-21 observed with *HMO1*-overexpressing cells. Moreover, our observations that there was no significant degradation of Rpa190 in *rdnΔ*/pPol II yeast strains were in good correlation with findings in human cell lines demonstrating that significant degradation of the large Pol I subunit does not occur in cells lacking active Pol I transcription (Wei et al., 2018). As another line of investigation, ChEC assays provided mechanistic insights, indicating that Pol I occupancy at the rDNA locus is differentially affected by BMH-21 treatment, depending on the Hmo1 expression level. Interestingly, while we observed a marginal increase in Pol I occupancy in wild-type cells upon exposure to BMH-21 - a finding that

potentially conflicts with results from (Jacobs et al., 2021) - BMH-21 treatment led to a substantial reduction in Pol I occupancy in *hmo1Δ* cells . In contrast, in cells overexpressing *HMO1* Pol I accumulated in rRNA genes in the presence of BMH-21, indicating that Hmo1 may stabilize Pol I's engagement with rDNA chromatin under drug-induced stress (Fig. 18, Fig. 19).

Our observations are paralleling Nagler's findings, suggesting that BMH-21 treatment may influence Pol I occupancy and Hmo1 recruitment at rRNA genes (Nagler, 2022). Consistent with our results, Nagler observed a modest increase in Pol I occupancy at 35S rRNA gene sequences in yeast strains carrying a wild-type rDNA locus following exposure to BMH-21. He also found that Hmo1 association with the rDNA increased significantly in this condition, supporting our interpretation that Hmo1 binding may promote recruitment of Pol I or stabilize the enzyme at 35S rRNA gene sequences in the presence of BMH-21.

Finally, our experiments showed clearly that BMH-21 treatment significantly increases psoralen accessibility of the rDNA, which indicates that the BMH-21 DNA-intercalation may alter the DNA-topology. It is important to note that we did not examine whether BMH-21 specifically alters psoralen accessibility at the rDNA locus or if similar changes occur broadly across other genomic regions. Thus, future experiments aimed at dissecting the genomic specificity of BMH-21's effects could greatly enhance our understanding of its mechanisms of action (Fig. 20, Fig. 21). Comparing the roles of Hmo1 and UBF1, both proteins may similarly stabilize Pol I complexes at rRNA genes, influencing sensitivity to Pol I inhibitors such as BMH-21 (Mais et al., 2005; Stefanovsky et al., 2001; reviewed in Sanij & Hannan, 2009). However, so far it has not been investigated if UBF1 plays a role in the cellular response to BMH-21 in higher eukaryotes.

7.4 Summary and Outlook

In this study, we successfully replicated and expanded previous findings from our working group, providing new insights into how designated Pol I specific inhibitors act in *Saccharomyces cerevisiae*. We were able to confirm that CX-5461 cytotoxicity in yeast was not strictly Pol I-specific. This observation calls for further research to elucidate the compound's precise mechanisms, especially given its documented roles in triggering replication stress and DNA damage responses. A deeper understanding of CX-5461's multifaceted mode of action could prove

vital for optimizing its therapeutic potential, particularly in the context of combination treatments targeting ribosome biogenesis in cancer.

Our experiments strongly support that BMH-21 primarily targets Pol I transcription, and that Hmo1 has a significant impact on the Pol I-specific effects of the compound in yeast. Notably, our ChEC and ChEC-Psoralen assays were each performed only once, so replicating these experiments will be essential to validate and refine our preliminary findings.

Overall, our findings and future studies may deepen our understanding of how small-molecule inhibitors target and affect Pol I transcription and rDNA chromatin structure, laying the groundwork for refined therapeutic strategies that exploit vulnerabilities in ribosome biogenesis**.**

8. Supplements

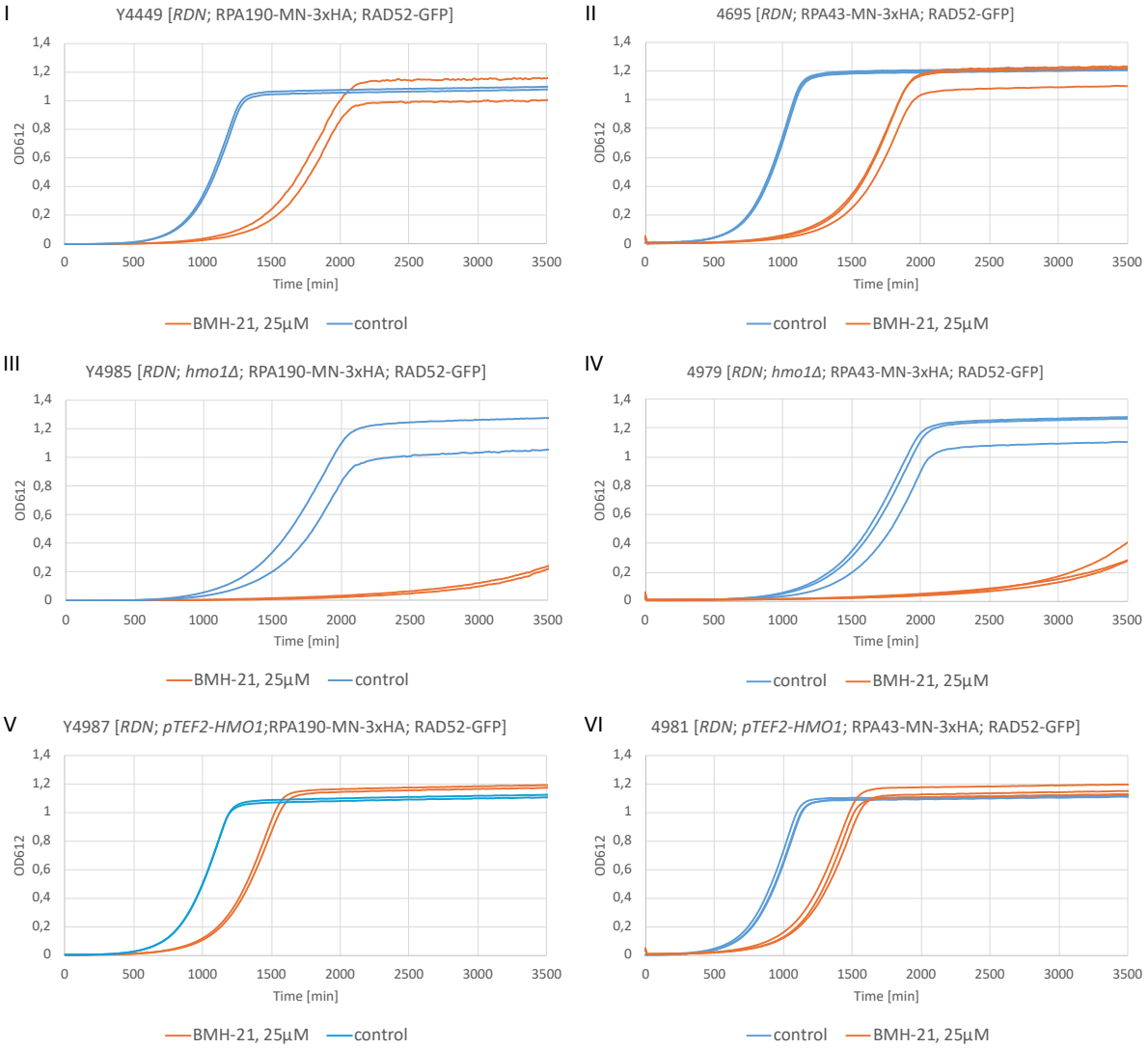

Supplementary Figure 1: Yeast strains expressing either Pol I subunit Rpa43 or Rpa190 in fusion with MNase and varying in endogenous Hmo1 levels behave identical in their response to BMH-21
Growth graphs (OD612) were recorded over time for six yeast strains cultured in a TECAN plate reader at 30 °C, with cells exposed to either 25 µM BMH-21 or an equivalent volume of DMSO (control). The six genotypes examined were: **(I)** Y4449 [*RDN*; RPA190-MN-3×HA; RAD52-GFP], which carries a wild-type RDN gene locus as well as an MNase tag on Rpa190; **(II)** Y4695 [*RDN*; RPA43-MN-3×HA; RAD52-GFP], which carries a wild-type RDN gene locus as well as an MNase tag on Rpa43; **(III)** Y4985 [*RDN*; *hmo1Δ*; RPA190-MN-3×HA; RAD52-GFP], which lacks Hmo1 and is tagged at Rpa190; **(IV)** Y4979 [*RDN*; *hmo1Δ*; RPA43-MN-3×HA; RAD52-GFP], which lacks Hmo1 and is tagged at Rpa43; **(V)** Y4987 [*RDN*; *pTEF2-HMO1*; RPA190-MN-3×HA; RAD52-GFP], which overexpresses Hmo1 and is tagged at Rpa190; and **(VI)** Y4981 [*RDN*; *pTEF2-HMO1*; RPA43-MN-3×HA; RAD52-GFP],. The optical density at 612 nm (OD612) was measured every 15 minutes and plotted against the time of growth. The growth graphs for the different conditions are color-coded as indicated in the legend. Cells were grown in two (I, II, V) or three (II, IV, VI) independent cultures for each condition, respectively. Two technical replicates have been created of this experiment.

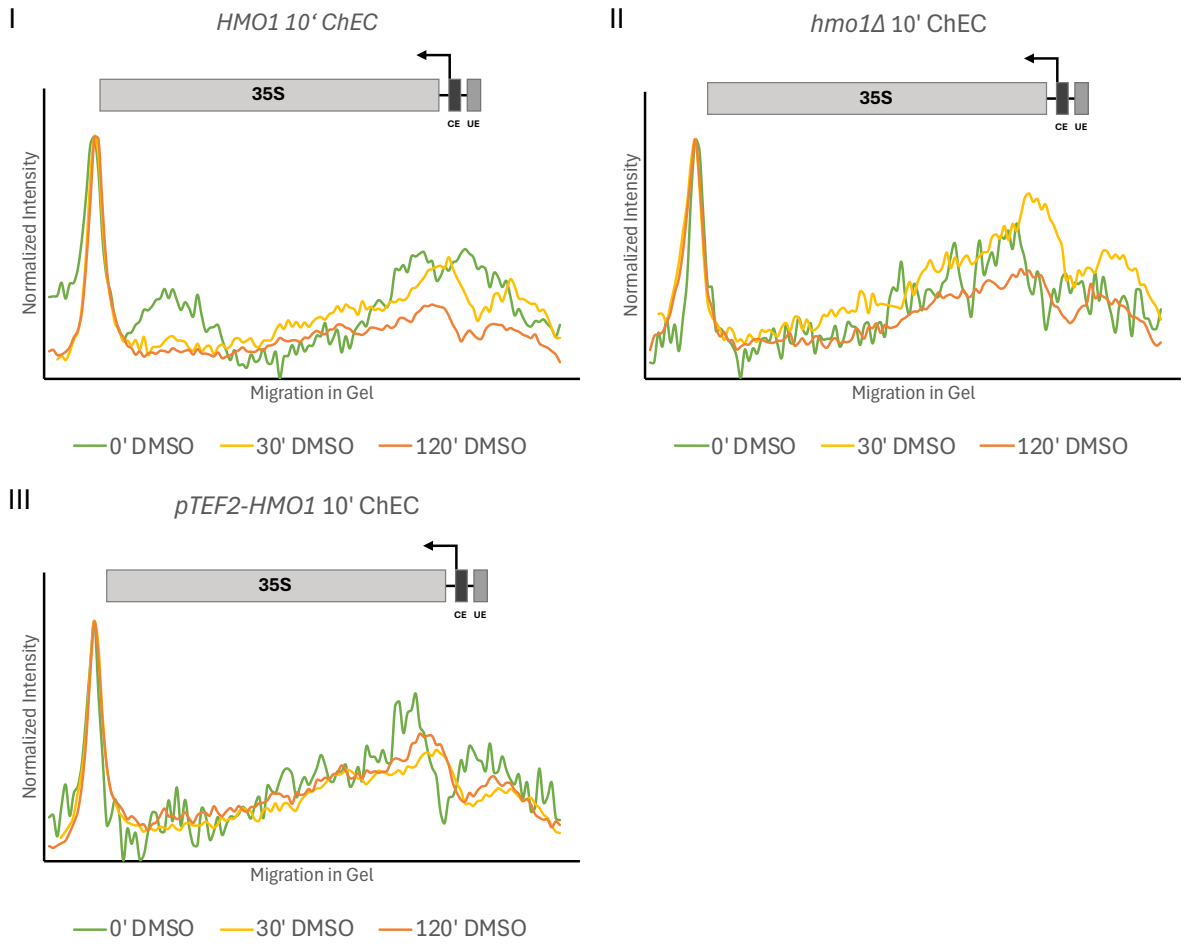

Supplementary Figure 2: Profile analysis of Rpa190-MN mediated cleavage events at the endogenous rRNA gene after BMH-21 treatment

The Figure displays profiles of radioactive signal intensities plotted against the migration of DNA fragments on Southern membranes, as presented in Figure 18. The data were generated following the protocols detailed in section 5.3.4. Profiles were obtained from ChEC experiments at 10 minutes for DMSO control samples at 0 (green graphs), 30 (yellow graphs) and 120 minutes (orange graphs). The data were generated using MultiGauge software, which quantitatively captures the cleavage patterns. The profiles were generated using Microsoft Excel. Intensity values were normalized to the highest value, respectively. Schematics positioned above the profiles illustrate the XcmI-digested fragments and their corresponding features, in line with the descriptions provided in Figure 18.

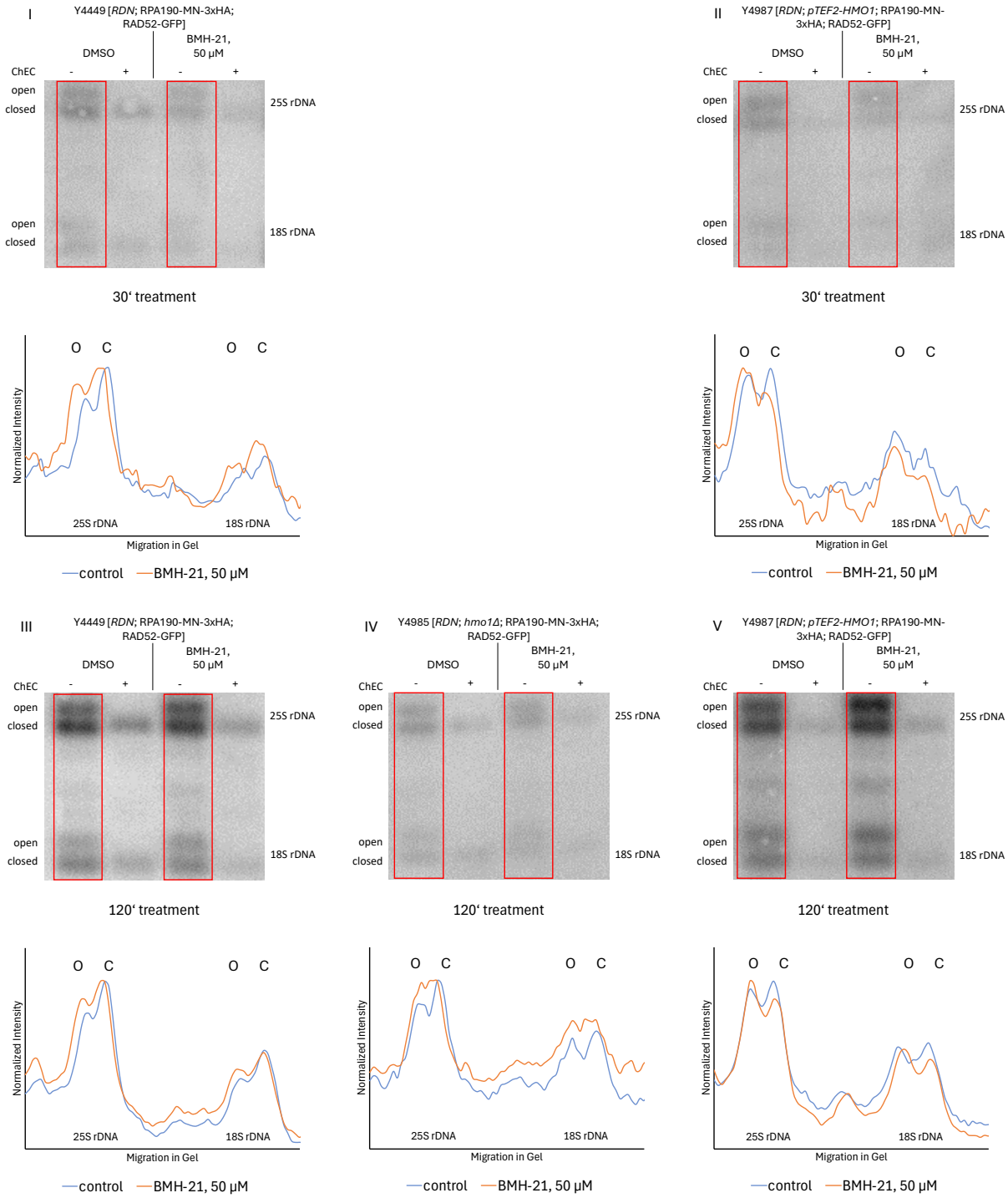

Supplementary Figure 3: Autoradiograms and profile analyses of 25S and 18S rDNA regions
Yeast strains Y4449 [*RDN*; RPA190-MN-3xHA; RAD52-GFP], Y4985 [*RDN*; *hmo1Δ*; RPA190-MN-3xHA; RAD52-GFP], and Y4987 [*RDN*; *pTEF2-HMO1*; RPA190-MN-3xHA; RAD52-GFP] were cultured in YPAD medium and treated as described in Figure 20. The autoradiograms display the 0 and 60-minute ChEC samples from cells pretreated with DMSO and 50 µM BMH-21. The upper two bands correspond to the same 25S rDNA region and are annotated as representing either fragments derived from open state chromatin (O) or closed state chromatin (C). The lower two bands correspond to the same 18S rDNA region and are annotated accordingly. Profiles derived from the autoradiograms are provided, with the intensities of the bands (reflecting open and closed chromatin states) plotted against their migration in the agarose gel and normalized to the highest value of each graph, respectively, thus offering a quantitative representation of the chromatin state at the 25S and 18S rDNA regions under the various treatment conditions

9. List of Figures

10. List of Tables

11. References

Achar, Y. J., Adhil, M., Choudhary, R., Gilbert, N., & Foiani, M. (2020). Negative supercoil at gene boundaries modulates gene topology. *Nature*, *577*(7792), 701–705. https://doi.org/10.1038/s41586-020-1934-4

Albert, B., Colleran, C., Léger-Silvestre, I., Berger, A. B., Dez, C., Normand, C., Perez-Fernandez, J., McStay, B., & Gadal, O. (2013). Structure-function analysis of Hmo1 unveils an ancestral organization of HMG-Box factors involved in ribosomal DNA transcription from yeast to human. *Nucleic Acids Research*, *41*(22), 10135–10149. https://doi.org/10.1093/nar/gkt770

Albert, B., Leger-Silvestre, I., Normand, C., Ostermaier, M. K., Perez-Fernandez, J., Panov, K. I., Zomerdijk, J. C. B. M., Schultz, P., & Gadal, O. (2011). RNA polymerase I-specific subunits promote polymerase clustering to enhance the rRNA gene transcription cycle. *The Journal of Cell Biology*, *192*, 277–293. https://doi.org/10.1083/jcb.201006040.

Baudin, F., Murciano, B., Fung, H. Y. J., Fromm, S. A., Mattei, S., Mahamid, J., & Müller, C. W. (2022). Mechanism of RNA polymerase I selection by transcription factor UAF. *Science Advances*, *8*, 5725. https://doi.org/10.1126/sciadv.abn5725.

Beckouet, F., Labarre-Mariotte, S., & Albert, B. (2008). Two RNA polymerase I subunits control the binding and release of Rrn3 during transcription. *Molecular and Cellular Biology*, *28*(5), 1596–1605. https://doi.org/10.1128/MCB.01501-07.

Bell, S. P., Jantzen, H. M., & Tjian, R. (1990). Assembly of alternative multiprotein complexes directs rRNA promoter selectivity. *Genes & Development*, *4*(6), 943–954. https://doi.org/10.1101/gad.4.6.943

Bell, S. P., Learned, R. M., Jantzen, H. M., & Tjian, R. (1988). Functional cooperativity between transcription factors UBF1 and SL1 mediates human ribosomal RNA synthesis. *Science (New York, N.Y.)*, *241*(4870), 1192–1197. https://doi.org/10.1126/science.3413483

Berger, A. B., Decourty, L., Badis, G., Nehrbass, U., Jacquier, A., & Gadal, O. (2007). Hmo1 Is Required for TOR-Dependent Regulation of Ribosomal Protein Gene Transcription. *Molecular and Cellular Biology*, *27*(22), 8015–8026. https://doi.org/10.1128/MCB.01102-07

Bermejo, R., Capra, T., Gonzalez-Huici, V., Fachinetti, D., Cocito, A., Natoli, G., Katou, Y., Mori, H., Kurokawa, K., Shirahige, K., & Foiani, M. (2009). Genome-Organizing Factors Top2 and Hmo1 Prevent Chromosome Fragility at Sites of S phase Transcription. *Cell*, *138*(5), 870–884. https://doi.org/10.1016/j.cell.2009.06.022

Bird, A. P. (1986). CpG-rich islands and the function of DNA methylation. *Nature*, *321*(6067), 209–213. https://doi.org/10.1038/321209a0.

Brachmann, C. B., Davies, A., Cost, G. J., Caputo, E., Li, J., Hieter, P., & Boeke, J. D. (1998). Designer deletion strains derived from Saccharomyces cerevisiae S288C: A useful set of strains and plasmids for PCR-mediated gene disruption and other applications. *Yeast (Chichester, England)*, *14*(2), 115–132. https://doi.org/10.1002/(SICI)1097-0061(19980130)14:2<115::AID-YEA204>3.0.CO;2-2

Brewer, B. J., & Fangman, W. L. (1988). A replication fork barrier at the 3' end of yeast ribosomal RNA genes. *Cell*, *55*(4), 637–643. https://doi.org/10.1016/0092-8674(88)90221-0.

Brill, S. J., DiNardo, S., Voelkel-Meiman, K., & Sternglanz, R. (1987). DNA topoisomerase activity is required as a swivel for DNA replication and for ribosomal RNA transcription. *NCI Monographs: A Publication of the National Cancer Institute*, *4*, 11–15.

Bruno, P. M., Liu, Y., & Park, G. Y. (2020). A small molecule targeting topoisomerase II via a topoisomerase poisoning mechanism in cancer therapy. *Cancer Cell*, *37*(3), 484-498 9. https://doi.org/10.1016/j.ccell.

Burger, K., Mühl, B., Harasim, T., Rohrmoser, M., Malamoussi, A., Orban, M., Kellner, M., Gruber-Eber, A., Kremmer, E., Hölzel, M., & Eick, D. (2010). Chemotherapeutic drugs inhibit ribosome biogenesis at multiple levels. *Journal of Biological Chemistry*, *285*(16), 12416–12425. https://doi.org/10.1074/jbc.M109.074211.

Bywater, M. J. (2012). Inhibition of RNA polymerase I as a therapeutic strategy to promote cancer-specific activation of p53. *Cancer Cell*, *22*(1), 51–65. https://doi.org/10.1016/j.ccr.2012.05.008.

Canadian Cancer Trials Group. (2022). Results of the phase I CCTG IND.231 trial of CX-5461 in patients with advanced solid tumors enriched for DNA-repair deficiencies. *Nat Commun*. https://doi.org/10.1038/s41467-022-31199-2.

Cherry, J. M., Hong, E. L., & Amundsen, C. (2012). Saccharomyces Genome Database: The genomics resource of budding yeast. *Nucleic Acids Research*, *40*(D1), 700–705. https://doi.org/10.1093/nar/gkr1029

Cioci, F., Vu, L., Eliason, K., Oakes, M., Siddiqi, I. N., & Nomura, M. (2003). Silencing in yeast rDNA chromatin. Reciprocal relationship in gene expression between RNA polymerase I and II. *Molecular Cell*, *12*, 135–145. https://doi.org/10.1016/S1097-2765(03)00238-6.

Conconi, A., Widmer, R. M., Koller, T., & Sogo, J. M. (1989). Two different chromatin structures coexist in ribosomal RNA genes throughout the cell cycle. *Cell*, *57*(5), 753–761. https://doi.org/10.1016/0092-8674(89)90788-2

Cormack, B. P., & Struhl, K. (1992). The TATA-binding protein is required for transcription by all three nuclear RNA polymerases in yeast cells. *Cell*, *69*(4), 685–696. https://doi.org/10.1016/0092-8674(92)90274-U.

Cornelison, R., Dobbin, Z. C., & Katre, A. A. (2017). Targeting RNA polymerase I to inhibit ribosome biogenesis in both chemosensitive and chemoresistant ovarian cancer cells. *Clinical Cancer Research*, *23*(3), 652–663.

Daiß, J. L., Griesenbeck, J., Tschochner, H., & Engel, C. (2023). Synthesis of the ribosomal RNA precursor in human cells: Mechanisms, factors and regulation. *Biological Chemistry*, *404*(11–12), 1003–1023. https://doi.org/10.1515/hsz-2023-0214

Dammann, R., Lucchini, R., Koller, T., & Sogo, J. M. (1993). Chromatin structures and transcription of rDNA in yeast Saccharomyces cerevisiae. *Nucleic Acids Research*, *21*(10), 2331–2338. https://doi.org/10.1093/nar/21.10.2331.

Deisenroth C., & Zhang Y. (2010). Ribosome biogenesis surveillance: Probing the ribosomal protein–Mdm2–p53 pathway. *Oncogene*, *29*(30), 4253–4260. https://doi.org/10.1038/onc.2010.189.

Drygin, D., Rice, W. G., & Grummt, I. (2010). The RNA polymerase I transcription machinery: An emerging target for the treatment of cancer. *Annual Review of Pharmacology and Toxicology*, *50*, 131–156. https://doi.org/10.1146/annurev.pharmtox.010909.105844.

Drygin, D., Rice, W. G., & Grummt, I. (2011). Targeting RNA polymerase I with an oral small molecule CX- 5461 inhibits ribosomal RNA synthesis and solid tumor growth. *Cancer Research*, *71*(4), 1418–1430. https://doi.org/10.1158/0008-5472.CAN-10-1728.

Elion, E. A., & Warner, J. R. (1984). An RNA polymerase I enhancer in Saccharomyces cerevisiae. *Cell*, *39*(3 Pt 2), 663–673. https://doi.org/10.1016/0092-8674(84)90476-0.

Engel, C., Plitzko, J., & Cramer, P. (2016). RNA polymerase I–Rrn3 complex at 4.8 Å resolution. *Nature Communications*, *7*(1), 12129. https://doi.org/10.1038/ncomms12129

Espinoza, J. A., Kanellis, D. C., Saproo, S., Leal, K., Martinez, J. F., Bartek, J., & Lindström, M. S. (2024). Chromatin damage generated by DNA intercalators leads to degradation of RNA Polymerase II. *Nucleic Acids Research*, *52*(8), 4151–4166. https://doi.org/10.1093/nar/gkae069

Fahy, D., Conconi, A., & Smerdon, M. J. (2005). Rapid changes in transcription and chromatin structure of ribosomal genes in yeast during growth phase transitions. *Experimental Cell Research*, *305*(2), 365–373. https://doi.org/10.1016/j.yexcr.2005.01.016

Ferreira, R., Schneekloth, J. S., Jr, Panov, K. I., Hannan, K. M., & Hannan, R. D. (2020). Targeting the RNA Polymerase I Transcription for Cancer Therapy Comes of Age. *Cells*, *9*(2), 266. https://doi.org/10.3390/cells9020266

Finch, J. T., & Klug, A. (1976). Solenoid model for superstructure in chromatin. *Proceedings of the National Academy of Sciences*, *73*(6), 1897–1901. https://doi.org/10.1073/pnas.73.6.1897.

French, S. L., Osheim, Y. N., Cioci, F., Nomura, M., & Beyer, A. L. (2003). In exponentially growing Saccharomyces cerevisiae cells, rRNA synthesis is determined by the summed RNA polymerase I loading rate rather than by the number of active genes. *Molecular and Cellular Biology*, *23*(5), 1558–1568. https://doi.org/10.1128/MCB.23.5.1558-1568.2003.

French, S. L., Sikes, M. L., Hontz, R. D., Osheim, Y. N., Lambert, T. E., El Hage, A., Smith, M. M., D., T., Smith, J. S., & Beyer, A. L. (2011). Distinguishing the roles of Topoisomerases I and II in relief of transcription-induced torsional stress in yeast rRNA genes. *Mol Cell Biol*. https://doi.org/10.1128/MCB.00589-10.

Friedrich, J. K., Panov, K. I., Cabart, P., Russell, J., & Zomerdijk, J. C. B. M. (2005). TBP-TAF Complex SL1 Directs RNA Polymerase I Pre-initiation Complex Formation and Stabilizes Upstream Binding Factor at the rDNA Promoter. *Journal of Biological Chemistry*, *280*(33), 29551–29558. https://doi.org/10.1074/jbc.M501595200

Fu, X., Xu, L., Qi, L., Tian, H., Yi, D., Yu, Y., Liu, S., Li, S., Xu, Y., & Wang, C. (2017). BMH-21 inhibits viability and induces apoptosis by p53-dependent nucleolar stress responses in SKOV3 ovarian cancer cells. *Oncol Rep*. https://doi.org/10.3892/or.2017.5750.

Gadal, O., Mariotte-Labarre, S., & Chedin, S. (2002). A functional requirement for the HMG box protein Hmo1 in yeast rRNA transcription and ribosome biogenesis. *Molecular and Cellular Biology*, *22*(4), 6196–6207. https://doi.org/10.1128/MCB.22.18.6196-6207.2002.

Ganley, A. R. D., Hayashi, K., Horiuchi, T., & Kobayashi, T. (2005). Identifying gene-independent noncoding functional elements in the yeast ribosomal DNA by phylogenetic footprinting. *Proceedings of the National Academy of Sciences of the United States of America*, *102*, 11787–11792. https://doi.org/10.1073/pnas.0504905102.

Geiduschek, E. P., & Kassavetis, G. A. (2001). The RNA polymerase III transcription apparatus. *Annual Review of Biochemistry*, *70*, 791–828. https://doi.org/10.1146/annurev.biochem.70.1.79.1

Ghaemmaghami, S., Huh, W. K., & Bower, K. (2003). Global analysis of protein expression in yeast. *Nature*, *425*(6959), 737–741. https://doi.org/10.1038/nature02046.

Girbig, M., Misiaszek, A. D., & Müller, C. W. (2022). Structural insights into nuclear transcription by eukaryotic DNA-dependent RNA polymerases. *Nature Reviews Molecular Cell Biology*, *23*(9), 603–622. https://doi.org/10.1038/s41580-022-00476-9

Goetze, H., Wittner, M., Hamperl, S., Hondele, M., Merz, K., Stoeckl, U., & Griesenbeck, J. (2010). Alternative Chromatin Structures of the 35S rRNA Genes in *Saccharomyces cerevisiae* Provide a Molecular Basis for the Selective Recruitment of RNA Polymerases I and II. *Molecular and Cellular Biology*, *30*(8), 2028–2045. https://doi.org/10.1128/MCB.01512-09

Griesenbeck, J., M., W., R., C., & A, C. (2012). Chromatin Endogenous Cleavage and Psoralen Crosslinking Assays to Analyze RRNA Gene Chromatin In Vivo'. In A. Vancura (Ed.), *Transcriptional Regulation: Meth- ods and Protocols* (pp. 291–301). Springer. https://doi.org/10.1007/978-1-61779-376-9_20.

Hall, D. B., Wade, J. T., & Struhl, K. (2006). An HMG protein binds to the 5' ends of yeast GAL1–10 genes and cooperates with TFIID in promoter activation. *Genes & Development*, *20*(15), 2037–2048. https://doi.org/10.1101/gad.1439206.

Hamdane, N., Stefanovsky, V. Y., Tremblay, M. G., Németh, A., Paquet, E., Lessard, F., Sanij, E., Hannan, R., & Moss, T. (2014). Conditional Inactivation of Upstream Binding Factor Reveals Its Epigenetic Functions and the Existence of a Somatic Nucleolar Precursor Body. *PLoS Genetics*, *10*(8), e1004505. https://doi.org/10.1371/journal.pgen.1004505

Hamperl, S., Wittner, M., Babl, V., Perez-Fernandez, J., Tschochner, H., & Griesenbeck, J. (2013). Chromatin states at ribosomal DNA loci. *Biochimica et Biophysica Acta (BBA) - Gene Regulatory Mechanisms*, *1829*(3–4), 405–417. https://doi.org/10.1016/j.bbagrm.2012.12.007

Henderson, A. S., Warburton, D., & Atwood, K. C. (1972). Location of ribosomal DNA in the human chromosome complement. *Proceedings of the National Academy of Sciences*, *69*(12), 3394–3398. https://doi.org/10.1073/pnas.69.12.3394.

Herdman, C., Mars, J. C., & Stefanovsky, V. Y. (2017). A unique interdependence of UBF1 and RNA polymerase I in rDNA transcription and nucleolar integrity. *Genes & Development*, *31*(8), 822–834. https://doi.org/10.1101/gad.298307.117.

Hernandez-Verdun, D. (2006). Nucleolus: From structure to dynamics. *Histochemistry and Cell Biology*, *125*(1–2), 127–137. https://doi.org/10.1007/s00418-005-0026-4.

Hontz, R. D., French, S. L., Oakes, M. L., Tongaonkar, P., Nomura, M., Beyer, A. L., & Smith, J. S. (2008). Transcription of Multiple Yeast Ribosomal DNA Genes Requires Targeting of UAF to the Promoter by Uaf30. *Molecular and Cellular Biology*, *28*(21), 6709–6719. https://doi.org/10.1128/MCB.00703-08

Hori, Y., Engel, C., & Kobayashi, T. (2023). Regulation of ribosomal RNA gene copy number, transcription and nucleolus organization in eukaryotes. *Nature Reviews. Molecular Cell Biology*, *1-16. DOI*, 10 1038 41580-022-00573–00579.

Ide, S., Miyazaki, T., Maki, H., & Kobayashi, T. (2010). Abundance of ribosomal RNA gene copies maintains genome integrity. *Science (New York, N.Y.)*, *327*(5966), 693–696. https://doi.org/10.1126/science.1179044

Jackobel, A. J., Zeberl, B. J., Glover, D. M., Fakhouri, A. M., & Knutson, B. A. (2019). DNA binding preferences of S. cerevisiae RNA polymerase I core factor reveal a preference for the GC-minor groove and a conserved binding mechanism. *Biochimica et Biophysica Acta (BBA) - Gene Regulatory Mechanisms*, *1862*(9), 194408. https://doi.org/10.1016/j.bbagrm.2019.194408.

Jackson, S. P., & Bartek, J. (2009). The DNA-damage response in human biology and disease. *Nature*, *461*(7267), 1071–1078. https://doi.org/10.1038/nature08467.

Jacobs, R. Q., Huffines, A. K., Laiho, M., & Schneider, D. A. (2021). The small-molecule BMH-21 directly inhibits transcription elongation and DNA occupancy of RNA polymerase I in vivo and in vitro. *Journal of Biological Chemistry*, *298*(1), 101450. https://doi.org/10.1016/j.jbc.2021.101450.

Jantzen, H. M., Admon, A., Bell, S. P., & Tjian, R. (1990). Nucleolar transcription factor hUBF contains a DNA-binding motif with homology to HMG box proteins. *Nature*, *344*(6268), 830–836. https://doi.org/10.1038/344830a0.

Jordan, P., & Carmo-Fonseca, M. (1998). Cisplatin inhibits synthesis of ribosomal RNA in vivo. *Nucleic Acids Research*, *26*(12), 2831–2836. https://doi.org/10.1093/nar/26.12.2831

Kasahara, K., Ohtsuki, K., Ki, S., Aoyama, K., Takahashi, H., Kobayashi, T., Shirahige, K., & Kokubo, T. (2007). Assembly of regulatory factors on rRNA and ribosomal protein genes in Saccharomyces cerevisiae. *Molecular and Cellular Biology*, *27*(19), 6686–6705. https://doi.org/10.1128/MCB.00876-07

Kasahara, M., Ohyama, Y., & Kokubo, T. (2011). Yeast HMG-box protein Hmo1 is a transcription factor that requires the TATA-binding protein for its recruitment to the promoters of a large subset of ribosomal protein genes. *Journal of Biological Chemistry*, *286*(23), 20106–20117. https://doi.org/10.1074/jbc.M111.230342.

Keener, J., Dodd, J. A., Lalo, D., & Nomura, M. (1997). Histones H3 and H4 are components of upstream activation factor required for the high-level transcription of yeast rDNA by RNA polymerase I. *Proceedings of the National Academy of Sciences*, *94*(25), 13458–13462. https://doi.org/10.1073/pnas.94.25.13458.

Keys, D. A., Dodd, J. A., & Nguyen, T. T. (1994). Rrn7 is a gene uniquely required for yeast RNA polymerase I transcription. *Genes & Development*, *8*(19), 2349–2362. https://doi.org/10.1101/gad.8.19.2349.

Keys, D. A., Dodd, J. A., & Nguyen, T. T. (1996). The dynamics of yeast RNA polymerase I transcription initiation. *Genes & Development*, *10*(16), 2015–2028. https://doi.org/10.1101/gad.10.16.2015.

Kim, D. W., Wu, N., & Kim, Y. (2016). *Discovery of CX-5461 and preclinical evidence of efficacy in small cell lung cancer models*. https://doi.org/10.1101/gad.279307.116.

Knutson, B. A., & Hahn, S. (2011). *Yeast Rrn7 and human TAF1B are TFIIB-related RNA polymerase I general transcription factors. Science* (Vol. 333, pp. 1637–1640). https://doi.org/10.1126/science.1207699.

Kobayashi, T., & Ganley, A. R. D. (2005). Recombination regulation by transcription-induced cohesin dissociation in rDNA repeats. *Science*, *309*(5740), 1581–1584. https://doi.org/10.1126/science.1114936.

Kobayashi, T., Heck, D. J., Nomura, M., & Horiuchi, T. (1998). Expansion and contraction of ribosomal DNA repeats in Saccharomyces cerevisiae. Requirement of replication fork blocking (Fob1) protein and the role of RNA polymerase I. *Genes & Development*, *12*, 3821–3830. https://doi.org/10.1101/gad.12.24.3821.

Kobayashi, T., Hidaka, K., Nishizawa, J., & Horiuchi, T. (1992). Identification of a site required for the polar replication fork barrier in the rRNA gene cluster of Saccharomyces cerevisiae. *Molecular and General Genetics*, *233*(1–2), 355–362. https://doi.org/10.1007/BF00587521.

Kornberg, R. D. (1974). Chromatin structure: A repeating unit of histones and DNA. *Science*, *184*(4139), 868–871. https://doi.org/10.1126/science.184.4139.868.

Kornberg, R. D., & Lorch, Y. (1999). Twenty-five years of the nucleosome, fundamental particle of the eukaryote chromosome. *Cell*, *98*(3), 285–294. https://doi.org/10.1016/S0092-8674(00)81991-1.

Lalo, D., Miyake, T., & Johnson, T. E. (1996). Mapping essential sequences of the yeast rRNA gene promoter with linker scanning mutations: Roles of upstream and core elements. *Journal of Biological Chem- Istry*, *271*(35), 21076–21082. https://doi.org/10.1074/jbc.271.35.21076.

Lane, D. P. (1992). P53, guardian of the genome. *Nature*, *358*(6381), 15–16. https://doi.org/10.1038/358015a0.

Lang, W., & Reeder, R. H. (1993). Transcription termination of RNA polymerase I due to a T-rich element and the TTFI factor. *Genes & Development*, *7*(9), 1735–1745. https://doi.org/10.1101/gad.7.9.1735.

Lang, W., & Reeder, R. H. (1995). Enhancer-directed termination: Intersection of rRNA processing and transcription termination. *Molecular and Cellular Biology*, *15*(8), 4863–4875. https://doi.org/10.1128/mcb.15.8.4863.

Longley, D. B., Harkin, D. P., & Johnston, P. G. (2003). 5-fluorouracil: Mechanisms of action and clinical strategies. *Nature Reviews. Cancer*, *3*(5), 330–338. https://doi.org/10.1038/nrc1074

Low, J. Y., Sirajuddin, P., Moubarek, M., Agarwal, S., Rege, A., Guner, G., Liu, H., Yang, Z., Marzo, A. M., Bieberich, C., & Laiho, M. (2019). Effective targeting of RNA polymerase I in treatment-resistant prostate cancer. *The Prostate*, *79*(16), 1837–1851. https://doi.org/10.1002/pros.23909

Luger, K., Mäder, A. W., Richmond, R. K., Sargent, D. F., & Richmond, T. J. (1997). Crystal structure of the nucleosome core particle at 2.8 Å resolution. *Nature*, *389*(6648), 251–260. https://doi.org/10.1038/38444

Mais, C., Wright, J. E., & Prieto, J. L. (2005). UBF-binding site arrays form pseudo-NORs and sequester the RNA polymerase I transcription machinery. *Genes & Development*, *19*(1), 50–64. https://doi.org/10.1101/gad.320405.

Mars, J.-C., Tremblay, M. G., Valere, M., Sibai, D. S., Sabourin-Felix, M., Lessard, F., & Moss, T. (2020). The chemotherapeutic agent CX-5461 irreversibly blocks RNA polymerase I initiation and promoter release to cause nucleolar disruption, DNA damage and cell inviability. *NAR Cancer*. https://doi.org/10.1093/narcan/zcaa032.

McClintock, B. (1934). The relationship of a particular chromosomal element to the development of the nucleoli in Zea mays. *Z. Zellforsch. Mikrosk. Anat*, *21*, 294–328. https://doi.org/10.1007/BF00374060

McStay, B. (2016). Nucleolar organizer regions: Genomic "dark matter" requiring illumination. *Genes & De- velopment*, *30*(15), 1598–1610. https://doi.org/10.1101/gad.283838.116.

Merz, K., Hondele, M., & Goetze, H. (2008). Actively transcribed rRNA genes in S. cerevisiae are nearly nucleosome-free. *Genes & Development*, *22*(9), 1190–1204. https://doi.org/10.1101/gad.465408.

Milkereit, P., & Tschochner, H. (1998). Components involved in yeast RNA polymerase I transcription. *Chro- Mosoma*, *107*(7), 469–480. https://doi.org/10.1007/s004120050327.

Misiaszek, A. D., Girbig, M., Grötsch, H., Baudin, F., Murciano, B., Lafita, A., & Müller, C. W. (2021). Cryo-EM structures of human RNA polymerase I. *Nature Structural & Molecular Biology*, *28*(12), 997–1008. https://doi.org/10.1038/s41594-021-00693-4

Moorefield, B., Greene, E. A., & Reeder, R. H. (2000). RNA polymerase I transcription factor Rrn3 is functionally conserved between yeast and human. *Proceedings of the National Academy of Sciences of the United States of America*, *97*, 4724–4729. https://doi.org/10.1073/pnas.080063997.

Moss, T., Langlois, F., Gagnon-Kugler, T., & Stefanovsky, V. (2007). A housekeeper with power of attorney: The rRNA genes in ribosome biogenesis. *Cellular and Molecular Life Sciences*, *64*(1), 29–49. https://doi.org/10.1007/s00018-006-6278-1

Moss, T., Mars, J.-C., Tremblay, M. G., & Sabourin-Felix, M. (2019). The chromatin landscape of the ribosomal RNA genes in mouse and human. *Chromosome Research*, *27*(1–2), 31–40. https://doi.org/10.1007/s10577-018-09603-9

Musso, L., Mazzini, S., Rossini, A., Castagnoli, L., Scaglioni, L., Artali, R., Nicola, M., Zunino, F., & Dallavalle, S. (2018). C-MYC G-quadruplex binding by the RNA polymerase I inhibitor BMH-21 and analogues revealed by a combined NMR and biochemical Approach. *Biochimica et Biophysica Acta. General Subjects*, *1862*(3), 615–629. https://doi.org/10.1016/j.bbagen.2017.12.002

Musters, W. (1989). A system for in vivo analysis of yeast rRNA gene transcription: Identification of three regions essential for transcription. *Nucleic Acids Research*, *17*(12), 5003–5018. https://doi.org/10.1093/nar/17.12.5003.

Nagler, C. (2022). *Studies on the effects of RNA-Polymerase-I-Inhibitors CX5461 and BMH-21 in Saccharomyces cerevisiae*.

Naidu, S., Friedrich, J. K., Russell, J., & Zomerdijk, J. C. B. M. (2011). *TAF1B is a TFIIB-like component of the basal transcription machinery for RNA polymerase I. Science* (Vol. 333, pp. 1640–1642). https://doi.org/10.1126/science.1207656.

Negi, S. S., & Brown, P. (2015). rRNA synthesis inhibitor, CX-5461, activates ATM/ATR pathway in acute lymphoblastic leukemia, arrests cells in G2 phase and induces apoptosis. *Oncotarget*, *6*(20), 18094–18104. https://doi.org/10.18632/oncotarget.4093

Nomura, M., Nogi, Y., & Oakes, M. (2013). Transcription of rRNA genes and ribosome biogenesis in eukary- otes. In *The Encyclopedia of Biological Chemistry* (2nd ed.). Elsevier.

Panday, A., & Grove, A. (2016). Yeast HMO1: Linker of genome integrity, gene expression, and nuclear architecture. *Biochimica et Biophysica Acta (BBA) – Gene Regulatory Mechanisms*, *1859*(6), 471–479. https://doi.org/10.1016/j.bbagrm.2016.01.014.

Pelletier, J., Thomas, G., & Volarević, S. (2018). Ribosome biogenesis in cancer: New players and therapeutic avenues. *Nature Reviews Cancer*, *18*(1), 51–63. https://doi.org/10.1038/nrc.2017.104.

Peltonen, K., Colis, L. C., Hällström, T. M., Liu, H., Jäämaa, S., Zhang, Z., Tuominen, E., & Laiho, M. (2014). Transcription inhibition by BMH-21 targets RNA polymerase I without causing DNA damage. *Cancer Re-Search*, *74*(23), 6653–6662. https://doi.org/10.1158/0008-5472.CAN-14-1531.

Peltonen, K., Colis, L., Liu, H., Jäämaa, S., Zhang, Z., Af Hällström, T., Moore, H. M., Sirajuddin, P., & Laiho, M. (2010). Small molecule BMH-21 inhibits RNA polymerase I and activates p53 in human tumor cells. *Cancer Cell*, *18*(1), 77–89. https://doi.org/10.1016/j.ccr.2010.05.028.

Petes, T. D. (1979). Yeast ribosomal DNA genes are located on chromosome XII. *Proceedings of the National Academy of Sciences*, *76*(1), 410–414. https://doi.org/10.1073/pnas.76.1.410.

Philippsen, P. (1978). The genes coding for the 5S rRNA of Saccharomyces cerevisiae. *Nucleic Acids Re- Search*, *5*(12), 4055–4072. https://doi.org/10.1093/nar/5.12.4055.

Pilsl, M., Crucifix, C., Papai, G., Krupp, F., Steinbauer, R., Griesenbeck, J., Milkereit, P., Tschochner, H., & Schultz, P. (2016). Structure of the initiation-competent RNA polymerase I and its implication for transcription. *Nature Communications*, *7*(1), 12126. https://doi.org/10.1038/ncomms12126

Potapova, T. A., & Gerton, J. L. (2019). Ribosomal DNA and the nucleolus in the context of genome organization. *Chromosome Research*, *27*(1–2), 109–127. https://doi.org/10.1007/s10577-018-9600-5

Ralser, M., Kuhl, H., Ralser, M., Werber, M., Lehrach, H., Breitenbach, M., & Timmermann, B. (2012). The Saccharomyces cerevisiae W303-K6001 cross-platform genome sequence: Insights into ancestry and physiology of a laboratory mutt. *Open Biology*, *2*(8), 120093. https://doi.org/10.1098/rsob.120093

Reeder, R. H., Guevara, P., & Roan, J. G. (1999). Saccharomyces cerevisiae RNA polymerase I terminates transcription at the Reb1 terminator in vivo. *Molecular and Cellular Biology*, *19*(11), 7369–7376. https://doi.org/10.1128/MCB.19.11.7369

Reiter, A., Hamperl, S., Seitz, H., Merkl, P., Perez-Fernandez, J., Williams, L., Gerber, J., Németh, A., Léger, I., Gadal, O., Milkereit, P., Griesenbeck, J., & Tschochner, H. (2012). The Reb1-homologue Ydr026c/Nsi1 is required for efficient RNA polymerase I termination in yeast. *The EMBO Journal*, *31*(16), 3480–3493. https://doi.org/10.1038/emboj.2012.185

Sanij, E., & Hannan, R. D. (2009). The role of UBF in regulating the structure and dynamics of transcriptionally active rDNA chromatin. *Epigenetics*, *4*(6), 374–382. https://doi.org/10.4161/epi.4.6.9449

Sanij, E., Poortinga, G., Sharkey, K., Hung, S., Holloway, T. P., Quin, J., Robb, E., Wong, L. H., Thomas, W. G., Stefanovsky, V., Moss, T., Rothblum, L., Hannan, K. M., McArthur, G. A., Pearson, R. B., & Hannan, R. D. (2008). UBF levels determine the number of active ribosomal RNA genes in mammals. *The Journal of Cell Biology*, *183*(7), 1259–1274. https://doi.org/10.1083/jcb.200805146

Schultz, M. C., Brill, S. J., Ju, Q., Sternglanz, R., & Reeder, R. H. (1992). Topoisomerases and yeast rRNA transcription: Negative supercoiling stimulates initiation and topoisomerase activity is required for elonga- tion. *Genes & Development*, *6*(7), 1332–1341. https://doi.org/10.1101/gad.6.7.1332

Siddiqi, I. N., Dodd, J. A., Vu, L., Eliason, K., Oakes, M. L., Keener, J., Moore, R., Young, M. K., & Nomura, M. (2001). Transcription of chromosomal rRNA genes by both RNA polymerase I and II in yeast uaf30 mutants lacking the 30 kDa subunit of transcription factor UAF. *The EMBO Journal*, *20*(16), 4512–4521. https://doi.org/10.1093/emboj/20.16.4512

Siddiqi, I. N., Dodd, J. A., Vu, L., & Nomura, M. (2001). Role of TATA-binding protein (TBP) and TBP-associated factors in upstream activation factor-dependent transcription of yeast rRNA genes. *Molecular and Cellular Biology*, *21*(20), 6922–6932. https://doi.org/10.1128/MCB.21.20.6922-6932.2001.

Snodgrass, R. G., Collier, A. C., Coon, A. E., & Pritsos, C. A. (2010). Mitomycin C Inhibits Ribosomal RNA. *Journal of Biological Chemistry*, *285*(25), 19068–19075. https://doi.org/10.1074/jbc.M109.040477

Son, J., Hannan, K. M., & Poortinga, G. (2020). Active ribosomal DNA repeats are a key determinant of ovarian cancer cell sensitivity to CX-5461. *Cell Reports*, *30*(11), 3960-3973 4. https://doi.org/10.1016/j.celrep.2020.02.095.

Stefanovsky, V. Y., Bazett-Jones, D. P., Pelletier, G., & Moss, T. (1996). The DNA supercoiling architecture induced by the transcription factor xUBF requires three of its five HMG-boxes. *Nucleic Acids Research*, *24*(16), 3208–3215. https://doi.org/10.1093/nar/24.16.3208

Stefanovsky, V. Y., Pelletier, G., & Bazett-Jones, D. P. (2001). DNA looping in the RNA polymerase I enhancesome is the result of non-cooperative in-phase bending by two UBF molecules. *Nucleic Acids Re- Search*, *29*(16), 3241–3247. https://doi.org/10.1093/nar/29.16.3241.

Steffan, J. S., Keys, D. A., Dodd, J. A., & Nomura, M. (1996). Analysis of the role of TATA-binding protein (TBP) in yeast ribosomal DNA transcription by RNA polymerase I: factor interactions and DNA bending. *Journal of Biological Chemistry*, *271*(17), 10538–10544. https://doi.org/10.1074/jbc.271.17.10538.

Tan, X., & Awuah, S. G. (2019). A cell-based screening system for RNA polymerase I inhibitors. *MedChemComm*, *10*(10), 1765–1774. https://doi.org/10.1039/c9md00227h.

Taylor, K. R. (2019). Myc-driven cancers are highly susceptible to the anti-cancer activity of CX-5461. *Can Cer Research*, *79*(23), 6152–6163. https://doi.org/10.1158/0008-5472.CAN-19-0878.

Toussaint, M., Levasseur, G., Tremblay, M., Paquette, M., & Conconi, A. (2005). Psoralen photocrosslinking, a tool to study the chromatin structure of RNA polymerase I–transcribed ribosomal genes. *Biochemistry and Cell Biology = Biochimie et Biologie Cellulaire*, *83*, 449–459. https://doi.org/10.1139/o05-141.

van de Nobelen, S., Rosa-Garrido, M., Leers, J., Heath, H., Soochit, W., Joosen, L., Jonkers, I., Demmers, J., van der Reijden, M., Torrano, V., Grosveld, F., Delgado, M. D., Renkawitz, R., Galjart, N., & Sleutels, F. (2010). CTCF regulates the local epigenetic state of ribosomal DNA repeats. *Epigenetics & Chromatin*, *3*(1), 19. https://doi.org/10.1186/1756-8935-3-19

van Riggelen, J., Yetil, A., & Felsher, D. W. (2010). MYC as a regulator of ribosome biogenesis and protein synthesis. *Nature Reviews. Cancer*, *10*(4), 301–309. https://doi.org/10.1038/nrc2819

Warner, J. R. (1999). The economics of ribosome biosynthesis in yeast. *Trends in Biochemical Sciences*, *24*(11), 437–440. https://doi.org/10.1016/S0968-0004(99)01460-7.

Wei, T., Najmi, S. M., Liu, H., Peltonen, K., Kucerova, A., Schneider, D. A., & Laiho, M. (2018). Small-Molecule Targeting of RNA Polymerase I Activates a Conserved Transcription Elongation Checkpoint. *Cell Reports*, *23*, 404–414. https://doi.org/10.1016/j.celrep.2018.03.066.

White, C. L., Suto, R. K., & Luger, K. (2001). Structure of the yeast nucleosome core particle reveals fundamental changes in internucleosome interactions. *The EMBO Journal*, *20*, 5207–5218.

Wittner, M., Hamperl, S., & Stöckl, U. (2011). Establishment and maintenance of alternative chromatin structures at active rDNA repeats in S. cerevisiae. *Genes & Development*, *25*(5), 484–495. https://doi.org/10.1101/gad.607011.

Woolford Jr, J. L., & Warner, J. R. (1991). The ribosome and its synthesis. In *The Molecular and Cellular Biol ogy of the Yeast Saccharomyces: Gene Expression* (Vol. 2, pp. 587–626). Cold Spring Harbor Laboratory Press.

Xiao, L., Kamau, E., Donze, D., & Grove, A. (2011). Expression of yeast high mobility group protein HMO1 is regulated by TOR signaling. *Gene*. https://doi.org/10.1016/j.gene.2011.08.017.

Xu, H., Antonio, M., & McKinney, S. (2017). CX-5461 stabilizes G-quadruplex DNA and interferes with replication in cancer cells. *Nature Communications*, *8*, 14432. https://doi.org/10.1038/ncomms14432.

Yamamoto, R. T., Nogi, Y., Dodd, J. A., & Nomura, M. (1996). Rrn3 is an essential gene in Saccharomyces cerevisiae required for a function that affects rRNA synthesis. *Proceedings of the National Academy of Sciences*, *93*(18), 8978–8982. https://doi.org/10.1073/pnas.93.18.8978.

Yan, Y., Zuo, X., & Wei, D. (2021). Targeting ribosomal RNA transcription by CX-5461: Synergies with topoisomerase I inhibition in ovarian cancer cells. *Cell Reports*, *37*(5), 10 1016.

Zentner, G. E., Saiakhova, A., Manaenkov, P., Adams, M. D., & Scacheri, P. C. (2011). Integrative genomic analysis of human ribosomal DNA. *Nucleic Acids Research*, *39*(12), 4949–4960. https://doi.org/10.1093/nar/gkq1326

12. Acknowledgments

An erster Stelle möchte ich meinem Doktorvater und Betreuer Prof. Dr. Joachim Griesenbeck danken. Nur durch deine Unterstützung war es mir möglich, dieses große Projekt erfolgreich zu bearbeiten und abzuschließen. Durch deine Anleitung durfte ich eine außergewöhnliche wissenschaftliche Ausbildung genießen, die mir in meinem weiteren Leben mit Sicherheit häufig weiterhelfen wird. Ich werde die vielen langen Diskussionen mit dir über mein und andere Projekte sehr vermissen.

Ich möchte mich bei Herrn Prof. Dr. Herbert Tschochner sowie Frau Prof. Dr. Neva Caliskan bedanken, die mir ermöglicht haben, den experimentellen Teil dieser Dissertation am Lehrstuhl für Biochemie durchzuführen.

Bei Herrn Prof. Dr. Ralf Wagner und Herrn Prof. Dr. Wolfgang Seufert möchte ich mich ausdrücklich dafür bedanken, dass sie sich die Zeit genommen haben, meine Dissertation als Zweit- und Drittgutachter zu beurteilen.

Als nächstes möchte ich mich bei Sebastian Kruse, Catharina Schmid, Michael Jüttner, Nicolas Alexandre, Eileen Schupper, Antonia Friedl und Jakob Stabl für die tolle Zeit am Lehrstuhl bedanken. Nicht nur durch die Ratschläge und lustigen Kaffeepausen im Labor, sondern auch durch die vielen Nachmittag und Abende, die wir gemeinsam verbracht haben, habt ihr dazu beigetragen, dass es doch erträglich war, wenn ein Experiment nicht ganz so gelaufen ist, wie es sollte.

Ich möchte Kristin Hergert, Tobias Fremter, Gisela Pöll sowie allen anderen Mitarbeitenden des Lehrstuhls für viele gute Ratschläge danken.

Ein großer Dank gilt meiner Familie, ohne deren Unterstützung es mir nicht möglich gewesen wäre, die Zeit für dieses Projekt einzuräumen.

Als letztes möchte ich mich bei meiner Freundin Nane von Bargen bedanken, die jederzeit für mich da ist und mich in allen Lebenslagen unterstützt.

13. Statement on the use of Large Language Models (LLMs)

In the research and writing processes of this thesis, Large Language Model (LLM)-based tools (e.g., GPT-4o) have been utilized as an assisting resource. Specifically, these tools have supported the transformation of initial ideas into coherent sentences, the generation and sorting of lists or tables for data analysis, the refinement of formatting, and the linguistic polishing of paragraphs. At every stage, the content produced by LLMs has been rigorously reviewed and proofread, ensuring that the final text meets academic standards and accurately reflects the intended arguments and findings.